# The Leading Edge®

Special section: Offshore technology

SEG SOCIETY OF EXPLORATION GEOPHYSICISTS

April 2020 · Volume 39, No. 4
ISSN 1070-485X

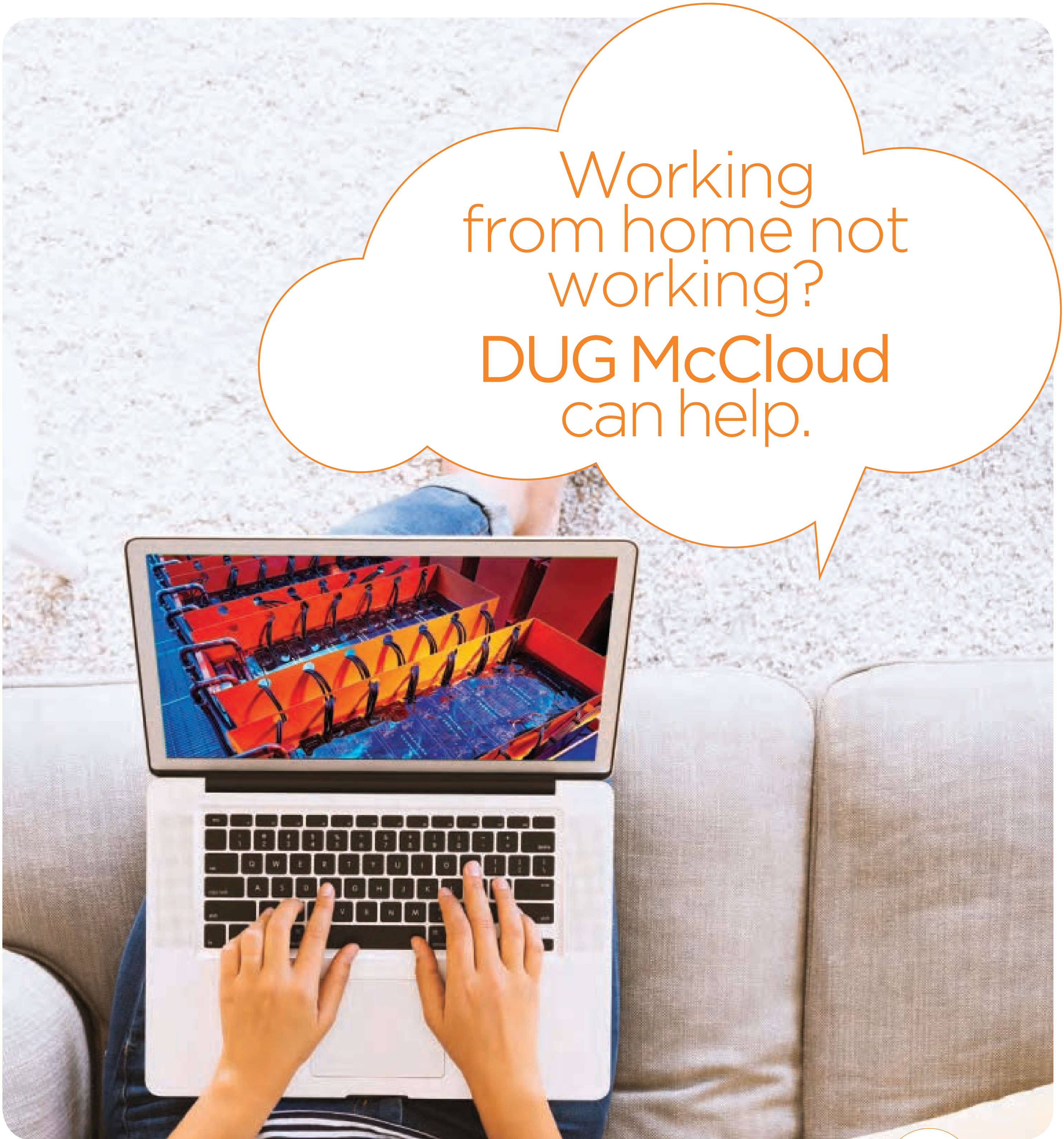
Working from home not working?
DUG McCloud can help.

# Table of Contents

## Special Section: Offshore technology



## Departments



**On the cover:** Seismic research vessel tows air guns on the open sea. Photo credit: Leo Francini/Shutterstock

THE LEADING EDGE

# SEG Board of Directors

PRESIDENT
**Rick Miller**
Kansas Geological Survey
University of Kansas
Lawrence, KS, USA

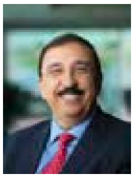

PRESIDENT-ELECT
**Maurice M. Nessim**
WesternGeco
Houston, TX, USA

FIRST VICE PRESIDENT
**Manika Prasad**
Colorado School of Mines
Center for Rock Abuse
Petroleum Engineering Dept.
Golden, CO, USA

SECOND VICE PRESIDENT
**Scott W. Singleton**
Independence Resources Management
Houston, TX, USA

TREASURER
**Dan Ebrom**
Katy, TX, USA

VICE PRESIDENT, PUBLICATIONS
**Baishali Roy**
ConocoPhillips
Houston, TX, USA

PAST PRESIDENT
**Robert R. Stewart**
University of Houston
Dept. of Earth and Atmospheric Sciences
Houston, TX, USA

DIRECTOR AT LARGE
**Bob Brook**
Lexden Energy
Brazoria, TX, USA

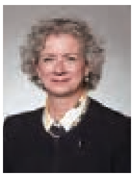

DIRECTOR AT LARGE
**Maria Angela Capello**
Kuwait Oil Company
Al Ahmadi, Kuwait

DIRECTOR AT LARGE
**David E. Lumley**
University of Texas at Dallas
Dept. Earth, Energy, and Environment
Richardson, TX, USA

DIRECTOR AT LARGE
**Kurt J. Marfurt**
School of Geoscience
The University of Oklahoma
Norman, OK, USA

DIRECTOR AT LARGE
**Tad Smith**
Tad Smith Consulting, LLC
Houston, TX, USA

DIRECTOR AT LARGE
**Kenneth M. Tubman**
Houston, TX, USA

CHAIR OF THE COUNCIL
**Gustavo Jose Carstens**
South American Seismic
Buenos Aires, Argentina

**Board of Directors members can be contacted via the SEG website at https://seg.org/board**

*The Leading Edge*® (Print ISSN 1070-485X; Online ISSN 1938-3789) is published monthly by the Society of Exploration Geophysicists, 8801 S. Yale Ave., Suite 500, Tulsa, Oklahoma 74137 USA; phone 1-918-497-5500. Periodicals postage paid at Tulsa and additional mailing offices.

Print subscriptions for professional members of the Society in good standing are included in membership dues paid at the World Bank III or World Bank IV rates. Dues for Active and Associate Members for 2020 vary depending on the three-tiered dues structure based on World Bank classification of the member's country of citizenship or primary work residence. Students may purchase print subscriptions by paying a discounted fee during dues renewal or by contacting members@seg.org. Nonmembers may obtain online subscriptions by contacting books@seg.org. Copies of single issues of *The Leading Edge*® may be purchased by inquiry to books@seg.org.

Corporations, universities, and other institutions can purchase access to *The Leading Edge*® via standalone subscriptions or one of several available subscription package options. SEG's subscription pricing features two academic and two corporate tiers, providing affordable access to applied-geophysics content for institutions of any size. SEG subscription packages offer significant savings on the price of single-publication subscriptions. Special pricing is available for organizations with multiple sites and for institutional consortia. For more information on package pricing, including single-site and multisite institutional subscriptions, please contact Patrick Riley at sales@seg.org or 1-918-497-5531. Institutional subscriptions for print delivery are available only with the purchase of a digital subscription. Rates are subject to change without notice. For more information, please visit http://seg.org/Publications/Subscriptions.

Advertising rates for *The Leading Edge*® will be furnished upon request. No advertisement will be accepted for products or services that cannot be demonstrated to be based on accepted principles of the physical sciences. For more information, contact kgamble@seg.org.



**JOHN KOEHR**, Executive Director
**TED BAKAMJIAN**, Associate Executive Director, Publications and Communities
**JENNIFER COBB**, Director, Journals and Books
**STEVE BROWN**, Managing Editor
**KELSY TAYLOR**, Associate Editor
**MARIA GEE**, Graphic Designer
**CALLIE LEE-PETRICEK**, Manuscript Submissions Specialist

**Editorial information:** 1-918-497-5503, sbrown@seg.org

**Advertising information and rates:**
1-918-497-5524
Kathy Gamble, kgamble@seg.org

**Subscription information:**
Members, members@seg.org
Nonmembers, books@seg.org
Institutions, Patrick Riley, 1-918-497-5531, priley@seg.org

**POSTMASTER:** Send changes of address to
**The Leading Edge**
8801 S. Yale, Suite 500
Tulsa, OK 74137 USA

THE LEADING EDGE

# Editorial Calendar

| Issue | Special section theme | Due date | Guest editors |
|---|---|---|---|
| May 2020 | Near-surface imaging and modeling | past due | Daniel Feigenbaum<br>Steve Sloan[1] |
| June 2020 | Middle East | past due | Abdullatif Al-Shuhail<br>Youcef Bouzidi<br>Saleh Al-Dossary<br>Yongyi Li[1] |
| July 2020 | Reservoir monitoring | past due | David Johnston<br>Arpita Pal Bathija[1] |
| August 2020 | Southeast Asia | past due | Roberto Fainstein<br>Soman Chacko<br>Chengbo Li[1] |
| September 2020 | Smart city geophysics | 1 May 2020 | Steve Sloan[1]<br>Yongyi Li[1] |
| October 2020 | Machine learning and AI | 1 Jun 2020 | Olga Brusova<br>Michael Pyrcz<br>Margarita Corzo[1] |
| November 2020 | Distributed acoustic sensing | 1 Jul 2020 | Kyle Spikes[1] |
| December 2020 | Geothermal | 1 Aug 2020 | TBD |
| January 2021 | Remote sensing | 1 Sep 2020 | Yongyi Li[1] |
| February 2021 | Mining | 1 Oct 2020 | Steve Sloan[1] |
| March 2021 | Basin exploration | 1 Nov 2020 | Margarita Corzo[1] |

[1] *TLE* Editorial Board coordinator

*TLE* publishes special sections and standalone articles covering all aspects of applied geophysics and related disciplines. Submission of articles is open to all. Please submit articles via the online manuscript submission system at https://mc.manuscriptcentral.com/tle. Submission instructions can be found at https://seg.org/Publications/-The-Leading-Edge/Information-for-Authors. For full descriptions of special section themes, see https://library.seg.org/page/leedff/tle-special-sections. *TLE* Editorial Board coordinators work with guest editors to coordinate and support the review process and also may serve as guest editors. For additional assistance, contact tle@seg.org.

# Houston needs more SEG presence

Dan Ebrom, SEG Treasurer

SEG has addressed the challenges of meeting the needs of a global membership with the opening of regional offices in the Middle East, China, and Malaysia. The China office is now financially self-supporting, and the Middle East office is running a positive net budget with multiple events each year. The success of these offices in addressing the needs of our membership and our profession has led us to look at Houston. Ironically, in Houston, where the SEG was founded and which continues to serve as a technical and organizational center for many oil companies and geophysical service companies, there is only a minimal permanent SEG presence.

Of course, Houston is only one of dozens of cities in which significant geophysical communities work and create, but it is the largest center to lack a local SEG office. This has been dealt with in the past by utilizing the talents of Houston-area SEG volunteers, working in concert with Tulsa-based SEG staff. While this approach succeeded in the past during boom times in the oil patch, the current low commodity prices have prompted an urgent need to better serve the major oil companies, independent oil companies, and service companies in Houston.

The fundamental role of SEG, in my opinion, is to facilitate exchanges of information among geophysicists. With the exception of the SEG Advanced Modeling Program, which creates modeled seismic data, SEG is primarily a facilitator of information exchange rather than a creator of information. Individual geophysicists, and teams of geophysicists, create information. It is the job of SEG to connect individuals (and organizations) who have a message to deliver with those individuals (and organizations) who want to hear that message. SEG makes these connections possible through a variety of vehicles: journals, annual meetings and associated commercial expositions, regional meetings, traveling distinguished and honorary lectures, specialized workshops, web-based training courses, onsite training courses, and on and on. A key point is that SEG should not compete with the already existing information-transfer activities of the Geophysical Society of Houston (and other local geophysical societies) but should augment and complement those information-transfer activities.

These activities do not occur in a vacuum. The Tulsa-based SEG staff spend significant amounts of time and effort on the logistics of these information-transfer exercises. For the staff to adequately serve the world's largest geophysical market, constant interaction is required with the local working geophysicists (and geophysical managers) who are based in Houston. Video conferencing works well for highly structured meetings, but spontaneous interactions (and creative problem solving) are best handled on the ground, which leads back to the need for Houston-based staff who are continually available and proactive in interacting with the Houston geophysical community.

Additionally, SEG relies on the generosity of donors to the SEG Foundation to fund the scholarships and charitable activities (such as Geoscientists *Without* Borders®) that make concrete the Society's goals of giving back to the communities of the world. These donors make their donations voluntarily of course, but staff is vital to connect with potential donors and let them know of the many different ways Foundation donations can positively impact the globe. Many of the donors are based in Houston, and so staff have to identify and meet donors here in the Bayou City. A Houston regional office makes a natural center for fund-raising efforts touching both individual and corporate donors.

Houston is also a global hub with direct airline connections to much of the world and, significantly, to the major urban centers of Latin America. As SEG expands its presence in the major oil-producing countries to the south, Houston is a natural place to meet decision makers and influencers from countries ranging from Mexico down to Venezuela, Brazil, and Argentina. Many national oil companies (from Latin America as well as from Asia and the Middle East) have offices in Houston, facilitating discussions of their needs and how they would best like to see those needs met.

So far, I have laid out the case for the utility of a Houston regional office for SEG. The good news is that plans, and funding, for such an office are underway already. Office space in Houston has been rented in the office building housing the Society of Petroleum Engineers (SPE). There are already two SEG staff members dedicated to the Houston office (Bill Barkhouse and Annabella Betancourt), but there is a need for a Houston-based business development full-time equivalent and an administrative employee (perhaps shared with SPE) to support this staff. When this staff is at full strength, we will expect to see better interaction with Houston-based stakeholders and donors and improved meetings that benefit both individual geophysicists and exhibiting companies. This is the level of SEG involvement that we need, and this is what must be delivered!

Thanks for reading. See you in the future! TLE

*This President's Page editorial, like every President's Page editorial, reflects the opinions of the author and is not reflective of official SEG policy.*

Executive Perspectives

# Looking back and ahead

John J. Koehr, Executive Director

I am pleased for the opportunity to update SEG members on the successes of our past year and provide a view further into this year. SEG's 2019 Annual Report will be available soon and will include much more detail about the year's activities. As a Society, we had much to be proud of in 2019. I would like to summarize key SEG accomplishments from my perspective:

- Finished 2019 with strong statements relative to activities (profit and loss), financial position (balance sheet), and cash flows. We are fortunate to be in this position, which provides us the foundation on which to grow our mission impact.
- Realigned staff resources with SEG's new portfolio structure. This includes Meetings, Publications, Constituent Engagement, Professional Development, Student and Early Career Programs, Regional Offices, Business Development and Expanding Markets, and Support.
- Completed a refresh of the SEG strategy including the work of presidential task forces addressing key strategic imperatives. Members can expect more communication as the Board achieves consensus on the road map.
- Completed the sale of SEG's Tulsa real estate. I am pleased to report that the campus name remains the Geophysical Resource Center, and the Doodlebugger statue remains prominently on display in the main lobby.
- Expanded SEG's global presence by establishing a new office in Kuala Lumpur, Malaysia, to address opportunities in the Asia-Pacific region.
- Launched a successful new partner event, Energy in Data, which is managed by SEG and cohosted with our good friends at the American Association of Petroleum Geologists and the Society of Petroleum Engineers.
- Launched the new EVOLVE Professional program.
- Held a successful 2019 Annual Meeting. This was my first SEG Annual Meeting, and I was impressed with all aspects of the event and community including our business and committee meetings, networking and social events, awards ceremony, plenary sessions, technical program, education program, exhibition, student and early-career programs, Student Leadership Symposium, Challenge Bowl, President's Jam, Wrap-Up Party, and member events. I was struck that geophysics is a true community with its own identity.
- Participated in alliance with a number of prestigious societies via GeoScienceWorld to launch a new open-access journal, *Lithosphere*. The journal will cover research in all areas of earth, planetary, and environmental sciences, providing a unique publishing choice for authors in the geoscience community.
- Launched the SEG Library on a new platform with a completely new design. The SEG Library continues to be cited as a top member benefit.

The Doodlebugger statue remains on display in the lobby of the Geophysical Resource Center in Tulsa, Oklahoma.

- Launched the new SEG Value in Partnering (VIP) program to enable corporate partners to bundle SEG offerings including membership, published content, industry events, education, and global networking opportunities.
- Initiated a new SEG Advanced Modeling (SEAM) project on artificial intelligence.
- Created a new staff Executive Perspectives column for *The Leading Edge*, written monthly by a member of the senior management team to share knowledge about the Society's products, programs, and services.

SEG's purpose is to promote the science of applied geophysics and related fields, to foster the common scientific interests of geophysicists, and to maintain a high professional standing among its members. In my view, this noble purpose includes engaging and serving our diverse global communities to advance applied geophysics for the benefit of humanity. Execution on our purpose can achieve a vision in which applied geophysics is recognized worldwide for what our members already know, enabling the best solutions to grand challenges that benefit humankind.

During my brief time with SEG, I have noted that staff and volunteers share values that include preserving the integrity of science; adhering to high standards of ethical professional conduct; embracing diversity of thought, culture, and demographics; treasuring the environment and the world's natural resources; celebrating the proud heritage and contributions of geophysicists; and serving as responsible stewards of Society resources. These shared values form a solid foundation, allowing SEG to confront market realities, advance our purpose, and take on our strategic imperatives.

Some key strategic imperatives that resurfaced through the Board's strategy refresh exercise include expanding global engagement, growing our constituent base in other applied-geophysics industries, engaging students and early-career professionals, attracting the next generation of geophysicists, improving diversity of the profession and membership, growing humanitarian contributions and impact, creating sustainable product and program solutions, meeting market needs, expanding cross-discipline collaboration and partnerships, enabling adoption of emerging technologies, and increasing utilization of geophysics.

To address these imperatives, SEG will implement a strategy road map to advance applied geophysics that includes continuing to grow the impact and excellence of our core knowledge-exchange channels, expanding diversity of our offerings and presence in new markets, expanding our global presence in support of applied-geophysics communities, increasing engagement with early-career professionals, and raising awareness of the role and relevance of applied geophysics. Our unfolding plans for 2020 are starting to move us more deliberately in this direction, and members can expect clear communications of the strategy and our progress. A preview includes:

- Celebration of SEG's 90th anniversary at the 2020 Annual Meeting in Houston
- Expanding the SEG global hub office in Houston supporting initiatives across all portfolios
- Further organizational alignment around a strategy addressing our imperatives
- Deeper collaboration with associations representing related science and engineering disciplines
- Renewed opportunities for mission and humanitarian impact enabled through philanthropy
- Focus on ensuring the sustainability of impactful programs within SEG's portfolios

Before closing this month's column, I want to comment briefly on SEG's response to the global coronavirus (COVID-19) outbreak. SEG leadership is monitoring the outbreak closely and taking all related developments very seriously. We are deeply concerned about the devastating and disruptive effects of the COVID-19 outbreak and consider as our highest priority ensuring the wellbeing of our global friends, colleagues, and constituents. We encourage all members to follow the guidance of local authorities and the World Health Organization.

Members can expect some disruption to planned activities over the next few months. SEG has taken action to reschedule lectures and workshops. Plans are underway to replace canceled lecture stops with virtual lectures, and the workshops will be rescheduled for later this year. Additionally, some partner events have been rescheduled. Please check the SEG events calendar (https://seg.org/events) for the latest information. Preparation continues unabated for this year's SEG Annual Meeting, SEG20, scheduled for 11–16 October in Houston. Please check https://seg.org/am/2020/ regularly for updates. Meanwhile, stay safe. TLE

# Two pivotal events are on the horizon

Rhianna Collier, Managing Director, Global Events

SEG's Meetings program is designed to bring together members from around the globe to discuss common threads of geophysics in numerous disciplines through a portfolio of events. This month, I want to highlight two upcoming events that are pivotal to the Meetings program. They are the 2020 SEG Annual Meeting (11–16 October 2020 in Houston, Texas) and the 2nd Annual Energy in Data Conference (21–24 February 2021 in Austin, Texas).

This year's Annual Meeting marks SEG's 90th anniversary celebration. For the past 90 years, SEG has engaged and served diverse global communities to advance applied geophysics for the benefit of humanity. I am delighted to announce that this year's technical program will feature nine special sessions. The Business of Applied Geophysics sessions will dive into four key strategic business discussions. In addition, the postconvention workshops will encompass 23 hands-on educational sessions.

### Special sessions:

- Geophysical exploration onshore and offshore Africa: Challenges and opportunities
- Geophysical exploration of the solar system by NASA
- Geophysics in medicine
- Geoscientists *Without* Borders® and humanitarian geophysics
- Geothermal exploration
- Machine learning in the near surface
- Recent advances and the road ahead
- SEG/AGU hydrogeophysics
- Urban geophysics

### Business of Applied Geophysics sessions:

- Doing geophysical business in Africa
- Will $CO_2$ sequestration become a viable geophysics business?
- What is the business model for near-surface geophysics?
- Where is the geophysical service industry headed?

### Postconvention workshops:

- 4D under complex overburden: Are we there yet?
- Anisotropic imaging velocity modeling — Preserving accurate structure and multiazimuth signal at the target — Current state and remaining challenges
- Applied geophysics addressing top challenges facing humanity
- $CO_2$ geophysical monitoring: Achievements, challenges, and road ahead
- DAS: Advances in fiber optic sensing over the last decade
- Full-wavefield imaging
- Geophysical challenges in presalt carbonates
- Geophysical solutions for oil field engineering applications
- Low-frequency FWI: How low do we need to go?
- Machine learning/artificial intelligence in mineral exploration
- Promises and challenges with sparse node ultra-long-offset OBN acquisition in imaging and earth model building
- Seismic attributes and DHI analysis in the age of artificial intelligence: Examples, challenges, and opportunities
- What is the latest in machine learning and data analytics for geoscience applications?
- Advancements in land seismic processing technologies
- Booking P1-3 oil and gas reserves using geophysical data
- Keeva Vozoff commemorative workshop
- Least-squares migration in complex overburden
- Machine learning blind-test challenge
- Microseismic monitoring: Proven versus nonproven
- Next-generation geoscience using machine learning
- Professor Azra Tutuncu's workshop — Integrated geophysical and geomechanical evaluation of induced seismicity
- SimPEG for mineral explorationists
- Values in elastic imaging and elastic full-waveform inversion

In addition to a robust educational program, there will be a number of networking and business development opportunities. Kicking things off will be our annual golf tournament 10 October at the Golf Club of Houston. The following days will feature multiple networking events designed to allow delegates the opportunity to make key connections with potential clients and partners.

I hope you will plan to join us in Houston as we celebrate a rich history of innovation. For more information about the technical program, exhibition, and networking events, visit https://seg.org/am/2020/.

SEG has a new event in its portfolio, Energy in Data (EID), in partnership with the American Association of Petroleum Geologists and the Society of Petroleum Engineers. EID is a data conference exclusively designed for the energy sector, providing a unique experience for multidisciplinary teams to influence the direction of the industry through the digital transformation process.

EID engages digital practitioners focused on describing and solving problems around data analytics, machine learning, cross-disciplinary integration, data management storage, oil and gas developments, drilling and production, and more. The event provides four days of hands-on workshops, interactive panels, technical sessions, design contests, hackathons, networking events, and an exhibition featuring innovative technologies and practices.

The EID organizational committee is working diligently to set the vision and development of the event regarding digital transformation pertinent to the energy sector, specifically for geoscientists, engineers, data scientists, IT specialists, and managers from all types of companies and academia. The call for abstracts will open in June 2020. Visit https://energyindata.org for more information.

To learn more regarding SEG's meetings and events, please contact me at rcollier@seg.org. TLE

# Introduction to this special section: Offshore technology

Ulrich Zimmer[1]

https://doi.org/10.1190/tle39040237.1

In this *TLE* special section on offshore technology, four papers outline advances in marine seismic acquisition and processing. The first paper, by Manin et al., describes the concept, tank trials, and sea trials of the "FreeCable" system, which relies on a fleet of small autonomous vessels to provide stability and flexibility in the positioning of seismic cables. The trials and pilot surveys show promising results with respect to signal improvement, acquisition efficiency, and cost effectiveness.

Blanch et al. describe a methodology of using full-waveform inversion and basement refraction events to improve velocity estimates under thick salt canopies. They show that this methodology can recover checkerboard perturbations that were introduced into a realistic velocity model. They apply this methodology to a data set obtained from an ocean-bottom network and show an improvement in determining the subsalt velocities.

Orji et al. describe a new marine vibrator source technology using folded surface concepts and resonance frequency tuning that improves the efficiency and robustness of the source. This design uses a large surface area with comparatively small displacements to achieve a lower sound exposure level without significantly compromising data quality.

Finally, in a proof of concept, Long and Martin showcase an application of data analytics and supervised learning to reduce the processing time for a marine data set from approximately 90 days to just a few days. This is achieved largely through automation of otherwise time-consuming steps such as quality control and multiple reiteration over processing steps and especially velocity model building and optimization. The paper shows that this approach is robust even in cases in which the starting velocity model differs by up to 15% from the optimized model. TLE

[1]Shell, Houston, Texas, USA. E-mail: ulrich.zimmer@shell.com.

# Full-azimuth, full-offset, high-fidelity vector marine seismic acquisition

Michel Manin[1], Luc Haumonté[1], and Eric Bathellier[1]

https://doi.org/10.1190/tle39040238.1


## Abstract

Ten years ago, Kietta launched a project to develop a new method of marine seismic acquisition using midwater stationary cables and autonomous surface vehicles. We present the concept and the technology bricks and recount the successful performance of a commercial pilot survey. The objective of the technology is to enable flexible acquisitions and deliver high-quality, high-fidelity seismic data without sacrificing productivity. After reviewing existing marine seismic acquisition methods, we describe the technology development, including sea trials. The geophysical advantages of acquiring true 3D/four-component data are demonstrated by seismic data analysis, including simultaneous sources and associated productivity calculation.


## Introduction

Existing marine seismic acquisition methods can be grouped in two main categories: towed-streamer techniques and ocean-bottom techniques, such as ocean-bottom cable, ocean-bottom node, and ocean-bottom seismometer (OBS). The offset and azimuth distribution obtained from the streamer technique is naturally narrow because the relative position of the sources with respect to the receivers is fixed (narrow azimuth). The improvement obtained through multiazimuth, wide-azimuth, rich-azimuth, and full-azimuth acquisition configurations comes with substantial additional operating cost and does not deliver full-offset, full-azimuth data in an isotropic bin. In addition, the method generates different types of noise: flow noise and mechanical noise, which are proportional to the square of the water velocity (Schoenberger and Mifsud, 1974; Elboth et al., 2010), and swell noise (Elboth et al., 2009). Mechanical vibrations affect the geophone signals, and the sea surface effects of the swell have an exponential decay with depth (Haumonté and Manin, 2017).

Ocean-bottom techniques do not suffer from the same limitations as streamers do. The receivers are stationary, positioned away from the sea surface, and not subject to mechanical tensions. Due to the source being independent of the receivers, the geometry is flexible, and the method is capable of performing full-azimuth, full-offset acquisition. The recording is theoretically broadband since the combination of hydrophone and geophone signals yields a flat signal spectrum through receiver deghosting. The reality is more complex, and being on the seabed, which is the interface between water and the subsurface, raises several issues (Mougenot, 2018). First, the survey quality is impacted by a variety of surface-related noise (Kugler et al., 2005; Le Meur et al., 2010; Socco et al., 2010). Second, the coupling with the seabed is a complicated problem. The receiver response is not isotropic because the receiver partially senses the sea and partially senses the sea bottom. Depending on whether it is coupled to a soft or a hard soil and depending on the rock properties beneath, the impedance and the overall sensor response varies a lot (Parsons and Duncan, 2011). Other challenges include the strong velocity contrast exhibited by the seabed interface, datuming for nonflat seafloor, and limited productivity because the laid-out receivers need to be launched and recovered continuously.

A step change in laying out and picking up receivers can be achieved from full automation of the seismic units. Disruptive technology that uses robotization and automation for the deployment and retrieval of autonomous underwater vehicles (AUVs) (Buisson, 2019; Uzan and Pellet, 2019) as seismic sensors has been introduced (Tsingas et al., 2018; Mancini et al., 2019). An alternative autonomous seismic acquisition technique is to use midwater stationary cables (MSCs) held by two autonomous surface vehicles (ASVs) (Haumonté et al., 2016a). In this article, we present the FreeCable technology and method and recount the main steps of the technology's development starting from the original idea to the performance of a commercial pilot survey. After presenting the principle and technology bricks of the system and its two acquisition modes (patch and progressive), we describe the proof of concept and prototype building. Finally, we demonstrate the system advantages from a geophysical and an operational perspective.

## FreeCable principle and technology bricks

The principle of the acquisition method is to operate MSCs controlled individually by a pair of ASVs. Each MSC is equipped with four-component seismic sensors and tied at both extremities to a recording autonomous vessel (RAV) (Figure 1). The MSC embeds specifically developed equipment to control the immersion depth at low speed. The operations are supervised from a master vessel that communicates with the RAV fleet through wireless radios. Real-time quality control is performed onboard. Each MSC is typically 8 km long and includes a four-component station every 25 m (320 stations per cable). The receiver spread consists of up to 20 parallel cables spaced 400 m apart, leading to a 64 km$^2$ receiver area. Immersion depth ranges from 7 to 100 m. Several shooting strategies are possible since sources and receivers are independent. For the sake of clarification, two operational modes are introduced: a more qualitative method (patch) and a more productive method (progressive). In patch mode, the 20 cables are stationary with respect to the seabed. The shooting vessel sails perpendicularly to the receiver lines and shoots every 25 m, with an interline spacing of 400 m. Overshoot of 4 km is used on each side of the spread (Figure 2). This is a stop-and-go method. Once the 64 km$^2$ area is

[1]Kietta, Marseille, France. E-mail: mmanin@kietta.com; lhaumonte@kietta.com; ebathellier@kietta.com.

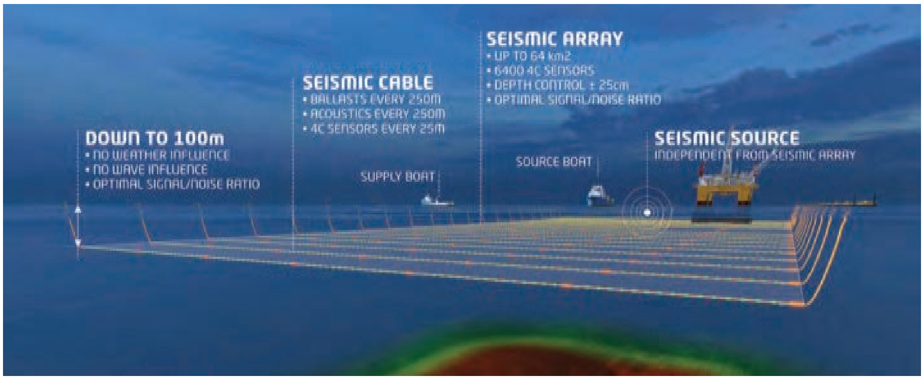


**Figure 1.** Overview of the FreeCable system.

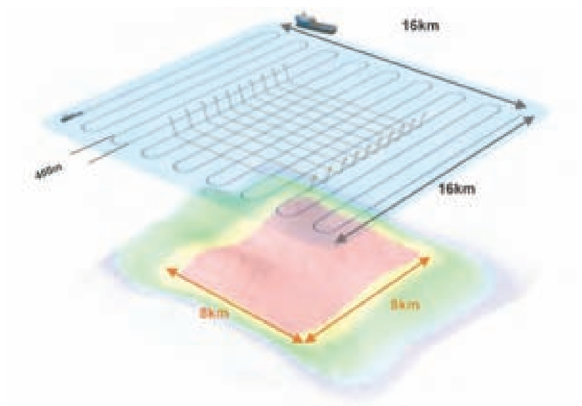


**Figure 2.** Patch acquisition mode with 10 cable-spread configuration.

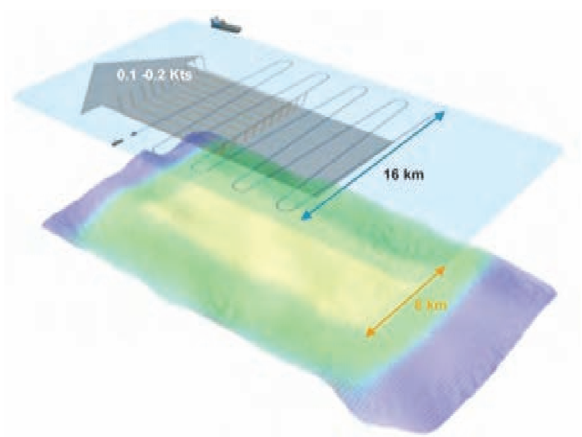


**Figure 3.** Progressive acquisition mode with 10 cable-spread configuration.

covered, the receiver spread moves to the next contiguous patch. In progressive mode (Figure 3), the 20 cables are moving slowly, e.g., 0.1–0.2 knots, along a predetermined route. The shooting vessel sails perpendicularly to the cables and shoots every 25 m with an overshoot of 4 km on each side. The cable speed is such that the shooting vessel has time to shoot a complete line while the cables move 400 m.

The first technology brick is the RAV (Figure 4a). The vehicle can be seen as a miniature tugboat capable of hauling and powering MSCs at low speed. It must accommodate a certain quantity of payload equipment onboard and command and control the position of the seismic cable, which is tied through a lead-in cable. The stability of the tension control must be reversible as the direction of the spread displacement can be reversed. The boat must be as quiet as possible to be undetectable in the seismic bandwidth, corresponding to an objective of acoustic level below 0.1 μbar. Its robust design enables the ship to be operational in rough seas, up to sea state 6. To build this ship and design the shape of its hull, in-tank tests were performed on scaled models, and studies were conducted with the support of a naval architect.

A second technology brick is the seismic cable itself (Figure 4b). It includes four-component seismic stations (hydrophone and triaxial geophone) and must be balanced accurately to have a neutrally buoyant weight in water and no hydrodynamic effect. The variation of the mechanical tension can range from 1 to 30 kilonewtons. Special care was used in mechanically embedding the seismic sensors to guarantee optimal coupling with the acoustic wave and maximum isolation of the vibrations propagating along the MSC so as to maximize the signal-to-noise ratio (S/N) for each component. Prototypes of the seismic subassembly were manufactured to check the quality of the seismic records.

A third technology brick is made up of dynamic ballasting units (Figure 4c). These units are designed to accurately control the cable depth all along the MSC. Due to the cable's low velocity with respect to the water, the "birds" of the seismic streamer were replaced by a technology capable of functioning in the absence of hydrodynamic effect. Ballasting units generate a negative or positive strength depending on the error between the targeted depth and the real depth. By inflating or deflating an external bladder, the ballasts stabilize the depth of the immersed cable in real time and compensate for local variations in seawater density.

Finally, a fourth technology brick corresponds to the real-time command and control system, including full seismic data harvesting and quality control (Figure 4d). Supervision comes from a control room installed onboard a master vessel, which accommodates the operational team. A performing telecom architecture was developed to enable bidirectional radio communications. Extensive sea trials were performed to characterize the range and the achievable transmission rates in different environment conditions. The cable positioning is accurately computed in the control room. A command and control algorithm coordinates the ASV fleet to guarantee that the spread is at the right location, taking into account the effects of the sea current. Its performance was analyzed by numerical simulation.

## Proof of concept and prototype building

***Hydrodynamic behavior and tank test.*** A model test program was conducted to evaluate three control drone concepts for towing and controlling the submerged buoyant seismic cables — a round drone with single azimuthal thruster, a round drone with twin azimuthal thrusters, and a tug-shaped drone with twin azimuthal thrusters. The model test program was conducted in two distinct phases. During the initial phase, small drone models were tested in a flume tank in current and regular waves. These tests showed that all three concepts were capable of producing the towline tensions and were controllable within the confines of the small test facility. During the second phase, working scale models were built, and a test program was performed with much larger models in simulated current and waves. The test results showed that all three concepts could provide the towline tensions required in calm water and waves, but the tug-shaped drone had the least increase in power with increasing speed and wave height and had the least pitch motions. For the simulation of hydrodynamic behavior in time domain of an underwater cable (the MSC) towed at both ends by the RAVs, a computing code was developed. This code was interfaced with another code that has been used to simulate the cable behavior with different sea current models. The cable is represented as a series of rigid bars between which the links are considered as perfect. Each bar undergoes weight, inertia, and drag forces.

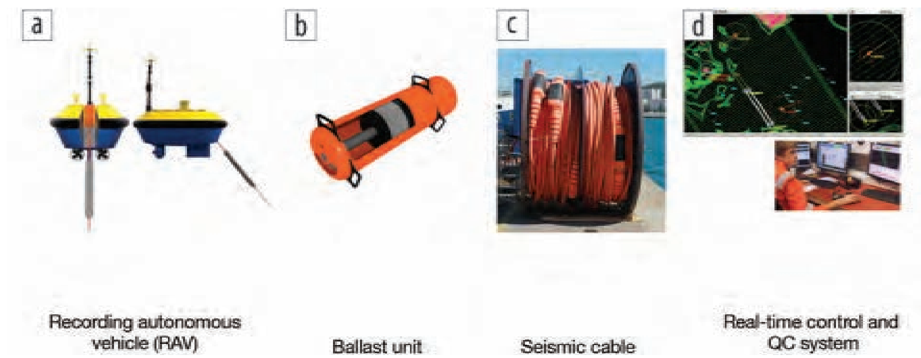


**Figure 4.** The four technology bricks.

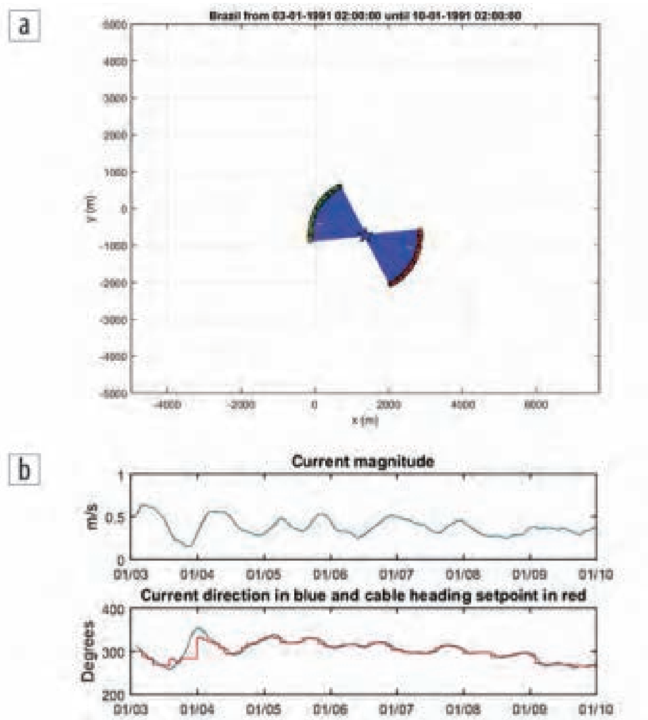


**Figure 5.** Simulations of the command and control algorithm. (a) Cable heading. (b) Sea current magnitude and matching between the current direction and cable heading setpoint.

***Command and control.*** To manage the MSC array and the RAV fleet, a command and control algorithm was developed. It is implemented onboard the master vessel, and its main functions are to control the positioning of the MSC array, the positioning of the MSCs, and the RAVs. The aim of the control strategy is to reduce the inline and crossline errors of the cable while keeping the cable straight. It is also possible to control the cable heading. In the absence of sea current, this heading can be imposed, but it is variable by default, and its setpoint depends on the azimuth and magnitude of the current. The sea current is the main disturbance impacting the cable. For a better algorithm performance, the current must be considered in order to limit the tensions applied by the RAVs and to keep the cables aligned with the main current azimuth as much as possible. The algorithm mainly relies on the forecasted current to anticipate potential changes in the cable heading. Figure 5 shows simulation results of the command and control algorithm applied to data from Brazil where the current is varying in azimuth but is mainly oscillating around 200°. (The magnitude of the current is variable and can go up to 0.8 m/s.) In this case, from 3 to 10 January 1991 the sea current was oscillatory and varying. The algorithm smoothed and filtered the variations. The cable heading remained within a 60° range. Despite the fact that the current is strong in magnitude, being aligned with the current makes the cable behavior stable and satisfactory.

***Survey design and modeling.*** The FreeCable acquisition configuration — 12.5 m inline sampling from receiver spacing and 12.5 m crossline sampling from shot point interval — is an optimized compromise from the wavefield sampling point of view. It also explains why other acquisition methods are different. To illustrate the impact of acquisition geometry on both the resolution and the illumination, the focal beam analysis was used (Delphi Consortium, 2018). The focal detector beam shows the focusing capability of the detector geometry (receiver array), and the focal source beam shows the focusing capability of the source geometry. Their multiplication in the space domain enables estimating the resolution of the acquisition geometry (resolution function representing the averaged reflectivity), and their multiplication in the Radon domain enables estimating the angle illumination function of the acquisition geometry (amplitude versus ray parameter representing angle-dependent reflection information). The simulations were run with the MATLAB code of the Delphi consortium (Blacquière and Verschuur, 2018) and used a simple model consisting of a single reflector set at 1250 m with a 2200 m/s velocity. In Figure 6a, it can be observed that the resolution is excellent as the dot represents the image of a point diffraction. This also confirms that the geometry provides equal offsets in inline and crossline directions, optimum spatial sampling, and symmetrical decomposition in both directions (Vermeer, 2012). We can also see that the angles are regularly illuminated even if the circle is obviously not fully filled (as in the

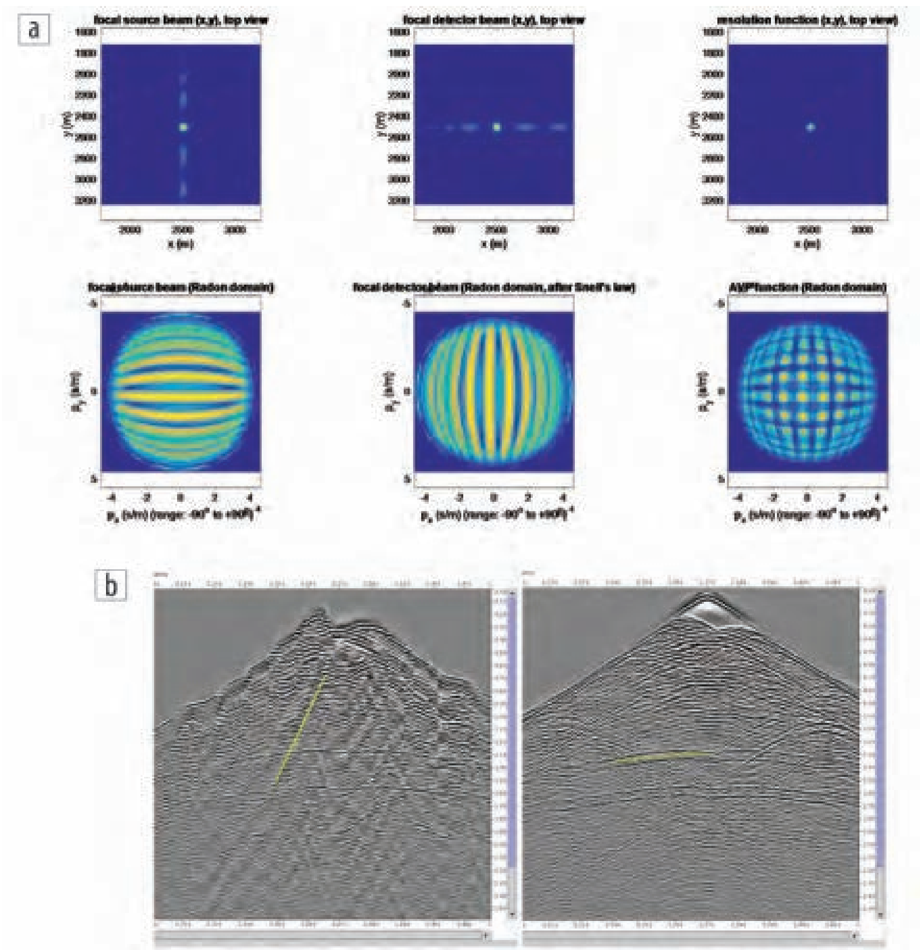


**Figure 6.** Modeling. (a) Resolution and illumination of the FreeCable acquisition geometry. (b) Hydrophone shot gathers for OBS (left) and FreeCable (right).

ideal geometry case) due to discretization. Finite difference 2D elastic modeling in the context of a complex seabed was also performed to provide a qualitative comparison between the MSC and OBS methods (Manin and Haumonté, 2018). A model with rough seabed and flat reflectors underneath was used, and Figure 6b shows a hydrophone common-shot gather for a shot point approximately in the middle of the model. The modeling used a 5 and a 25 Hz Ricker wavelet with a 1 m cell size in both directions. The comparison of the OBS and MSC displays shows that the subsurface reflections are cleaner in the MSC case (see for instance the yellow marker added) and that the near surface is consistently sampled. The OBS image is strongly impacted by a wave train of strong low-frequency perturbations propagating at a low apparent velocity, as depicted for example by the yellow straight line. These disturbances are Scholte waves (Zheng et al., 2013). Moreover, in the OBS case the near surface is significantly distorted due to the irregular seabed. Notice that in these simulations the 5 Hz multiples were turned off to limit the perturbations and to be able to interpret the OBS display. Further work (not presented here) consisted of analyzing the multicomponent data quality and using geophone signals to get information on the wave propagation and particle motion directions. The MSC displays enable observation of the waves, i.e., strong direct arrivals, reflections on the flat layers, and directly reflected waves on slanted cliffs. On the other hand, the OBS displays are hazy where direct arrivals, reflected, and refracted P-waves are hardly observable. The sole events that can be visible are S-waves. The polarization analysis demonstrated that MSC raw data provide an easy means to analyze seismic events and interpret the subsurface geology.

***Real-size test.*** Once preliminary studies and unit testing were completed, a full-scale test was performed with the system prototype. The trial occurred at Seneca Lake (USA) — a deep lake equipped with a naval base, which made it possible to perform acoustic tests. The equipment configuration to be tested was made up of three ballasts and two sections of the seismic cable. A small-volume air gun was used to generate the acoustic waves. During this experiment, the MSC was set at different depths. The test allowed us to check that the seismic cable was capable of recording weak signals with an excellent coupling on all four-component sensors and measuring the beneficial effect to operate the cable at greater depth (Haumonté and Manin, 2017). Ghost suppression was validated at the different depths, with the ballasts providing an accurate depth control of the cable. This lake trial demonstrated that the proof of concept worked and delivered high-quality seismic data. The back analysis allowed us to improve some system components and correct some defaults, in particular mechanical noise generated by the ballasts. The seismic cable was augmented by an elastic stretcher for linear noise attenuation, the integration of equipment necessary for acoustic positioning, and the design of the lead-in cable. The RAV concept was updated, particularly the set of onboard equipment and its software architecture, to make it smart and remotely controllable. From the perspective of system supervision, an integrated solution using, among other data, acoustic positioning data was developed. A solution of quality control of seismic data was also put in place. Finally, command and control algorithms were studied for various conditions, and a flexible version was implemented to enable an adaptive setting. This step terminated with a phase of system integration consisting of assembling, testing, and operating all the elements — four RAVs, 7 km of MSC, and the control room.

***Sea trials.*** First sea trials were conducted in the Toulon Bay of the Mediterranean Sea. These trials allowed us to close a certain number of issues with a progressive ramping up of the coverage of the system functionalities. Then, a full-scale test was performed in the deep offshore of the Mediterranean Sea, approximately 200 km from Marseille and Barcelona (Haumonté et al., 2016b).

At this location, the water depth is 2.4 km, and it is at the toe of the continental slope, which is the only place in the Gulf of Lion where the sedimentary column is complete (without major erosion and hiatuses). The test with the MSC immersed at 100 m made it possible to perform all the operational steps of a real survey: mobilization, transit to the survey area, deployment at sea, operations, recording of the seismic data, picking up of the system, and seismic data processing. This test validated the system operability and its capacity to deliver data in an efficient manner. A shooting vessel towing a small-volume source made up of two air guns (totaling 150 in$^3$) enabled confirmation of the extreme sensitivity of the system. Despite the low-energy source, geologic events were recorded beyond 7 s two-way time. The capability of the system to record a broadband spectrum at different depths was demonstrated again. Many lessons were learned from this experiment to enhance the system. At the end, a set of actions led to modifying some components, and additional tests were done to validate the changes. This made it possible to increase the system robustness and perform automation settings for performance optimization.

***Pilot survey.*** The next step was the planning and execution of a commercial pilot survey for an oil and gas operator. This survey was done in the Red Sea in a geologically and operationally complex environment, e.g., shallow water with islands, coral reefs, and rough seafloor topography (Khan et al., 2017). A standard-volume seismic air gun was used for this work. During the pilot survey, the capability of the system to operate and deliver high-quality data in a challenging environment was demonstrated (Haumonté and Wang, 2017). In particular, all of the four-component sensors recorded useful signals because the reflections came from any direction. The ideal coupling with the water enabled suppression of the receiver ghost in a simple and robust manner, delivering a flat spectrum ranging from low to high frequencies. In Figure 7, the P-Z summation is applied to remove the receiver-side ghosting and water-column reverberation. For this orthogonal acquisition patch, the average receiver depth was set at 15 m, and the ghost frequency notch appears at 52 Hz at the zero offset (assuming the water velocity is 1550 m/s). Figure 7 shows a hydrophone shot record where we can see the ghost notches. The vertical geophone component of the same shot and the P-Z summation are also shown on this figure. We can observe that

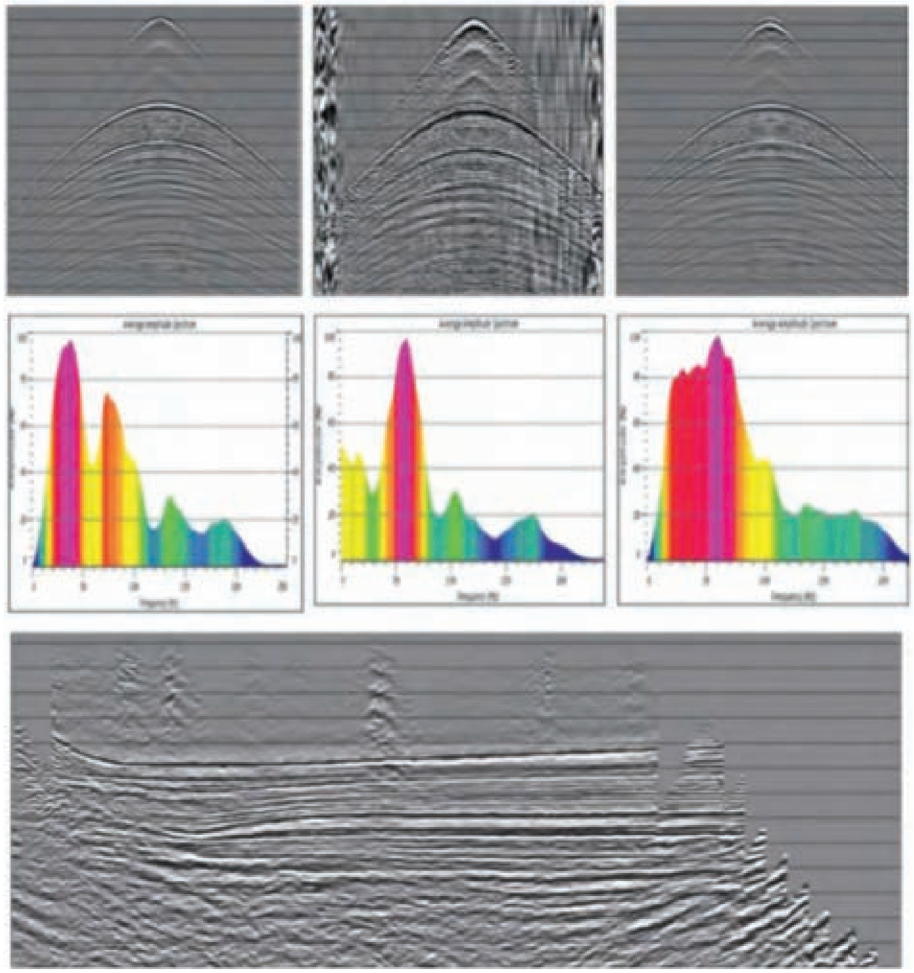

**Figure 7.** Hydrophone data and vertical geophone data after P-Z summation (gathers, spectrums, and stack).

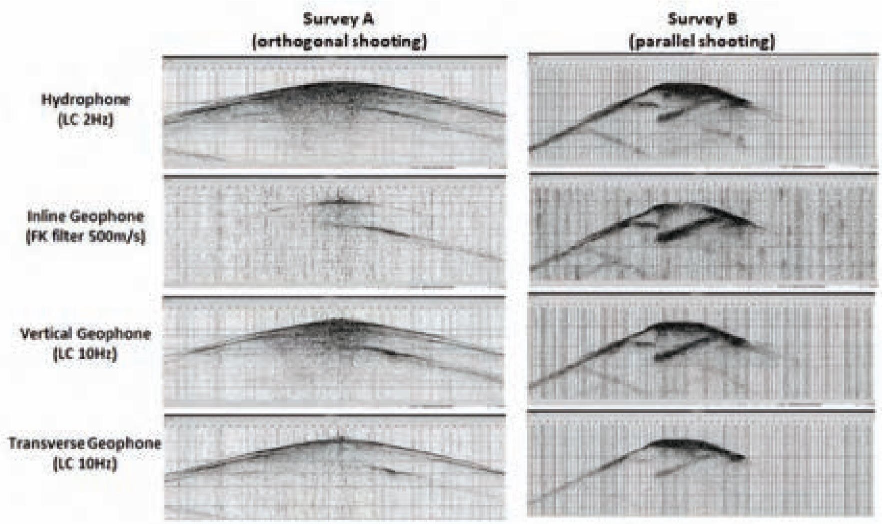


**Figure 8.** Four-component receiver gathers in crossline (left) and inline (right) configuration.

the P-Z summation has done an excellent job of removing the ghosts and broadening the spectrum. The broadband enhancement is also seen on the stack section shown in the same figure.

## Geophysical advantages

***High-fidelity vector wavefield.*** The hydrophones measure the sound pressure wave, while the geophones capture the particle velocity vector: in the acoustic medium constituted by water it is simply related by the water acoustic impedance, which is deterministically estimated from its density and the sound velocity. The temporal and spatial variations of the impedance are limited, and the receivers are considered as perceiving the same impedance. Figure 8 shows four-component receiver gathers for two shooting lines, respectively, in crossline and inline configuration of the pilot survey. Note that the seismic reflections and refractions are coherently visible on all four components. Hence, those signals recorded in an isotropic, homogeneous, and repeatable media have no amplitude and phase distortion. It is potentially well suited for amplitude and inversion analysis and reservoir characterization studies.

***Full-offset, full-azimuth distribution.*** Figure 9a displays a hydrophone record from the Red Sea orthogonal patch, where a shot is almost directly on the top of the MSC. We can see that the noise level is a little stronger at the near offsets, so it is not a problem to fire on top of a cable. Figures 9b and 9c show a geophone that is 1.5 km away from the cables, where, except for those channels close to one of the RAVs, good quality of the particle motion was recorded in the vertical component (Figure 9b), and there is still quite strong energy left in the *y*-component after the three-component rotation (Figure 9c).

***Low noise level.*** Figure 10 presents experimental results from the test performed at Seneca Lake. In this extremely quiet environment, measurements are not disturbed by flow noise and mechanical noise. This figure compares the signal recorded from a single small airgun (3 in$^3$) at 30 m and 120 m depth. The spectrum exhibits signature modulations. It is clearly visible that the noise level below 20 Hz is much higher at 30 m than at 120 m, as predicted by the theory.

***High-quality coupling.*** In the FreeCable method, the sensor coupling is with the midwater and hence is accurate, of high fidelity, and repeatable. To prove the high-quality coupling of the MSC, water-bottom reflections of the deep offshore seismic data were analyzed from both the hydrophone and vertical geophone in terms of amplitudes. The data are 2D, and the amplitude maps displayed in Figure 11 are in the prestack common midpoint (CMP)-offset plan. The yellow bands are due to the variations of the reflection coefficient of the seawater bottom. Those bands are common to the hydrophone and vertical geophone, and the division of the two maps yields the acoustic impedance eliminating the variation effects of the reflection coefficient. As we can observe, the

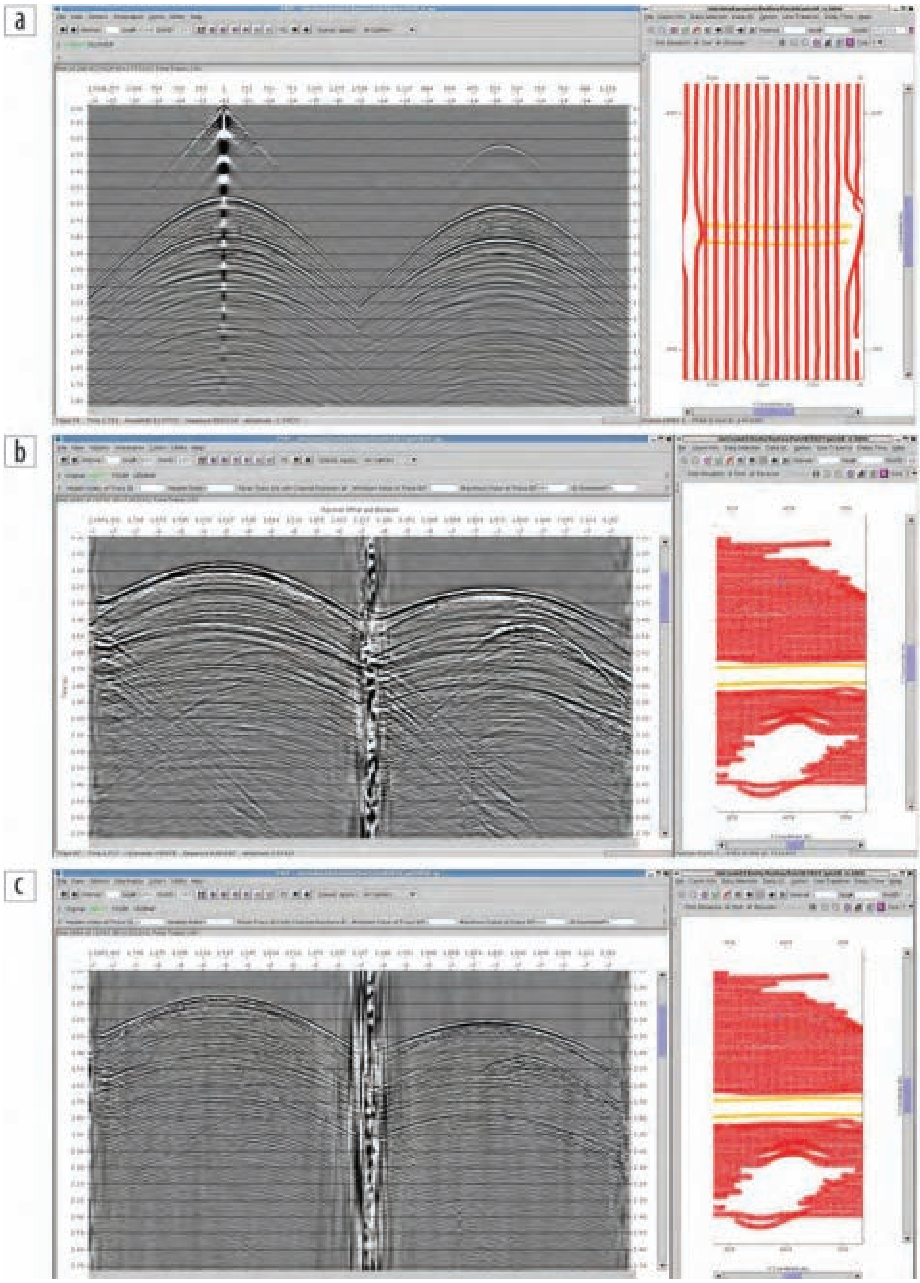


**Figure 9.** (a) Hydrophone record at the top of the cable. (b) Vertical geophone record 1.5 km away from the cables. (c) Y geophone.

acoustic impedance is very stable for every sensor and every CMP. The histogram confirms this stability around the theoretical acoustic impedance of the seawater.

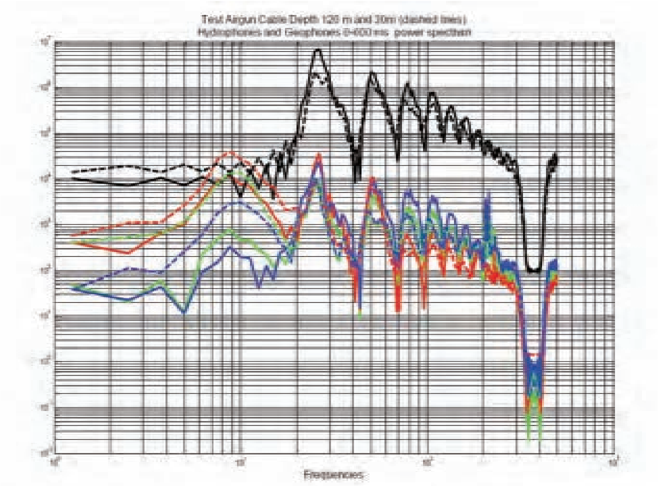


**Figure 10.** Single air gun four-component spectrum at 30 m (dashed line) and 120 m (solid line): hydrophone (black), inline geophone (red), and crossline geophones (green and blue) — unmatched absolute scale.

***Multicomponent deghosting and deblending.*** Receiver deghosting with P-Z summation is great because knowledge of the ghost variation is not necessary because two receivers record the ghost at the same time. The process works on elementary traces before stack and preserves signal. However, there are two sensitive issues: (1) taking into account the curve of the sensor response and (2) taking into account the directivity of the vertical geophone while the hydrophone is omnidirectional. As a consequence and to be rigorous, a scalar depending of the local incidence should be used. We did not look at this point, but there are other deterministic methods that are based on a precise knowledge of the ghosting operator. It can then be envisaged to deconvolve each elementary trace by its theoretical ghost. On one hand, it is known that such a deconvolution explodes because the holes of the ghost spectrum are close to zero. On the other hand, if small variations of depth or incidence are present, it can be built on those variations to render the process stable. The optimal formulation in the least squares sense is

$$R = \frac{\sum corr(tracei, ghosti)}{\sum autocorr(ghosti)}.$$

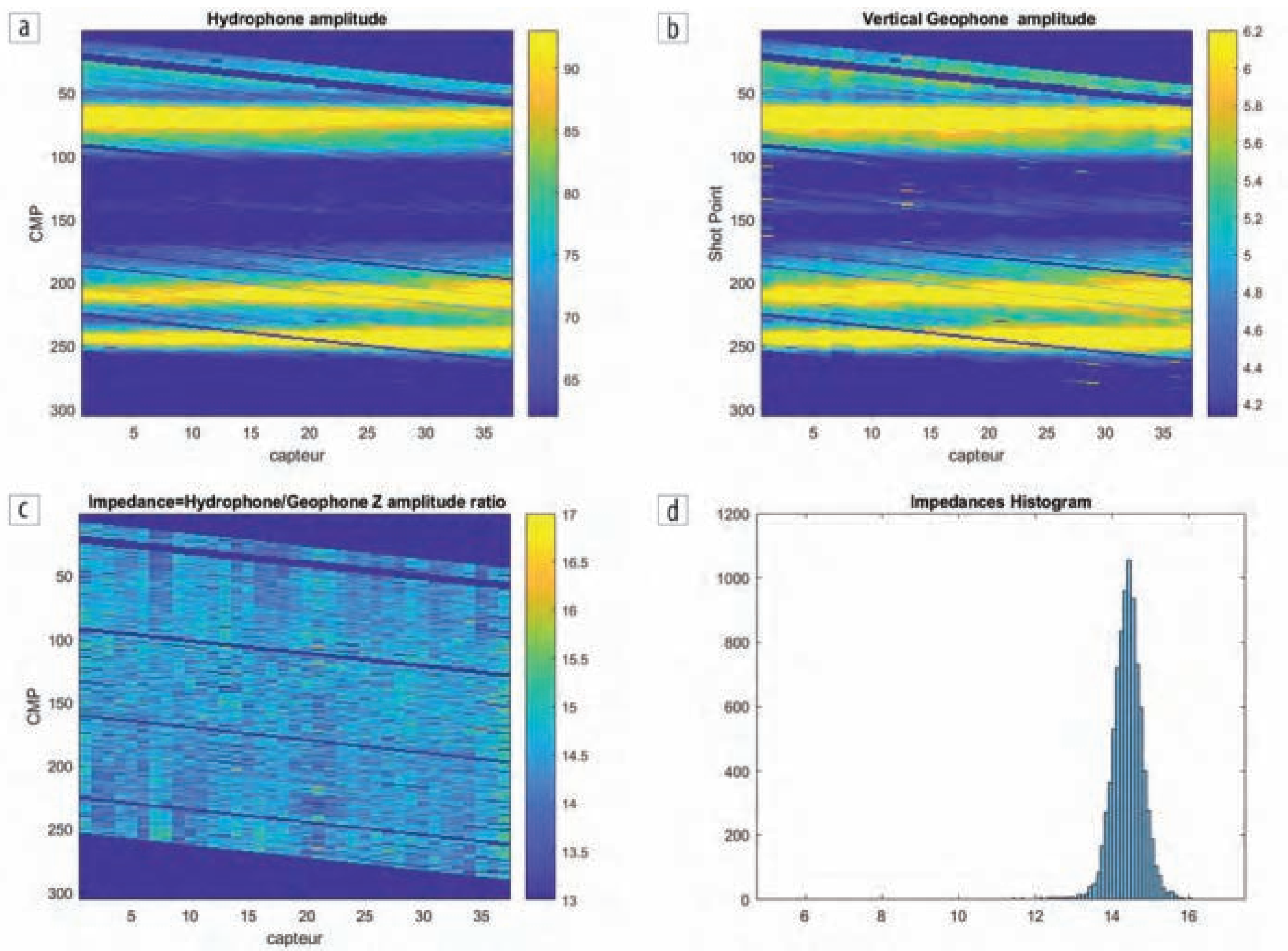


**Figure 11.** Amplitude fidelity. (a) Hydrophone amplitude. (b) Vertical geophone amplitude. (c) Impedance. (d) Histogram.

We place ourselves within a common CMP, and the *R* adapted stack is computed using this formula. It can be remarked that if individual ghosts are fluctuating a bit, the denominator will never be zero. This technique was applied separately to the hydrophone and vertical geophone component of the deep offshore Mediterranean data. We can observe on Figure 12 that the image of the ghost match stack of the hydrophone and vertical geophone set is better than the deghosted image of the upgoing wavefield obtained by P-Z summation. An effect of the process of the ghost match stack on the low-frequency noise is also visible, and the spectrum is sensibly smoother. On the same data set, the adaptive deghosting method was applied (Vrolijk and Blacquière, 2020). Using a multiwindow adaptive deghosting algorithm estimated the optimum ghost model parameters and almost all the ghost energy was removed and a promising result of the upgoing wavefield was obtained.

Another geophysical advantage of the FreeCable method that was demonstrated is its potential to deblend multicomponent simultaneous source data with a pattern-based approach (Jennings et al., 2018). The data set used was once again from the Mediterranean Sea, and the data were synthetically blended assuming two source vessels. When comparing the deblended data with the unblended data, it was clear that using the horizontal geophone components in addition to the hydrophone component removed more of the interfering shot. (The hydrophone data alone result in a S/N of 11.65 dB, and using the hydrophone and horizontal geophone components gives a S/N of 16.17 dB.)

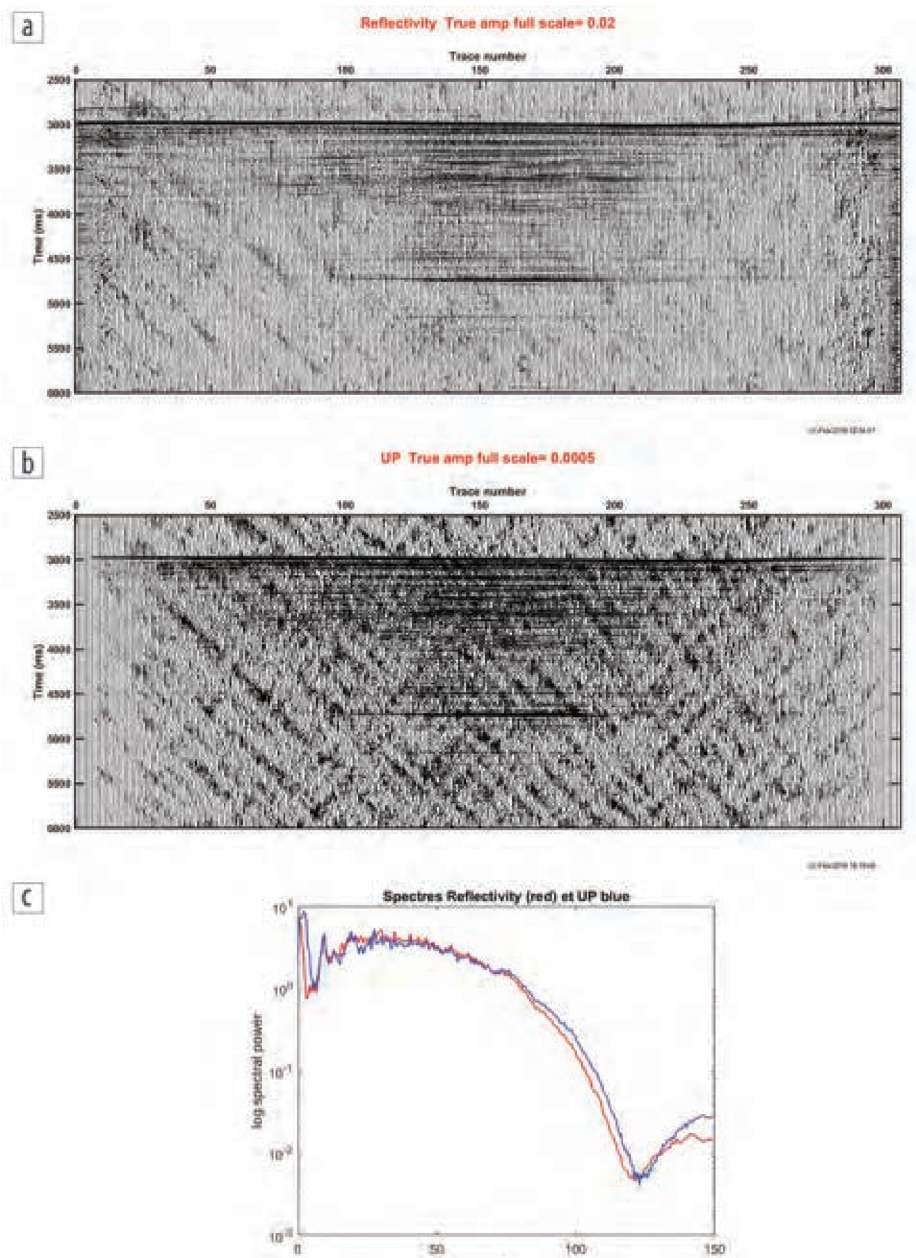


**Figure 12.** Receiver deghosting. (a) Ghost match stack. (b) Upgoing wavefield after P-Z summation. (c) Spectrums.

## Productivity and cost effectiveness

The FreeCable acquisition geometry has numerous degrees of freedom, and the technology has been designed to cope with this intrinsic flexibility. Hence, the method inherently allows sparse or dense geometries. The comparison of two acquisition design cases in patch and progressive modes showed that in progressive mode the productivity is doubled and the fold coverage is halved compared to the patch mode (Haumonté, 2018). In Table 1, some numerical examples are given with 10 MSCs of 8 km length and receiver line and source line intervals equal to 400 m. It was demonstrated that the productivity limitations come from the shooting time. Since the FreeCable system is always operational in water (no repetitive launch and recovery operations), using multiple simultaneous sources automatically multiplies the productivity since the shooting time is almost divided by the number of sources.

## Conclusions

The MSC seismic method and technology have been designed to offer full-azimuth, full-offset, high-fidelity data to the oil and gas exploration and production industry. The technological bricks that make up the acquisition system have been designed to maximize data quality and take advantage of the flexibility of the method. This acquisition method is able to provide an optimized survey design and a customized configuration to offer high productivity and cost effectiveness without the need to recover and relaunch the system. The acquired knowledge will pave the way for the development of vector processing algorithms. Multicomponent source deblending and receiver deghosting were illustrated, but suppression of seismic interference and maritime traffic noise can be implemented. The technology will evolve toward a fully autonomous and unmanned acquisition solution using simultaneous shooting boats with a low-carbon, low-environmental impact on marine life. TLE

**Table 1.** FreeCable raw productivity assuming two or four sources. See text for acquisition parameters.

| | 10 midwater stationary cables | |
|---|---|---|
| | Patch mode | Progressive mode |
| Fold (12.5 × 12.5 m bin) | 200 | 100 |
| Raw productivity — single source | 15 $km^2$/day | 34 $km^2$/day |
| Raw productivity — two simultaneous sources | 28 $km^2$/day | 63 $km^2$/day |
| Raw productivity — four simultaneous sources | 48 $km^2$/day | 117 $km^2$/day |

## Acknowledgments

The authors thank Saudi Aramco for allowing reproduction of their data as well as Kietta management for their support during the life of this project.

## Data and materials availability

The Mediterranean Sea data presented in this work are available and can be obtained by contacting the corresponding author.

Corresponding author: ebathellier@kietta.com

## References

Blacquière, G., and E. Verschuur, 2018, Masterclass: Assessing resolution in the value chain: Presented at Delphi Consortium meeting.

Buisson, N., 2019, Bridges project: DXP and UXP gliders bring together research and industry for the development of glider environment services: Proceedings of Oceans 2019 — Marseille, https://doi.org/10.1109/OCEANSE.2019.8867569.

Delphi Consortium Masterclass, 2018, https://delphi-consortium.com, accessed 17 March 2020.

Elboth, T., D. Lilja, B. Reif, and Ø. Andreassen, 2010, Investigation of flow and flow noise around a seismic streamer cable: Geophysics, **75**, no. 1, Q1–Q9, https://doi.org/10.1190/1.3294639.

Elboth, T., B. Reif, and Ø. Andreassen, 2009, Flow and swell noise in marine seismic data: Geophysics, **74**, no. 2, Q17–Q25, https://doi.org/10.1190/1.3078403.

Haumonté, L., 2018, Digging into the technology of the midwater stationary cable (MSC) acquisition: Presented at New Advances in Marine Geophysical Acquisition Technologies Workshop, SEG.

Haumonté, L., and M. Manin, 2017, A paradigm shift in marine seismic: Broadband full-offset full-azimuth 4-C acquisition with midwater stationary cable: 87th Annual International Meeting, SEG, Expanded Abstracts, 5948–5952, https://doi.org/10.1190/segam2017-17743172.1.

Haumonté, L., and W. Wang, 2017, Survey results obtained in a complex geological environment with midwater stationary cable: 87th Annual International Meeting, SEG, Expanded Abstracts, 196–200, https://doi.org/10.1190/segam2017-17742882.1.

Haumonté, L., L. Velay, and M. Manin, 2016a, A novel marine exploration method offering true 4-C 3D full-offset full-azimuth full-bandwidth seismic acquisition (Freecable): 86th Annual International Meeting, SEG, Expanded Abstracts, 230–234, https://doi.org/10.1190/segam2016-13869474.1.

Haumonté, L., L. Velay, and M. Manin, 2016b, In situ test results obtained in the Mediterranean Sea with a novel marine seismic acquisition system (FreeCable): 86th Annual International Meeting, SEG, Expanded Abstracts, 51–55, https://doi.org/10.1190/segam2016-13865545.1.

Jennings, J., R. Clapp, B. Biondi, and S. Ronnen, 2018, Multicomponent deblending of marine data using a pattern-based approach: 88th Annual International Meeting, SEG, Expanded Abstracts, 236–240, https://doi.org/10.1190/segam2018-2997838.1

Khan, A., T. Al-Ghamdi, and F. Al-Somali, 2017, Cutting-edge marine seismic technologies — Some novel approaches to acquiring 3D seismic data in a complex marine environment: First Break, **35**, no. 11, 77–85.

Kugler, S., T. Bohlen, S. Bussat, and G. Klein, 2005, Variability of Scholte-wave dispersion in shallow-water marine sediments: Journal of Environmental & Engineering Geophysics, **10**, no. 2, 203–218, https://doi.org/10.2113/JEEG10.2.203.

Le Meur, D., N. Benjamin, L. Twigger, K. Garceran, L. Delmas, and G. Poulain, 2010, Adaptive attenuation of surface-wave noise: First Break, **28**, 83–88.

Mancini, F., H. Debens, and B. Hollings, 2019, Low-powered autonomous underwater vehicles for large-scale ocean-bottom acquisition: First Break, **37**, no. 11, 49–55.

Manin, M., and L. Haumonté, 2018, Qualitative comparison between midwater stationary cable and seabed acquisitions based on a 2D elastic modeling in irregular seabed conditions: 88th Annual International Meeting, SEG, Expanded Abstracts, 3848–3852, https://doi.org/10.1190/segam2018-2996995.1.

Mougenot, D., 2018, Marine, seabed, and land seismic equipment for broadband acquisition: A review: Geophysical Prospecting, **66**, no. 5, 922–933, https://doi.org/10.1111/1365-2478.12537.

Parsons, M., and A. Duncan, 2011, The effect of seabed properties on the receive beam pattern of a hydrophone located on the seafloor: Acoustics Australia, **39**, no. 3, 106–112.

Schoenberger, M., and J. F. Mifsud, 1974, Hydrophone streamer noise: Geophysics, **39**, no. 6, 781–793, https://doi.org/10.1190/1.1440466.

Socco, L. V., S. Foti, and D. Boiero, 2010, Surface-wave analysis for building near-surface velocity models — Established approaches and new perspectives: Geophysics, **75**, no. 5, 75A83–75A102, https://doi.org/10.1190/1.3479491.

Tsingas, C., A. Muhaidib, T. Brizard, and C. Walker, 2018, SpiceRack: An autonomous seafloor seismic acquisition system: Presented at New Advances in Marine Geophysical Acquisition Technologies Workshop, SEG.

Uzan, L., and F. Pellet, 2019, A new acoustic payload for gliders: Proceedings of Oceans 2019 — Marseille, https://doi.org/10.1109/OCEANSE.2019.8867335.

Vermeer, G., 2012, 3D seismic survey design, 2nd edition: SEG, https://doi.org/10.1190/1.9781560803041.

Vrolijk, J.-W., and G. Blacquière, 2020, Adaptive estimation of the upgoing wavefield from a variable-depth recording in the case of a dynamic sea surface: Geophysics, **85**, no. 1, V45–V56, https://doi.org/10.1190/geo2019-0035.1.

Zheng, Y., X. Fang, J. Liu, and M. C. Fehler, 2013, Scholte waves generated by seafloor topography: arXiv:1306.4383.

# Designing an exploration-scale OBN: Acquisition design for subsalt imaging and velocity determination

Joakim Blanch[1], Jon Jarvis[1], Chris Hurren[1], Alex Kostin[1], Yan Liu[2], and Lingli Hu[2]

https://doi.org/10.1190/tle39040248.1


## Abstract

Direct wave arrivals are the most robust signals to determine velocity. They have been used for almost a century in hydrocarbon exploration. This is because the arrival time is explicitly available and provides a direct measurement of the average velocity of the subsurface raypath. To acquire these direct arrivals in a seismic experimental setting, it is necessary that the waves turn back to the surface after they start traveling into the earth. As is well known, it is possible to turn waves back up if they encounter faster propagation velocities than previously experienced. Using these simple concepts, we show how it is possible to design a seismic acquisition to measure subsalt velocities when the salt cover is very thick and potentially not homogeneous. Until now in marine seismic surveying, the physical limitations of the earth meant that the use of direct wave arrivals was restricted to relatively shallow depths of investigation. By combining the application of node technology with a well-established physical phenomena (i.e., refraction in the basement), it is possible to retrieve subsalt velocities from seismic surveys.


## Introduction

The conventional methodology to image below salt is to go through an elaborate interpretation workflow. The shape of salt is determined, which enables subsalt imaging. However, the methodology is not adequate for determining subsalt velocity. In many cases, this is not necessary because the base-of-salt interface is fairly flat. It is possible to get an image (albeit not accurate depth) below salt (Figure 1). The subsalt velocity model can also be improved by using velocity measured in wells. However, in areas where there are few well penetrations and the base of salt is fairly rugose, the conventional methodology is no longer applicable (Figure 1). A new methodology is required to determine the shape of complex salt and subsalt velocity through seismic measurements.

Using direct arrivals for velocity estimation is one of the oldest seismic exploration methods and appears to have been used as early as 1910 (Weatherby, 1940). One early method is called "fan shooting" in which earlier than expected arrivals are used to identify areas of higher velocity, indicating the presence of salt domes. Subsequently, direct arrivals have been used for refraction tomography with many applications (Dines and Lytle, 1979; Ivansson, 1985; Zelt and Smith, 1992).

These methods are labor intensive, as individual events need to be identified manually. Since the amount of seismic data collected has increased in recent years, there has been a growing need to automate this process. There is a family of such methods, and full-waveform inversion (FWI) is currently the most used methodology that works directly with recorded data without the need to pick direct arrivals. It requires less labor than traditional methods. These methods are also likely less sensitive to low signal to noise because they do not require identification of wavefront arrivals in raw data. FWI was designed for accurate amplitude inversion of reflected energy (Lailly, 1983), but because its kernel mimics a velocity inversion kernel when the method is applied to direct arrivals, it is suitable for velocity inversion as well. Other methods with specifically designed objective functions, such as surface source extension (Huang et al., 2019), work equally well.

Previous works that apply FWI to determine salt geometry and/or subsalt velocity use starting models that only take some

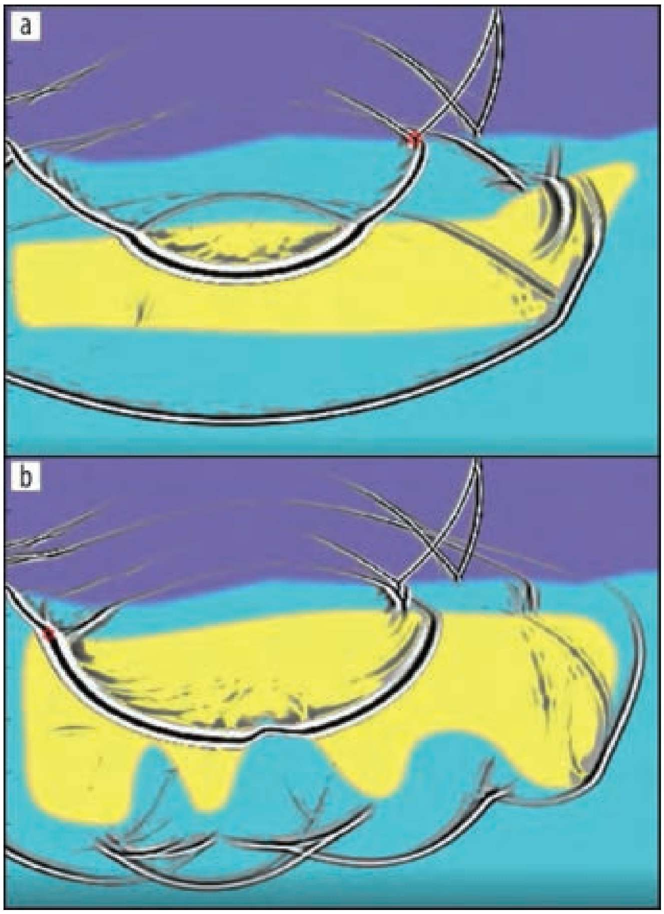


**Figure 1.** Simulation snapshots through different salt shapes. A wavefront is almost flat after passing through a flat base-of-salt interface as shown in (a). However, a rugose base of salt generates a complicated wavefront, and as in the case in (b), with triplication points. To image below salt with a rugose base, it is necessary to have a more accurate subsalt velocity than for a flatter base of salt.

[1]BHP, Houston, Texas, USA. E-mail: joakim.blanch@bhp.com; jon.jarvis@bhp.com; chris.hurren@bhp.com; alex.kostin@bhp.com.
[2]CGG, Houston, Texas, USA. E-mail: yan.liu@cgg.com; lingli.hu@cgg.com.

of the velocity properties of the earth into account. Subsequently, the application is somewhat limited to areas with thin salt sheets, which have an edge toward conventionally compacted sediments, such that the waves could turn back upward in the sediment layer and enter the salt from the side.

There are, however, areas where the salt forms a very thick canopy from the seafloor to approximately 10 km depth and where these models are not functional. In such cases, the solution is to add the basement to the velocity model and to use the direct arrivals that are turned upward in the basement for velocity model building. These direct arrivals are key enablers to determine salt geometry and subsalt velocity. For this current methodology combined with available data to work, it is necessary to approximately determine the depth and velocity at the top of basement.

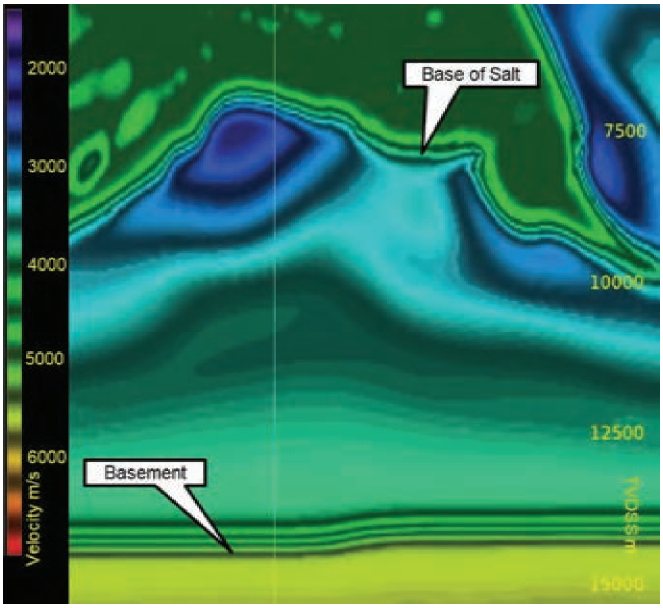


**Figure 2.** Part of the detailed initial model, which includes basement used as a starting velocity model for the survey design. The color bar shows the velocity in meters per second, and the axis on the right is the depth in meters.

Because low-frequency data are important in handling large velocity errors for FWI (i.e., methods that are based on a straightforward least-squares data-fitting objective function), it is necessary to be able to acquire such data. However, conventional sources generate little energy at low frequencies. Hence, it is necessary to understand the behavior of FWI for realistic noise levels at these lower frequencies. Because ocean-bottom nodes (OBNs) are stationary (unlike streamers) and generally deep below the sea surface, the signal recorded by the nodes has a better signal-to-noise ratio. Subsequently, the proposed design will utilize OBNs. In addition, OBNs enable acquisition of data recorded at long offsets, which would be difficult to achieve using a streamer survey.

## Survey design methodology

The objective of the survey design is to enable the creation of an accurate subsalt velocity model in an environment where complex salt bodies cover subsalt clastic sediments. Additionally, it is necessary to determine salt-body geometries and potentially variable intrasalt velocity. As mentioned previously, to acquire long-offset data, we consider OBNs with a sea-surface source.

The first step in the survey design is to build a velocity model that is the best estimate available of the actual subsurface velocity. We use a velocity model derived through standard subsalt imaging and add an estimated basement surface based on interpretation of the existing seismic image (Figure 2).

The starting velocity model contains a thick salt canopy consisting of mixed salt and sediment inclusions. The subsalt succession consists of alternating sand and shale sediments of an unknown velocity. We believe that the basement is either continental granitic crust or oceanic basaltic crust. However, what is considered to be the top basement could also be prerift or synrift deposits. Still, and perhaps most important, the top basement is represented by a large velocity contrast/discontinuity. Figures 3 and 4 show ray tracing and finite-difference modeling through one of the velocity models. Diving waves (seismic waves that return to the surface) are generated below salt at and below the basement. It is also apparent that there is no energy transmitted into the basement at larger incidence angles (i.e., seismic waves experience total reflection, which can be used as diving waves for the purpose of FWI). At a certain smaller incidence angle, there will be conventional reflection and transmission at the basement boundary.

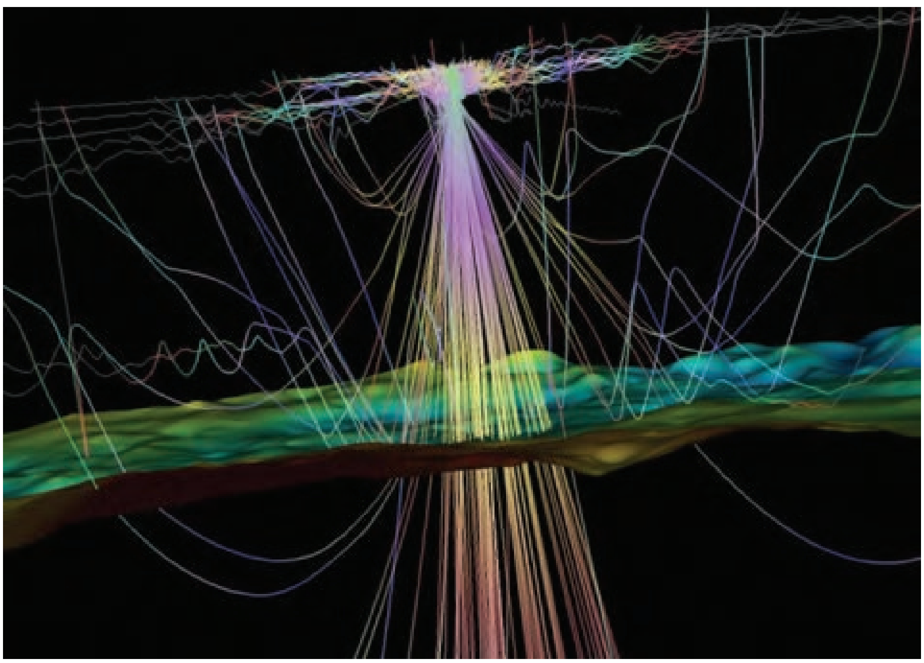

**Figure 3.** Ray cone with basement horizon. Rays with a high takeoff angle are turned either at water bottom or at top of salt. Rays with a small takeoff angle are not turned. However, a few rays with moderate takeoff angles are turned within the basement.

Rays/wave energy that is refracted in the basement has almost vertical takeoff at the seafloor, because the shallow salt effectively screens rays/energy with large takeoff angles. Thus, sources that direct energy vertically could be more efficient than sources with a uniform radiation pattern for a seismic survey designed to determine subsalt velocity.

The velocity at the top of basement is somewhat uncertain, and we decided to work within the 5–6 km/s range. The most likely velocity at the top of the basement is 6 km/s, but since we believed that a slower velocity would put a higher demand on an actual survey in terms of offsets, we opted to use the lower range in order to design a robust survey. The range for the basement velocity is based on results of several refraction studies that have been performed in the Gulf of Mexico (e.g., Eddy et al., 2018). To investigate the impact of basement velocity on survey design parameters, we performed modeling using the same velocity model above the top basement interface and varied the velocity at the top of the basement. The velocity within the basement is a slow linear gradient, reaching 8 km/s at 25 km depth for all models. Figure 5 shows ray-tracing results for different top basement velocities. As expected, a lower velocity at the top basement requires longer offsets to be acquired in order to record energy that has turned at or within the basement. As such, we opted to use 5.5 km/s for the top basement velocity in the modeling study because we believe this to be in lower range of the velocity of a realistic top basement velocity.

To further evaluate and constrain offset requirements, ray tracing was used to generate statistics. A large number of rays was initiated from potential seafloor node locations. Rays that reached the basement or deeper depths and returned to the sea surface were used to generate statistics for offsets, traveltime, and azimuthal information. These statistics were used to limit the number of configurations to test using full-wave modeling and inversion. Figure 6 shows the offset, traveltime, and azimuth statistics from the ray tracing. From the statistical approach, it is evident that offsets longer than 20 km (suggested in Figure 5) are required for a succesful survey. To generate a large number of rays turning at the basement, at least 25 km of offset is required. It is worth noting that as the velocity in the basement is quite fast, the traveltime distribution cuts off sharply at approximately 20 s. Rays traveling through the basement spend less time in the basement than in the water compared to rays traveling through the water column and sedimentary sections.

It is not straightforward to generate a velocity model that is suitable for evaluation of success or failure of velocity model recovery. Common models include Marmousi and the SEG salt model. The model must contain the correct amount of uncertainty for the problem at hand. Hence, it is not productive to use, for

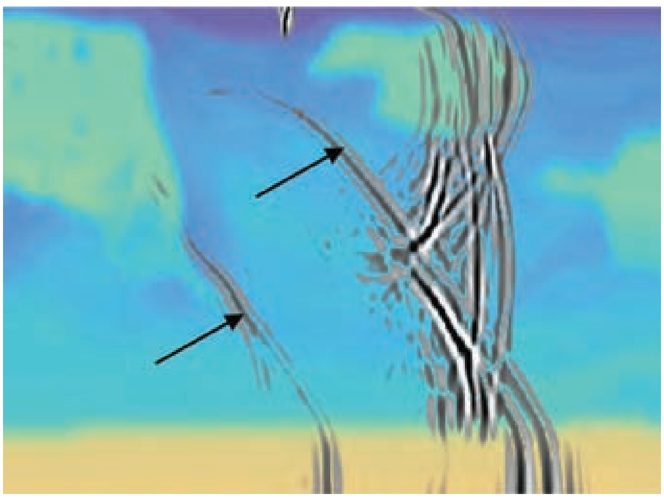

Figure 4. Finite-difference synthetic snapshot. Basement-refracted waves are indicated by arrows.

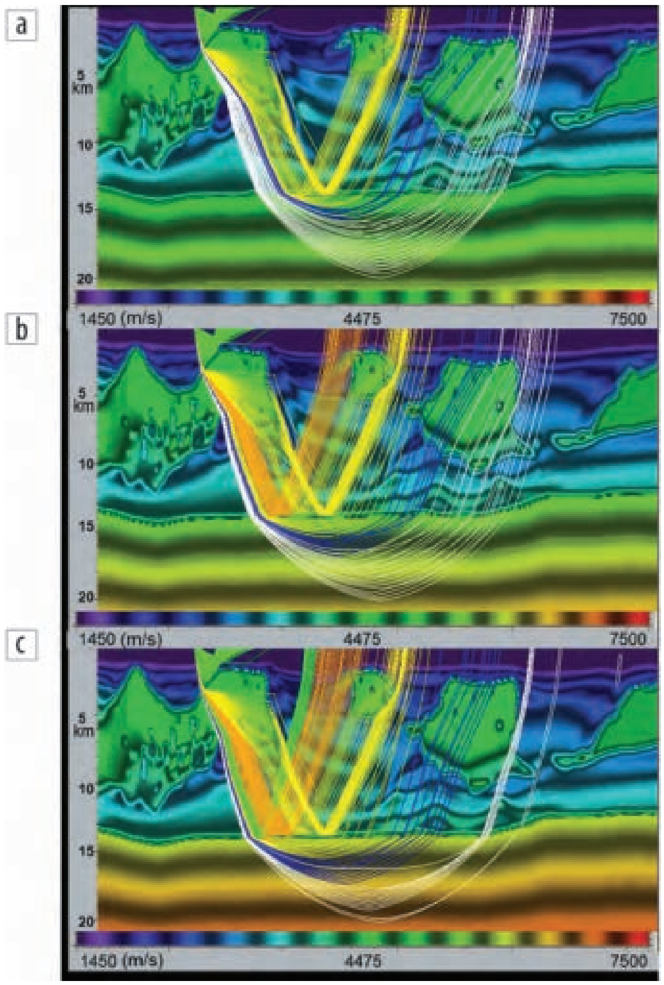


**Figure 5.** Ray tracing through the velocity model using different top basement velocity. Depths are in kilometers, and velocities are in meters per second. The figure shows turning rays for different top basement velocities for the same overburden velocity. The top basement velocity is 5.0 km/s in (a), 5.5 km/s in (b), and 6.0 km/s in (c). Rays belonging to different offset classes have different colors: 0–20 km are green, 20–30 km are orange, 30–40 km are yellow, 40–50 km are blue, and 50–60 km are white. It is clear that a slower top basement velocity results in longer offsets for events that turn at the top basement. The events that turn at the top basement are total reflections. Due to the presence of salt, there are gaps in offsets from fairly short offsets (which have turned up due to salt) to offsets of approximately 20 km. Hence, it appears that at least 20 km of offset is required to determine subsalt sedimentary velocity. A lower top basement velocity will result in more energy refracting through the basement, which would help determine basement velocity and location. In order to have a chance to determine basement depth and velocity, it appears that at least 30 km of offset is required.

instance, a pure gradient model. In this case, the velocity model is reasonably well known down to approximately 6–7 km depth. In addition, it is necessary to discard model perturbations that require seismic energy with frequencies that cannot be generated or propagated for the long distances that are required. This is clearly a limitation, but it is necessary to make an assumption that the velocity errors are such that it is possible to correct them. Otherwise, the survey design exercise is futile. A methodology that meets the requirements is to add a checkerboard perturbation to a background velocity model and try to recover the checkerboard perturbation. The checkerboard perturbation allows for the evaluation of resolution and extent of the recovered perturbation within the framework of the background velocity model. This further allows for the evaluation of the sensitivity to noise.

We started with what we believe is a realistic background velocity model and then added a checkerboard perturbation to the background model. The velocity models with the checkerboard perturbations were used to generate synthetic data, which were then used as input for velocity inversion algorithms and imaging. For a test to be considered successful, the checkerboard pattern had to be properly recovered (i.e., both accurate amplitudes and zero crossings).

We also tested more realistic scenarios in which we changed salt geometries as well as removed overpressure zones. To further understand what frequencies could be used for FWI, we added realistic field-measured noise levels to the synthetic data.

## Results

It is necessary to understand the actual offset required to receive basement-refracted events. Using a large model and simple ray tracing, it is possible to get an idea at which offset these arrivals start to appear. Figure 6 shows that the events start to appear at offsets of approximately 25 km. Subsequent to determining the required offsets, the node density, shot density, and required node patch size must be determined. To determine these factors, we used checkerboard perturbations added to the background velocity model. The checkerboard perturbations we employed had a size of 1 km. The 1 km size is sufficient as smaller checkerboard perturbations had limited effect on the imaging results beccause the subsalt imaging frequency is approximately 15–20 Hz.

By considering basement-refracted events, FWI successfully recovered checkerboard velocity perturbations as well as potentially more geologic velocity perturbation (Figures 7 and 8). For the noise-free data, the node spacing could be larger than 1.5 km while still recovering the velocity perturbations. The node and source spacing needed to recover the velocity model depended more on noise level than any other factor. Different densities of nodes and source locations could be thought of as generating different fold. Subsequently, use of higher densities of nodes and source locations results in more resilience to noise due to higher fold. The noise level is naturally dependent on specific geographic location and other factors. Thus, it is not possible to provide a recommended value for node and source spacing in general. It

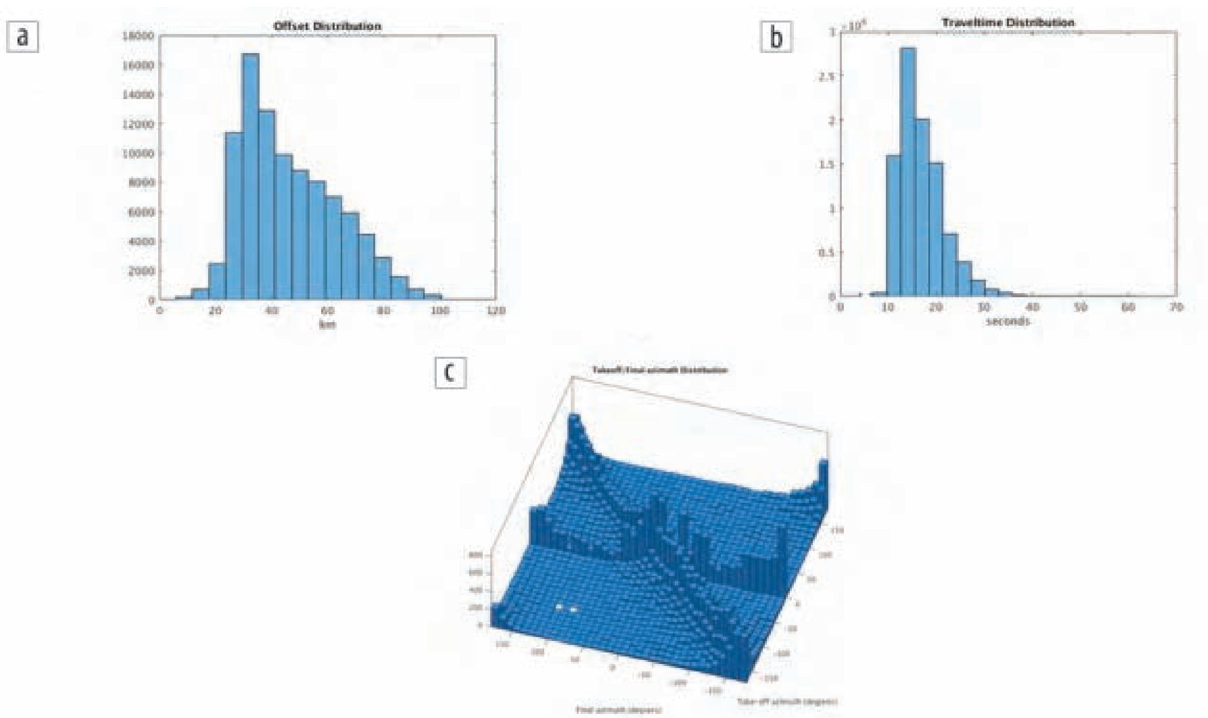


**Figure 6.** Statistics for a large set of rays that have reached the basement and returned to the surface, modeled through a representative velocity model. As can be seen in (a), very few rays return with an offset less than 25 km. The number of rays can also be seen to taper off for longer offsets. The taper with longer offsets is due to the model size, as the taper would be less with a larger model. The traveltimes shown in (b) are concentrated between 10 and 30 s, with a taper above 20 s. The longer offsets in (a) correspond to longer travel within the basement, but since the basement has considerably higher velocity than overlying water, salt, and sediments, the traveltimes for long offsets are not that much greater. The model is truly 3D, with widely varying salt bodies. There is still considerable correlation between takeoff angle and final azimuth for the rays, as can be seen in (c). The final azimuth is defined as the azimuth where the rays emerge at the surface compared to the takeoff location. Many rays with a completely vertical takeoff are diverted through the velocity and end up with a distribution of azimuths, which is indicated in (c) by the large count of rays along 0° takeoff angle.

is necessary to design surveys with the unique objective and constraints for the area of interest.

By evaluating the ability to recover a checkerboard pattern from noisy data, we found in this instance that a node spacing of 1.6 km should be sufficient, and the node patch size should be at least 25 km. For the source effort, 800 m line spacing would be sufficient, and the source effort should be performed with a 14 km halo around the node patch (Figure 9). In reality, it is advisable to use denser spacing for both nodes and sources in order to ensure good data quality in case of failed nodes and larger than expected noise.

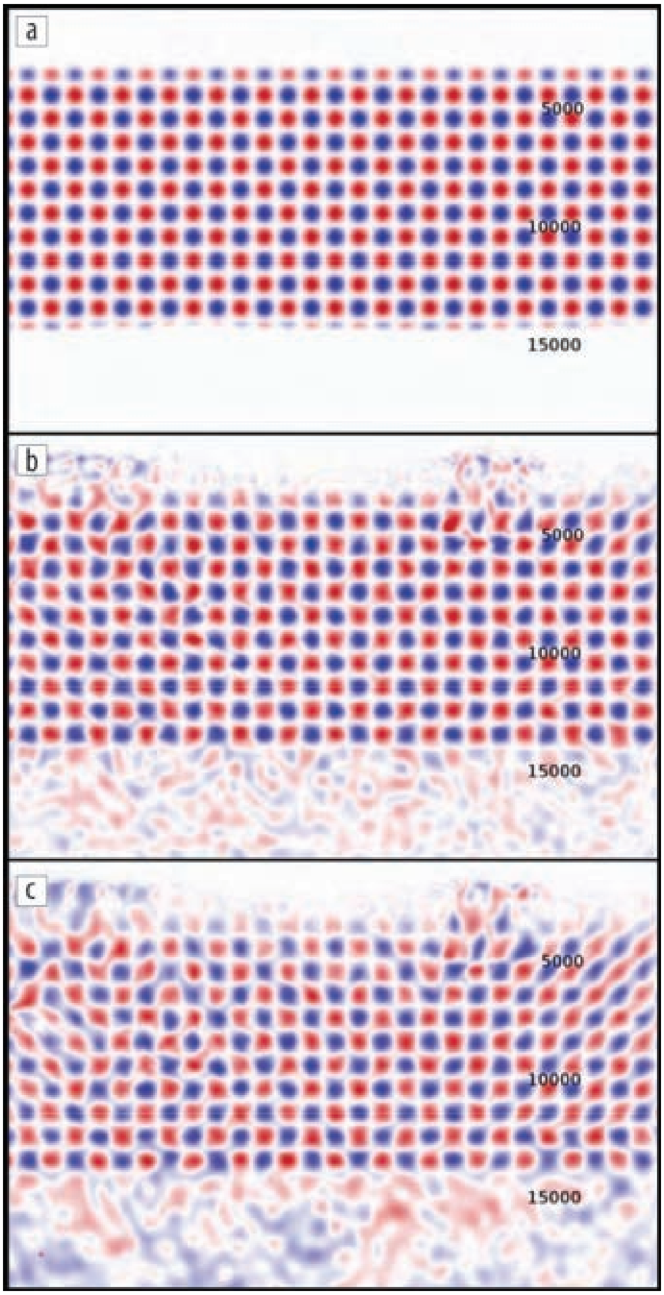


**Figure 7.** (a) True checkerboard velocity perturbation. (b) Recovered velocity perturbation. (c) Recovered velocity perturbation with noise in data. The signal-to-noise ratio of the input data is approximately 1. The velocity model can only be recovered in volumes with high ray density for the noisy data.

Figure 10 shows the imaging results for a model with perturbations that are geologically more realistic applied to the velocity model shown in Figure 8. Imaging using the incorrect velocity model clearly distorts the subsalt image. However, by using velocities obtained through FWI, it is possible to image the subsalt strata reasonably accurately. The FWI iterations were started using 2 Hz data and low noise. Hence, if the data were to contain more noise at low frequencies, it may not be possible to recover the velocity.

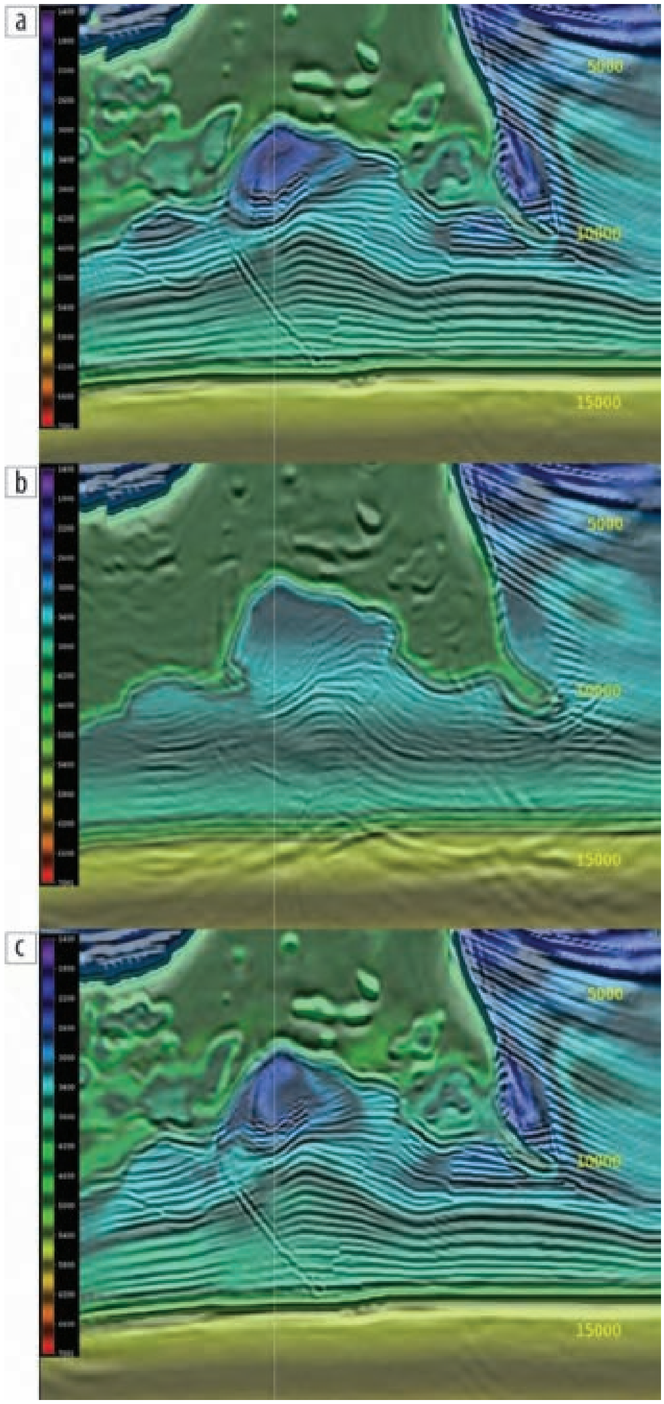


**Figure 8.** (a) The actual model with geologic-based perturbations. (b) The initial model. (c) The recovered model. The recovered model is accurate enough to enable imaging.

Another source of error would be node location accuracy coupled with water velocity accuracy. Nodes can be located accurately using direct arrivals, preferable from close to zero offset. For typical surveys, there are several of these arrivals to use that in turn enable determining water velocity simultaneously by requiring all measurements to be consistent. The node location error is typically less than 10 m, but we still evaluated the ability to recover the velocity model with node location errors uniformly distributed in the range of −50 to 50 m in all directions. The node location error had no detectable effect on the final recovered velocity model. This can be explained by the fact that it is uniformly random. A systematic location of the same scale would have a small but detectable effect. Hence, for subsalt velocity determination, the accuracy of current methodology to locate nodes is sufficient.

## Conclusions

Through forward modeling, we have shown that it is possible to retrieve subsalt velocities below thick and complicated salt canopies using basement-refracted events in conjunction with FWI. By combining these modeling efforts with modern OBN technology, we have successfully designed and optimized a seismic acquisition program whereby these velocity updates are expected to provide a step change in subsalt imaging for use in exploration. TLE


## Acknowledgments

The authors thank BHP for permission to publish the results.


## Data and materials availability

Data can be requested. Each request will be evaluated, but access to data may not be granted.


Corresponding author: joakim.blanch@bhp.com


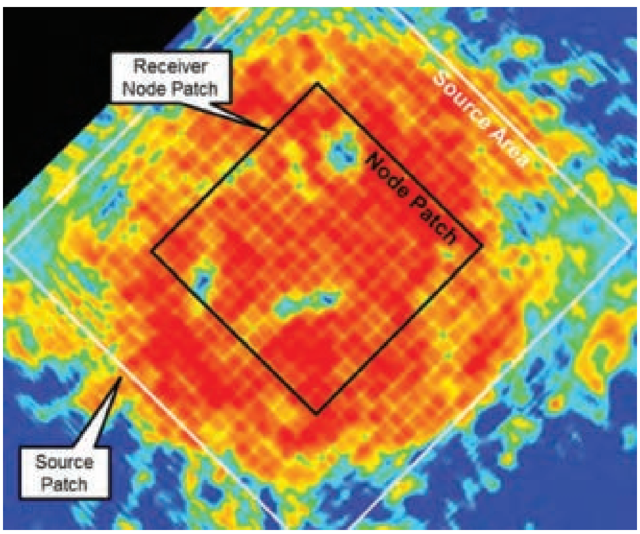


**Figure 9.** Evaluation of velocity perturbation recovery. The node patch is indicated by the black polygon, and the source area is indicated by the white polygon. Warmer colors indicate more successful velocity recovery. The fully red area, under the node patch, indicates that the source halo is sufficient to recover the velocity below the node patch. There are, however, areas that are not possible to recover, which correspond to illumination holes. The measure to evaluate the velocity is predictability: $(\sum_i A_i B_i)^2 / \sum_i (A_i)^2 \sum_i (B_i)^2$.


## References

Dines, K., and J. Lytle, 1979, Computerized geophysical tomography: Proceedings of the IEEE, **67**, no. 7, 1065–1073, https://doi.org/10.1109/PROC.1979.11390.

Eddy, D. R., H. J. A. Van Avendonk, G. L. Christeson, and I. O. Norton, 2018, Structure and origin of the rifted margin of the northern Gulf of Mexico: Geosphere, **14**, no. 4, 1804–1817, https://doi.org/10.1130/GES01662.1.

Huang, G., R. Nammour, W. W. Symes, and M. Dolliazal, 2019, Waveform inversion via source extension: 89th Annual International Meeting, SEG, Expanded Abstracts, https://doi.org/10.1190/segam2019-3216338.1.

Ivansson, S., 1985, A study of methods for tomographic velocity estimation in the presence of low-velocity zones: Geophysics, **50**, no. 6, 969–988, https://doi.org/10.1190/1.1441975.

Lailly, P., 1983, Seismic inverse problem as a sequence of before stack migrations: Presented at Conference on Inverse Scattering: Theory and Applications, SIAM.

Weatherby, B. B., 1940, The history and development of seismic prospecting: Geophysics, **5**, no. 3, 215–230, https://doi.org/10.1190/1.1441805.

Zelt, C. A., and R. B. Smith, 1992, Seismic traveltime inversion for 2-D crustal velocity structure: Geophysical Journal International, **108**, no. 1, 16–34, https://doi.org/10.1111/j.1365-246X.1992.tb00836.x.


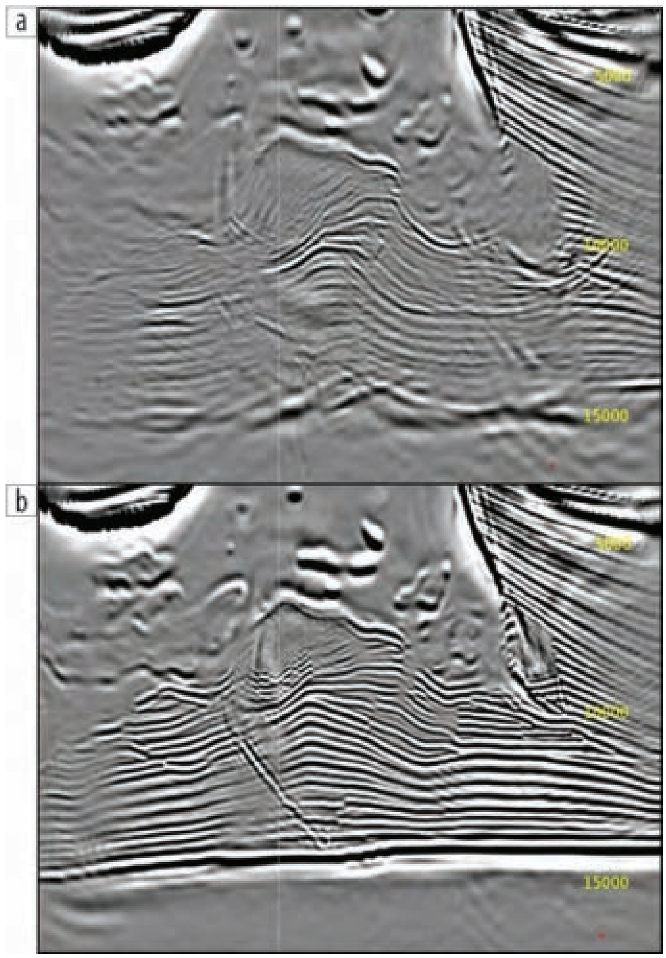


**Figure 10.** (a) The image using the initial velocity model (Figure 8b). (b) The image using the recovered velocity model (Figure 8c). The initial model is clearly not accurate enough to properly focus the imaging data, whereas using FWI to recover the subsalt velocity model enables focusing of the seismic data.

# The music of marine seismic: A marine vibrator system based on folded surfaces

Okwudili C. Orji[1], Mattias Oscarsson-Nagel[1], Walter Söllner[1], Endrias G. Asgedom[1], Øystein Trætten[1], and Rune Voldsbekk[1]

https://doi.org/10.1190/tle39040254.1

## Abstract

Marine vibrators have bespoke geophysical benefits that are yet to be harnessed because of robustness and efficiency issues. We have developed a new marine vibrator source technology that is efficient and stable. The source technology overcomes the historical problems of inefficiency and robustness by using folded surface technology and resonance frequency tuning. We show measured output examples that demonstrate that the folded surface concept combined with small displacements can provide the required output levels. Our source system consists of a low-frequency module covering 1–10 Hz and a high-frequency module covering 10–125 Hz. The source control system has shown high stability and precision and can handle harmonic distortion. With the aid of synthetic data examples, we demonstrate that seismic data acquired using marine vibrators in either intermittent or continuous mode can be processed. Finally, we demonstrate the environmental friendliness of the source in comparison to air gun-based sources.

## Introduction

Seismic data acquisition started on land where explosives were used as sources and quickly developed to using vibrators. The reasons for the quick transition are numerous and include health and safety of personnel and the environment as well as the desire for controlled seismic energy sources. In the marine environment, the operational and environmental consequences of using explosives is higher. In a bid to replace explosive sources in the marine environment, Conoco introduced vibrator sources in the 1960s (Proffitt, 1991). However, air gun sources proved to be more robust and reliable (Chelminski, 1961; Landrø and Amundsen, 2018), and they have since become the industry standard for marine seismic acquisition.

In recent times, the changing geopolitical landscape and technological advances have placed more stringent requirements on the received sound levels from marine seismic sources. The source must be efficient and environmentally friendly and must have sufficient low-frequency output as well as high output fidelity. These requirements are driving the industry to develop alternative source concepts. Marine vibrator sources are a leading candidate among the alternatives (Tenghamn, 2006; Dellinger et al., 2016; Feltham et al., 2018; Roy et al., 2018). In this paper, we discuss the development of one such system — the folded surface marine vibrator (FSMV). We discuss the theoretical background of generating acoustic energy using a marine vibrator and then present practical aspects of building a system that can generate the required energy levels. We then demonstrate specific acquisition scenarios and the processing steps that must be performed. Finally, we compare the output of the marine vibrator to other air gun-based acquisition methods and demonstrate the advantages of marine vibrators from an environmental perspective.

## Main benefits of marine vibrators

Marine vibrators possess a number of unique beneficial capabilities compared to air gun sources. Foremost among these is the nonimpulsive nature of signals generated by marine vibrators, which offers a high degree of control over the output. In contrast, traditional air guns can only generate impulsive signals. This capability provides a number of potential advantages for marine vibrators, including (1) better control of the amplitude and bandwidth of the emitted acoustic energy, which is important for addressing environmental concerns; (2) controlled signal output, which offers opportunities for new and flexible source geometries; and (3) the potential for ultra-low-frequency 1–6 Hz output to benefit full-waveform inversion (Rietsch, 1977; Dellinger et al., 2016; Brenders et al., 2018).

Moreover, marine vibrators are efficient, which in this context is measured by (1) the ratio between the generated acoustic energy and the energy expended and (2) the ratio between the useful energy (effective frequency band) that contributes to imaging the subsurface and the total acoustic energy generated. Conventional air guns require compressed air, which leads to a great deal of energy loss through heat dissipation, whereas electrical conversion to acoustic energy is much more efficient. In addition, much of the acoustic energy generated by air guns contributes energy at frequencies much higher than 250 Hz, which are not typically used for imaging the subsurface. By contrast, marine vibrators can generate tailor-made signatures with whatever frequency content, phase characteristics, and output level is desired. The ability of marine vibrators to generate coded signals can be exploited to mitigate residual shot noise (e.g., Laws et al., 2019) and seismic interference. Furthermore, air guns generate bubble oscillations that can be challenging to remove during processing, whereas marine vibrator signatures can operate with a simple linear sweep.

## Generating acoustic energy using marine vibrator elements

In this section, we introduce the theoretical background of generating acoustic energy from vibrating plates in a marine environment. Subsequently, we discuss the relation between the plate motion and the emitted signals and examine the consequences for generating low frequencies.

The basic element of a marine vibrator source is a pair of oscillating plates in water enclosing a volume of air under pressure.

[1]PGS, Oslo, Norway. E-mail: okwudili.orji@yahoo.com; mattias.oscarsson-nagel@pgs.com; walter.soellner@pgs.com; endrias.asgedom@pgs.com; oystein.traetten@pgs.com; rune.voldsbekk@pgs.com.

The pressure wavefield outside this volume may be derived from the motion of the vibrator plates caused by an increasing and decreasing enclosed volume (Figure 1).

Starting from the acoustic representation theorem, we consider the pressure wavefield inside the model enclosed by a spherical surface of radius $|r'|$ as the outer border and an idealized surface surrounding the oscillating plates as the inner border. This pressure wavefield is given by:

$$p(\boldsymbol{x}_R,t)=\int_{S_+ + S_-}\left(g(\boldsymbol{x},\boldsymbol{x}_R,t)^* \nabla p(\boldsymbol{x},t)-\nabla g(\boldsymbol{x},\boldsymbol{x}_R,t)^* p(\boldsymbol{x},t)\right)\cdot \mathbf{n}dS, \tag{1}$$

where $p$ is the pressure, and $g$ is the free space Green's function that describes propagation from the plate surface to a measuring location $\boldsymbol{x}_R$ (Morse and Feshbach, 1953).

In equation 1, we have assumed that the surface surrounding the total removed volume is given solely by the plate surfaces $S_+$ and $S_-$ (i.e., the distance between the plates is much smaller than the plate size). Choosing the direction of the normal vector to point from $S_-$ to $S_+$, the integral over the entire surface is:

$$p(\boldsymbol{x}_R,t)=\int_{S_+}\left(g(\boldsymbol{x},\boldsymbol{x}_R,t)^* \nabla p(\boldsymbol{x},t)-\nabla g(\boldsymbol{x},\boldsymbol{x}_R,t)^* p(\boldsymbol{x},t)\right)\cdot \mathbf{n}dS-\int_{S_-}\left(g(\boldsymbol{x},\boldsymbol{x}_R,t)^* \nabla p(\boldsymbol{x},t)-\nabla g(\boldsymbol{x},\boldsymbol{x}_R,t)^* p(\boldsymbol{x},t)\right)\cdot \mathbf{n}dS. \tag{2}$$

So far, no assumptions have been made about the Green's functions or wavefields on the plate surfaces. If we now assume continuity of the pressure fields across the surfaces, which is a valid assumption for thin synchronously oscillating plates separated by a small distance, and impose continuity of the Green's functions and their derivatives across the surfaces, the expression for the pressure reduces to

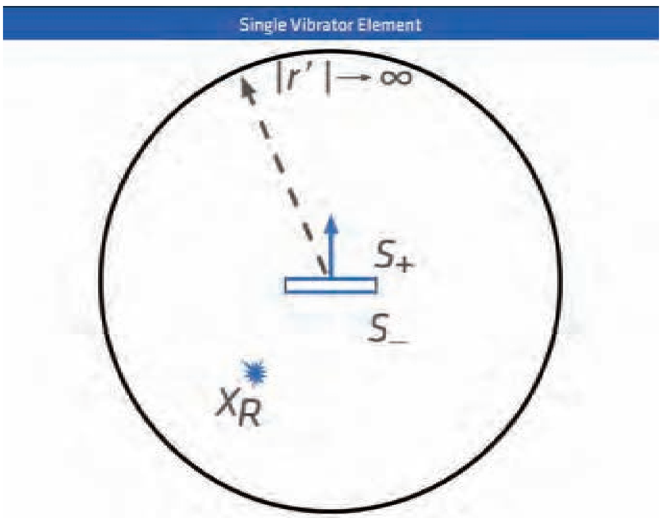


**Figure 1.** A sketch showing a single vibrator element consisting of a pair of plate surfaces enclosing a volume of air. The normal vector across the inner surface is indicated.

$$p(\boldsymbol{x}_R,t)=\int_{S_+} g(\boldsymbol{x},\boldsymbol{x}_R,t)^*[\nabla p(\boldsymbol{x},t)]\cdot \mathbf{n}dS\,. \tag{3}$$

The bracket [.] in equation 3 denotes the difference of values — in this case, of the gradients of the pressure wavefield across the plate surfaces. Substituting the pressure gradients in equation 3 by particle velocity $\mathbf{v}$ using $\rho i\omega \mathbf{v} = \nabla p$, we obtain, in the frequency domain,

$$p(\boldsymbol{x}_R,\omega)=i\omega\rho\int_{S_+} g(\boldsymbol{x},\boldsymbol{x}_R,\omega)[v_n(\boldsymbol{x},\omega)]dS\,, \tag{4}$$

where $i\omega v_n$ is the normal component of the plate acceleration, $\omega$ is the circular frequency, and $\rho$ is density.

Equation 4 is a general expression for calculating the emitted pressure wavefield everywhere inside the model generated by a pair of synchronously oscillating plates of arbitrary shape. Observe that the pressure wavefield is in phase with the acceleration of the plate oscillation. Consequently, to obtain a flat amplitude spectrum of the far-field pressure emitted by the source, the time function of the plate motion needs to be designed such that the acceleration becomes a flat function in the frequency domain. Generating a flat spectral plate displacement would instead result in an emitted far-field pressure wavefield with the low frequencies suppressed, following $(i\omega)^2$, corresponding to the second time derivative of the signal (Söllner and Orji, 2018). This relation between plate motion and output pressure illustrates the basic challenge of generating low frequencies.

To derive the normal force $F_n$ exerted on the plate surface by a time-harmonic acoustic wavefield, we derive the pressure wavefield at every point on the plate surface from equation 4 and integrate over the surface:

$$F_n \equiv \int_{S_+} p(\boldsymbol{x}_R,\omega)dS' = i\omega\rho\int_{S_+}\int_{S_+} g(\boldsymbol{x},\boldsymbol{x}_R,\omega)[v_n(\boldsymbol{x},\omega)]dSdS'. \tag{5}$$

For some simple shaped and rigid plates, equation 5 can be solved analytically for the total force (e.g., Blackstock, 2000):

$$F_n=\pi a^2 v_n \rho c\left[1-\frac{2J_1(2ka)}{2ka}+j\frac{2K_1(2ka)}{2ka}\right], \tag{6}$$

where, $a$ is the plate radius, $k$ is the wavenumber, and $J_1$ and $K_1$ are, respectively, the Bessel and Struve functions of order 1. From the definition of the acoustic impedance, as pressure divided by the particle velocity, the total impedance $Z$ at the plate surface is identified from equation 6 as:

$$Z=\rho c\left[1-\frac{2J_1(2ka)}{2ka}+j\frac{2K_1(2ka)}{2ka}\right]. \tag{7}$$

The real part of the complex radiation impedance is also known as radiation resistance, and the imaginary part is known as radiation reactance. For example, the radiation resistance is a measure of the radiation power, which may be obtained from the real part of the total force in equation 5 or 6 after multiplication by the plate velocity. The volume of water that must be displaced for a desired radiation power can be computed for different frequencies when the vibrator element is acoustically small (i.e., $ka$ << 1 and the real part of the bracket in equation 6 is expressed by $\frac{(ka)^2}{2}$, the first term of a series expansion). To output significantly more energy at the very low frequencies in comparison to air gun arrays, Figure 2a shows the enormous volume of water that must be displaced per cycle as frequency decreases in order to generate a constant output of 200 dB relative to 1 μPa at 1 m. About 707 liters of water must be displaced at 3 Hz. The required volume of water to be displaced is asymptotically approaching zero and approximately constant starting from about 10 Hz and above. The rapid increase for lower frequencies represents a fundamental physical challenge that applies to any acoustic source deployed in water. For marine vibrators, a consequence is that different engineering approaches must be used to generate frequencies above and below 10 Hz. For this reason, we have chosen to build two specific marine vibrator modules for different frequency ranges: a low-frequency module (LFM) covering 1–10 Hz and a high-frequency module (HFM) covering 10–125 Hz.

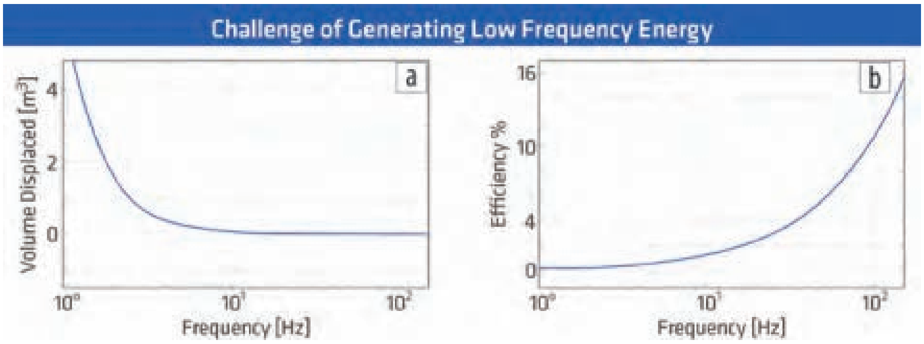


**Figure 2.** (a) The required volume of water to be displaced per cycle for a constant output of 200 dB relative to 1μ Pa @ 1 m. (b) A measure of the efficiency of generating acoustic output as a function of frequency.

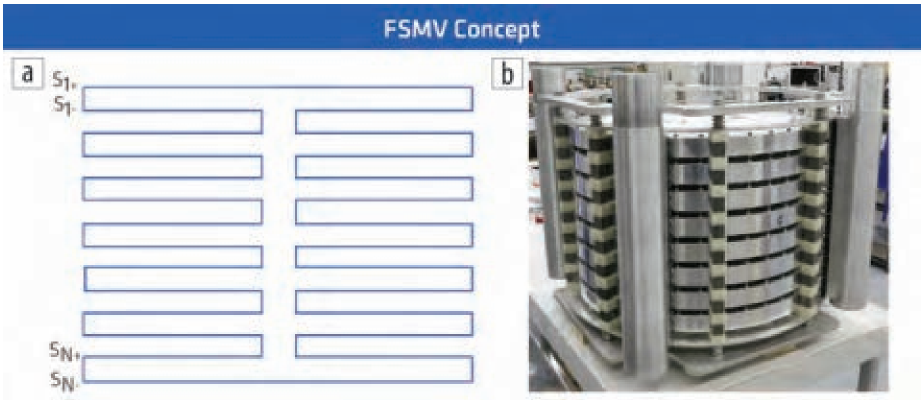


**Figure 3.** (a) Sketch of the FSMV concept and (b) a picture of the basic element of the prototype.

A measure of the efficiency of generating acoustic output can be calculated from equation 7 as the ratio of the radiation resistance to the absolute value of the sum of the radiation resistance and the radiation reactance. The efficiency for a unit diameter plate at 10 Hz is 1.2% (see Figure 2b). To overcome this inefficiency, the low-frequency source must be designed such that it resonates at an optimal frequency between 1 and 10 Hz.

## The FSMV development

***Vibrating membrane design.*** The opening and closing of an air gun shuttle can be repeated millions of times over a typical lifetime. As soon as the air shuttle opens and closes, the acoustic output is controlled by the surrounding water. Consequently, the sphere of influence is at the beginning of air release, before the passive reaction of water takes over. By contrast, all phases of water motion and sound generation for a marine vibrator are controlled by the membrane of the vibrator. Hence, selection of the size, shape, and material of the membrane are crucial. There are many aspects to consider for successful design of a robust and reliable marine vibrator source. The material of the membrane may deteriorate over time. It may crack or lose structural abilities, which can eventually lead to leakage and possible failure of the full system. These considerations are especially important when large displacements are used. In addition, marine vibrators are required to vibrate through millions of cycles in their lifetime. Hence, to achieve a robust and reliable design, especially for low-frequency output, small displacements and a large surface area must be used.

Simple calculations can show that source elements with several tens of square meters of effective surface area are unfeasible, especially from an operational point of view. Building a source array comprising many small vibrator elements could generate the desired output level but at very high cost due to the inefficiency of small independent source elements. In our source, the required large surface area is achieved by using a stack of vibrator elements enclosing one common internal volume, leading to an FSMV source. A simplified sketch and picture of the LFM source is shown in Figure 3. The advantage of this design is that the vibrating elements are exposed to lower vibration stresses, which implies a longer service life and lower acoustic distortion compared to alternative designs that use small surface area and large displacements. In addition, the small displacements can be accommodated by a bending metal interface, rather than rolling elastomeric or sliding seal interfaces required by large displacement vibrators.

***Resonance frequency tuning.*** To partially overcome the intrinsic inefficiency of generating low-frequency energy, the LFM unit

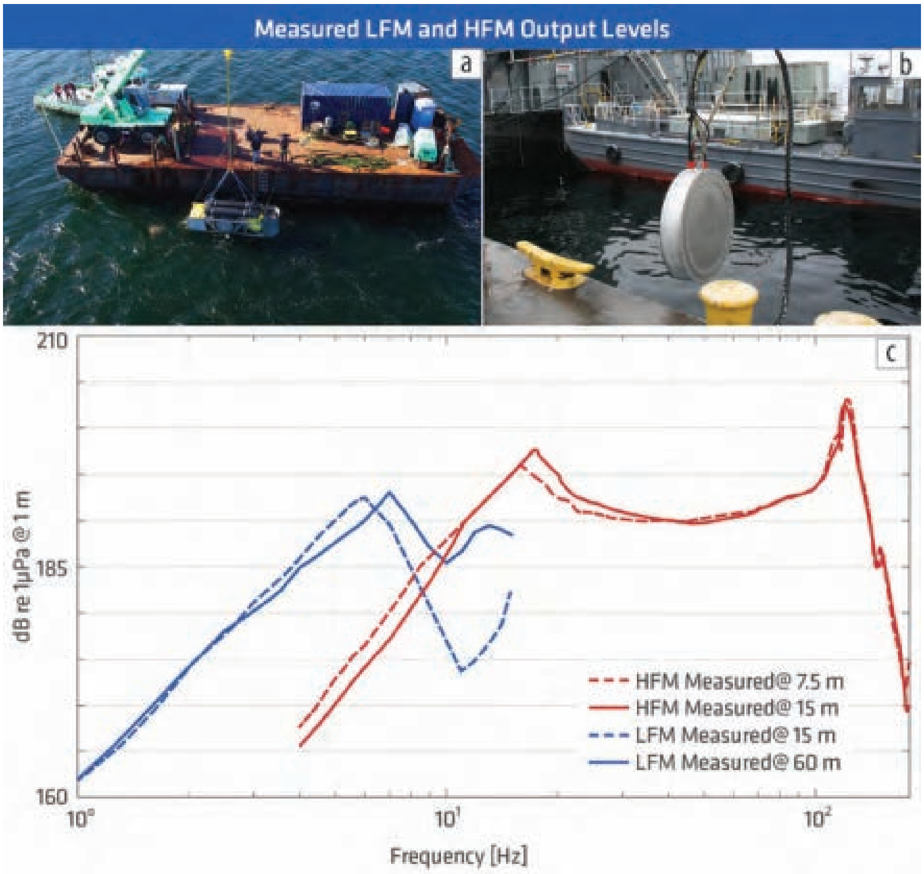


**Figure 4.** The (a) LFM and (b) HFM at the test site. (c) Measured output levels of the LFM and HFM at different depths.

single-module calibrations to multi-module full-band exercises. Figure 4c shows the measured output for single modules. The effective output from this prototype is above 190 dB from 4 to 125 Hz. The marine vibrator joint industry project (MV JIP) spectral density level specification is 190 dB re.1 μPa/Hz @ 1 m for 5–10 Hz and 200 dB re.1 μPa/Hz @ 1 m for 10–100 Hz (e.g., Feltham et al., 2018). However, acoustic output requirements depend on geologic and geophysical challenges and, for many field targets, might be below the MV JIP specifications.

The LFM unit was tested at 15 and 60 m depth, while the HFM unit was tested at 7.5 and 15 m depth. The change in resonance frequency is related to the increasing air stiffness with depth. The resonance frequency of the HFM unit is optimized for shallow depths, while that of the LFM unit is optimized for deep tow. Towing the LFM units shallower is beneficial because the resonance moves to lower frequencies, and it is also convenient since it is operationally more challenging to tow deeper. However, this benefit must be traded off against the geophysical advantages of a deep towed source to exploit the effect of constructive interference with the source ghost at low frequencies. Unity chirp rate is required to achieve the output levels shown in Figure 4c (for linear sweeps). The implication is that the sweep length required will affect source point sampling at normal acquisition speeds, which will be discussed in a later section. Figures 5a and 5b show plots of the computed 5 s output for two LFM and four HFM units. The output of the system for 5 s is above 180 dB for the frequencies covering 1–125 Hz. The computed signatures are based on predicted source levels.

has been designed to exploit resonance at an optimal frequency between 1 and 10 Hz. At resonance, the source impedance is given by the radiation resistance only (Kinsler et al., 2000). As a rule of thumb, the resonance frequency can be estimated using the mass of the vibrating plate, $m_b$, the mass of the water vibrating with the plate surface, $m_r$, the plate stiffness, $k_b$, and the stiffness of the air trapped between the plates, $k_a$:

$$f = 1/2\pi\sqrt{\frac{(k_b + k_a)}{(m_b + m_r)}}\,. \tag{8}$$

By varying the mass and the stiffness parameters, the resonance frequency can be tuned as desired. One way to achieve this is to stack (or fold) the vibrating plates. By stacking the plates, the resonance frequency decreases. The elastic properties and distances between the vibrator elements are designed based on finite element modeling to produce a controlled resonance of the source in order to increase the output efficiency. The optimal resonance frequency of the LFM was determined to be about 5–7 Hz and was chosen for the deepest depth of 75 m. The resonance frequency and tow depth were chosen considering operational feasibility and safety.

***FSMV output characteristics.*** Prototype modules have undergone multiple sea trials at different operating depths and locations and at various power levels (see Figure 4). Recent efforts have focused on proving operational reliability and scaling up from

***Timing and phase control.*** A central benefit of marine vibrators is that they are controllable. Hence, the transducers and the control system must be stable and show high fidelity. To achieve this, the combined transfer function of the transducers and the control system must be repeatable such that it can be accounted for during signal generation. Figure 6 shows measured output from the HFM unit. To demonstrate the timing accuracy and stability of the system, 10 continuous linear sweeps with randomized lengths ranging from 4 to 6 s covering 10–80 Hz were tested. The source was operated in both continuous (Figure 6a) and intermittent (Figure 6b) modes. In continuous mode, the continuous sweep was repeated several times by allowing different time intervals between each sequence. In intermittent mode, a fixed time interval (20 s) was allowed between each sweep. The red dots indicate the required (reference) trigger times of the source. The trigger time error is computed as the difference between the commanded trigger times (reference) and the measured trigger times. The computed error is far less than 1 ms (Figure 6c).

A further demonstration of source control is to verify the ability of the source to generate pseudorandom signals. In general, pseudorandom signals are more difficult to generate compared to linear sweeps due to the near random phase of the signals. Figure 7a shows plots of two pseudorandom signals emitted at different times. Figure 7b shows a 1 s zoom of Figure 7a, and Figure 7c shows a plot of the first shot overlaid with the scaled control signal. The two signals are in phase, which demonstrates the controllability and fidelity of the system.

***Harmonic distortion.*** When marine vibrators are operated with large displacements, they generate high harmonic distortion levels. The level of harmonic distortion is generally related to the total stiffness of the source. When the air inside the source is very stiff and large displacements are used, nonlinear performance occurs leading to high harmonic distortion. In addition, the distortion levels increase when the source is operated near or at its resonance frequency. Operating the source above the resonance frequency generates low levels of harmonic distortion. Figure 8a shows a spectrogram of the output in Figure 6a. There is little or no harmonic distortion, which demonstrates that the HFM unit is inherently a low-distortion system. However, the output of the LFM unit (Figures 8b and 8c) shows some harmonic distortion as expected. Increasing the depth of operation of the unit increases the air stiffness, which leads to more harmonic distortion (compare Figures 8b and 8c). To counteract this phenomenon, the source system has active distortion-reduction algorithms such as iterative learning control (ILC). Figure 8d shows a spectrogram of an LFM output with ILC applied for harmonic attenuation and clearly exhibits reduced levels of harmonic distortion.

***Towing and handling.*** The FSMV is modular and consists of a few modules combined in tow bodies (sleds). The sleds can either be connected to a surface float as in conventional source systems

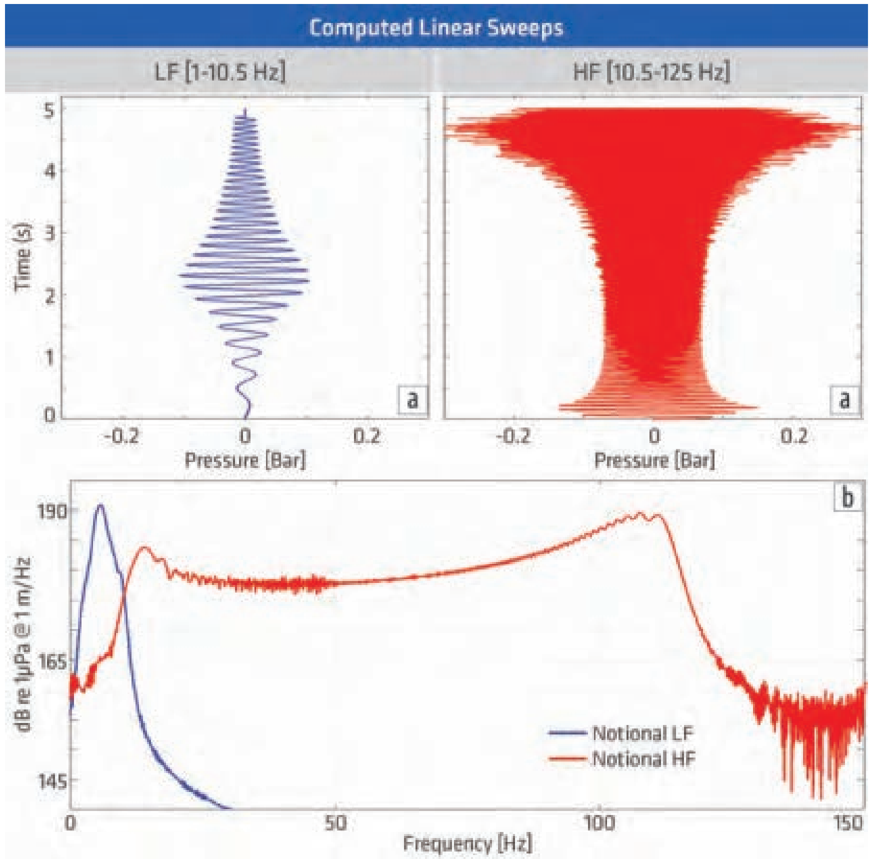


**Figure 5.** (a) Time plots and (b) frequency spectra. Computed 5 s linear sweeps based on the predicted output levels for two LFM units covering 1–10 Hz (blue) and four HFM units covering 10–125 Hz (red).

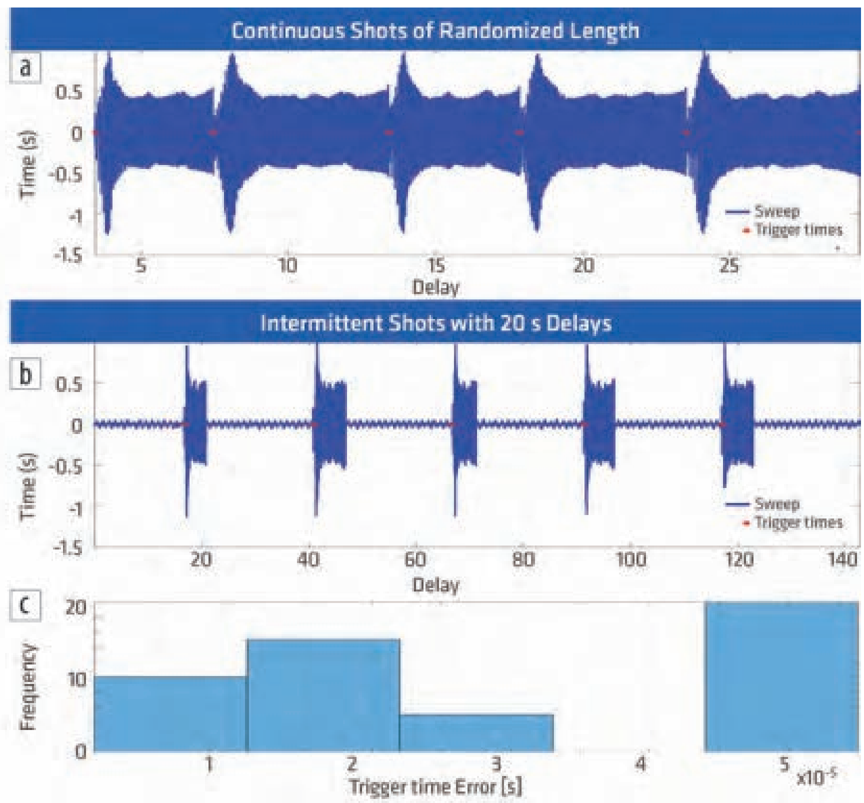


**Figure 6.** Measured HFM data for randomized sweeps in (a) continuous emission and (b) intermittent mode. (c) Histogram of the computed triggering time errors.

or towed directly from the body with built-in individual depth control. The system is designed to utilize existing vessel equipment as much as possible to facilitate a cost-efficient technology introduction. A key design focus of the overall system is seamless integration into the existing seismic vessel back-deck configuration envelope. These requirements place constraints on the overall size, weight, and output levels of the system. The deployment and recovery capability, using existing methods, must be balanced with optimal vessel back-deck space utilization of the current marine seismic source system. These have to function in a safe and reliable manner, including in marginal sea conditions. The number of LFM and HFM units that are configured into sleds, and the required number of sleds, will fit within the current marine seismic vessel back deck. Hence, the commercial system will require minimal adjustment of the existing marine seismic vessel back-deck layout and can be seamlessly integrated into existing seismic vessel platforms.

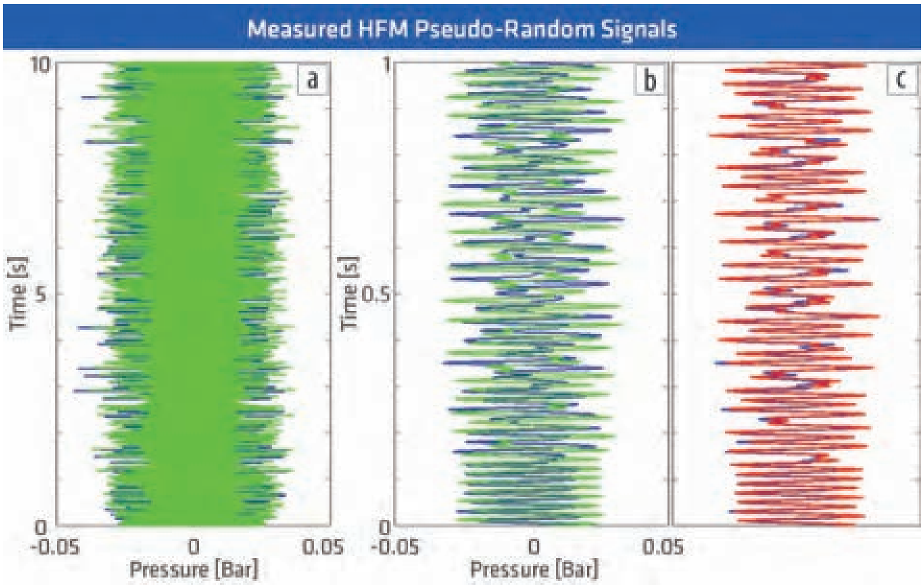


**Figure 7.** (a) Measured HFM pseudorandom signals repeated two times, (b) a 1 s zoom of the plots in (a), and (c) the first measured signal plotted with the scaled control signal.

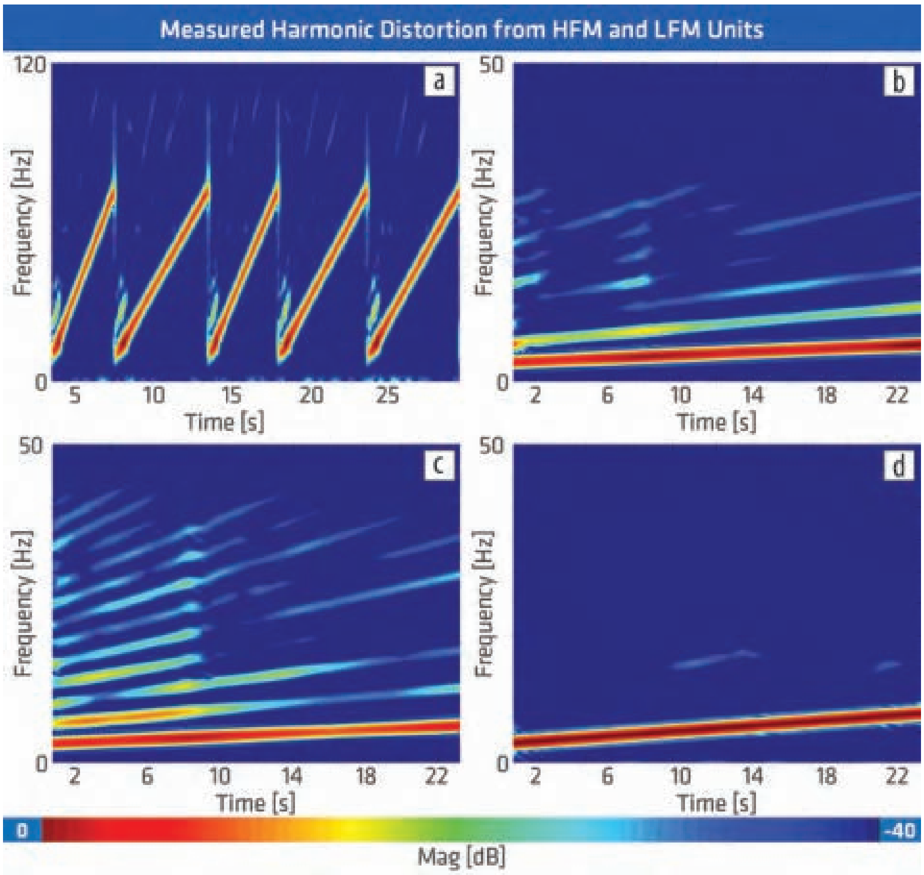


**Figure 8.** Spectrograms measured for different marine vibrator elements. (a) HFM continuous signal (shown in the left plot of Figure 6a). (b) LFM deployed at 15 m depth for a 24 s linear sweep covering 3–6 Hz. (c) LFM deployed at 60 m depth for the same sweep. (d) LFM with active distortion reduction applied for a 20 s, 3–8 Hz sweep when the source is deployed at 15 m depth.

Source separation is typically limited to 50–200 m for conventional seismic acquisition using air guns. This narrow towing configuration is limited by the specifications of the umbilical cable. This has implications for acquisition efficiency since increased source separation opens the possibility for increased sail line separation, meaning a given survey area could be covered in a shorter time. The FSMV is an electrical system and, although pressure compensation is required, the specification of the umbilical cable for the full system will allow for wider towing configurations subject to other operational limits. In the future, the sleds could be self-contained unmanned vessels with integrated propulsion and power supply systems. This concept would eliminate the limitation on tow width.

## Continuous versus intermittent acquisition: Synthetic examples

The ability to control marine vibrator output offers versatility in terms of survey design. Traditional intermittent emission and listening for a given time interval is suitable for air gun arrays since the air compressors need time to recharge. Some marine vibrators must be operated at 50% duty cycle due to limitations inherent in their design (e.g., overheating due to large displacements), and, for these designs, acquisition must also be performed in an intermittent manner similar to air gun acquisition. The FSMV does not suffer this limitation, which means the vibrator can be operated continuously if so desired. In this section, the implications of intermittent and continuous acquisition will be explored.

A synthetic data modeling and processing exercise was performed to evaluate different acquisition and processing solutions. Data examples were modeled using finite difference modeling for the Sigsbee 2B model. The source signatures used in modeling were prepared using the predicted output from Figure 5. For intermittent acquisition, the length of the signature was 5 s with 5 s of listening time. The source and the receivers were modeled as moving with a speed of 2.5 m/s at depths of 10 and 20 m, respectively, giving a shot point interval of 25 m. The temporal sampling interval was 4 ms with 12.5 m receiver spacing. The source wavefield containing the source motion is shown in Figure 9a.

To remove the effects of the source signature, trace-by-trace correlation with the far-field signature (pilot sweep) was performed. Figures 9b and 9c show the total pressure shot record before and after this correlation. Observe that, after the correlation, the resulting data in Figure 9c resemble seismic data from an impulsive source. Consequently, further data processing flows that are routinely applied to air gun data can be used from this point onward.

The primary difference between data acquired with air guns compared to that from a marine vibrator is the effect of source motion. An air gun emits energy at a single point in space, which can be assumed to be stationary. For a marine vibrator, the point at which energy is emitted is constantly changing as the source moves through the water. The processing demonstrated in Figure 9 neglects the effect of this source motion yet still yields a reasonable

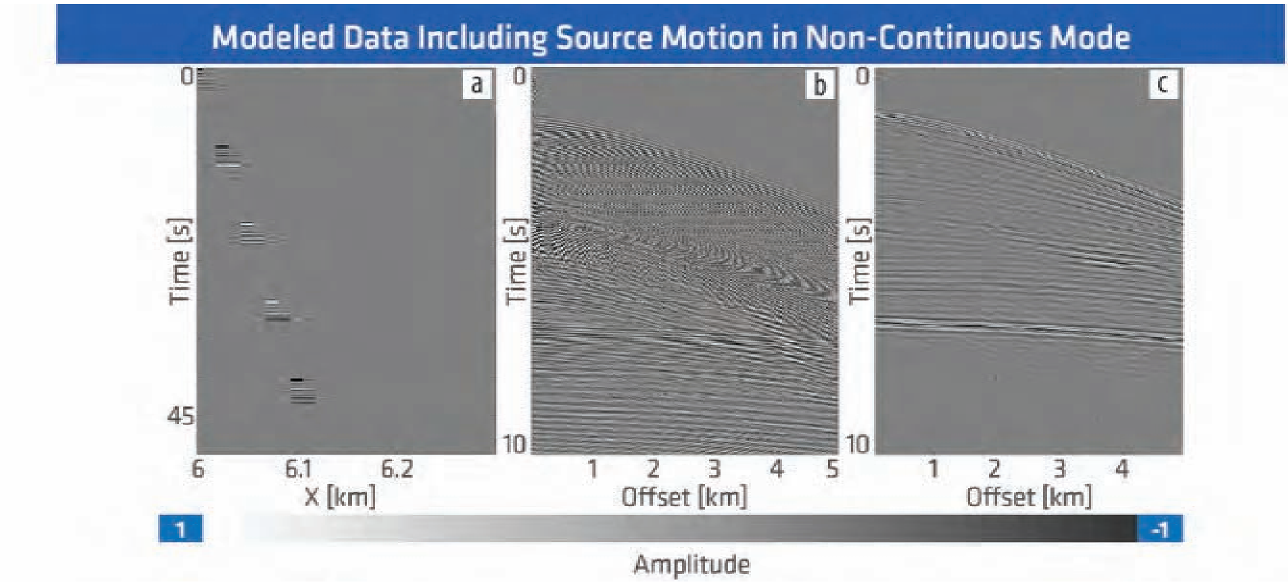


**Figure 9.** (a) The modeled source wavefield including the source motion for a FSMV source system used in intermittent mode. (b) The modeled total pressure wavefield obtained from this source for a single sweep. (c) The total pressure wavefield after crosscorrelation with the pilot sweep.

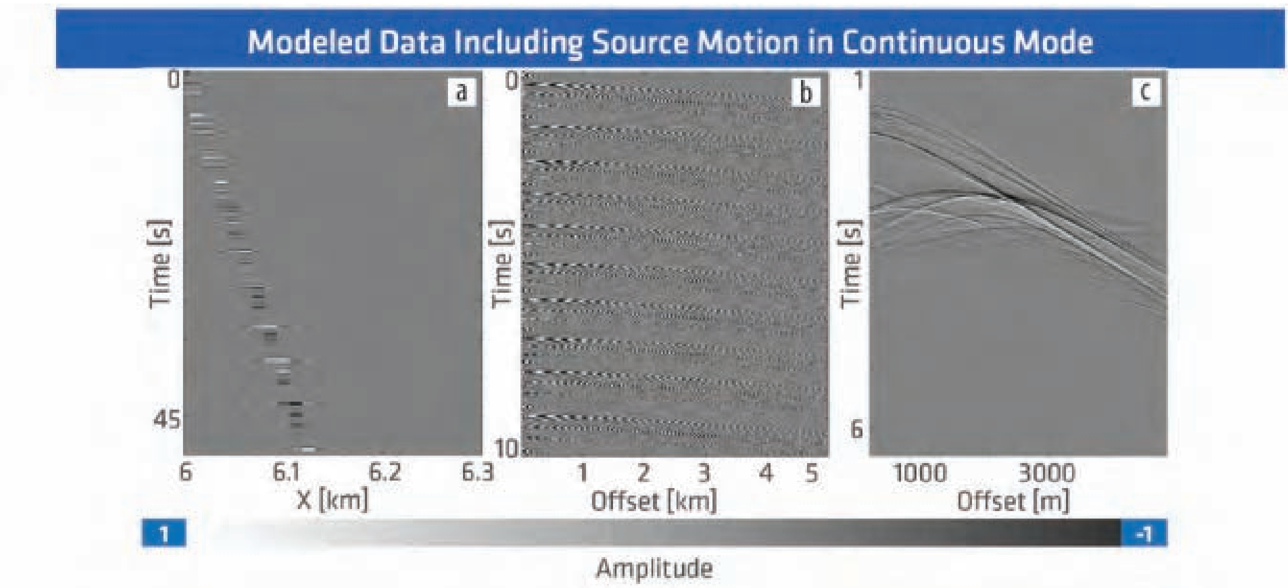


**Figure 10.** (a) The modeled source wavefield including the source motion for a FSMV system used in continuous mode. (b) The modeled continuous total pressure wavefield. (c) The upgoing pressure wavefield after source wavefield deconvolution.

result. Methods for correcting for source motion have been demonstrated (e.g., Dragoset, 1988; Hampson and Jakubowicz, 1995; Asgedom et al., 2019). This source motion correction must be applied in the common-receiver domain. Consequently, when marine vibrators are used to acquire data in an intermittent manner, spatial aliasing limits the possibility of applying a proper motion source correction. For the shot point interval of 25 m used in Figure 9, spatially unaliased signal can only be obtained up to 30 Hz. If the shot point interval were reduced to 12.5 m to partially mitigate this aliasing problem, the time interval between two shots would be 5 s, which is the length of the actual sweep resulting in blending of the data from successive sweeps.

The most efficient method for exploiting the full benefits of marine vibrators is to use them in continuous emission mode. Such acquisition will remove the spatial sampling limitations that arise from intermittent acquisition. The FSMV source system can emit signals that approximate the characteristics of band-limited white noise, which is the theoretically ideal continuous signal. This can be achieved by operating the source at 100% duty cycle (e.g., Figure 6a). A processing methodology that utilizes continuous wavefields on both the source and the receiver sides has been developed and demonstrated using an air gun source (Hegna et al., 2018). The same principles can be applied to continuous marine vibrator data.

Using the same data acquisition configuration as in Figure 9, data were modeled using a continuous wavefield (see Figure 10a). The randomized sweep length is from 4 to 6 s. The first 50 s of the continuous total pressure data is shown in Figure 10b. The effect of the continuous wavefield can be deconvolved following Hegna et al. (2019) (Figure 10c). The deconvolution removes all source motion effects and performs source deghosting and designature of the data. As in the case of intermittent acquisition, the output resembles impulsive data and can be processed similarly.

## Environmentally friendly seismic sources

The risk of potential harm and disturbance of marine life due to actuation of marine seismic sources is routinely assessed before carrying out any marine seismic survey. The two commonly used environmental metrics to assess the received sound levels are the peak sound pressure level (pSPL) and the sound exposure level (SEL). The pSPL is related to the maximum output of the source in the time domain, while the SEL is related to the total energy output of the source. The marine seismic industry is moving toward data acquisition methods that are more environmentally friendly using various techniques, including lower source output levels (e.g., Laws et al., 2017; Klüver et al., 2018), improved data acquisition

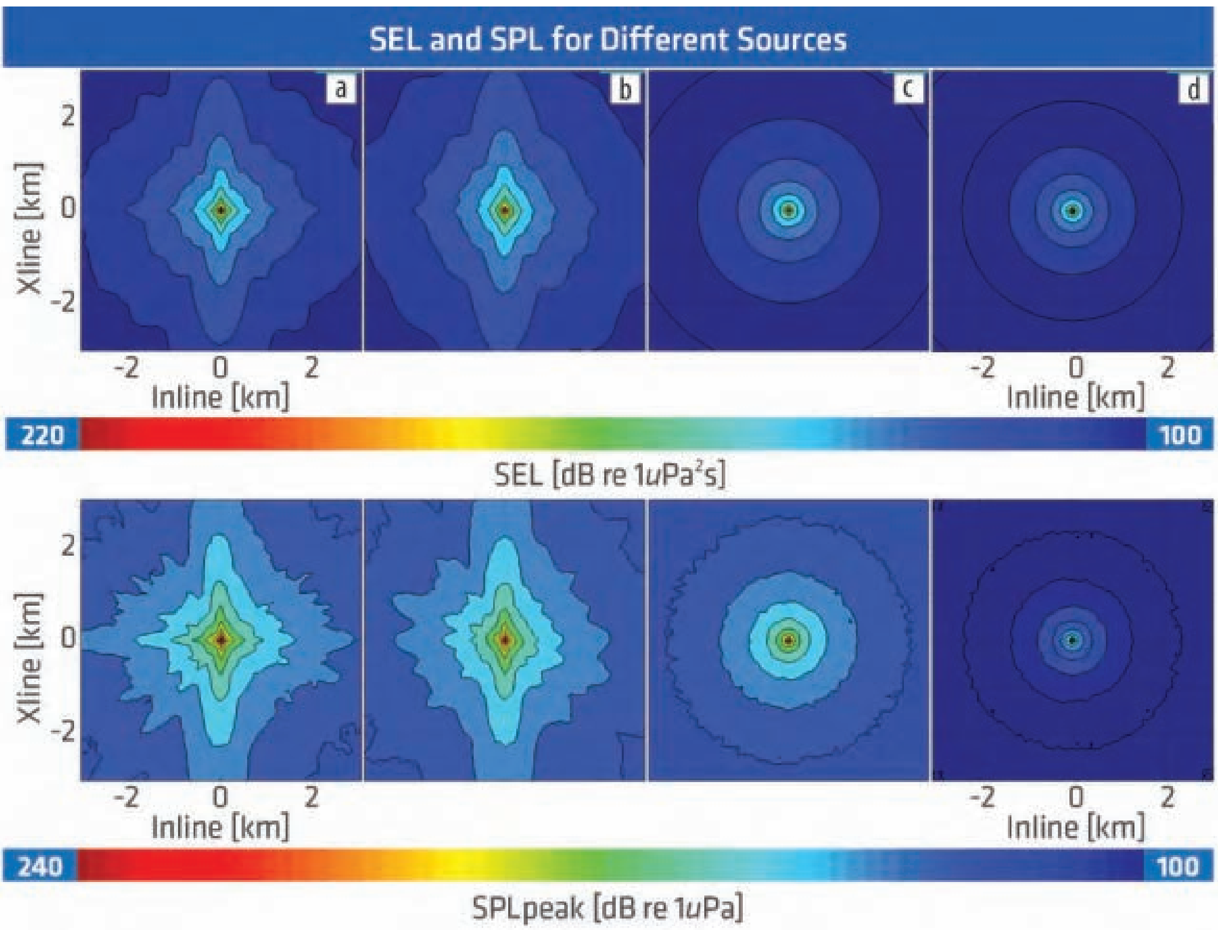


**Figure 11.** The emitted SEL (top panels) and pSPL (lower panels) for different sources. (a) A 4130 $in^3$ air gun array with 10 s shot interval. (b) A 3280 $in^3$ air gun array with 7.5 s shot interval. (c) Single-string continuous shooting air gun source. (d) PGS MV prototype used in continuous emission and recording mode. The recording time window considered is 10.5 s.

techniques (Abma, 2018; Hegna et al., 2018), new source technology (e.g., Laws et al., 2017; Orji et al., 2019), or a combination of the three (Hegna et al., 2019). The challenge is to achieve these goals without compromising data quality.

The output of different seismic sources used in different acquisition modes was modeled to assess their environmental impact. In the comparison, all the air gun sources were modeled at 6 m depth, while the marine vibrators were modeled at 10 m depth. The frequency band between 0 Hz and 1 kHz was considered for all sources; however, note that the marine vibrator source only delivers seismic energy between 1 and 100 Hz. The recording time window length considered is 10.5 s, and only the direct arrival and its ghost contributions were modeled from the sources to their corresponding receivers located 1 m below the source.

**Table 1.** Summary of the environmental metrics at 0.5 km exclusion zone in the inline direction.

| Inline | 4130 in$^3$ | 3280 in$^3$ | Air gun continuous | FSMV continuous |
|---|---|---|---|---|
| SEL[dBre1μPa2s] full band | 145.02 | 143.96 | 133.74 | 127.68 |
| SEL[dBre1μPa2s] 0–100 Hz | 140.6 | 140.38 | 126.97 | 127.68 |
| pSPL[dBre1μPa] full band | 170.46 | 166.57 | 158.23 | 126.39 |
| pSPL[dBre1μPa] 0–100 Hz | 162.71 | 158.61 | 142.66 | 126.39 |

Figure 11 shows the SEL (top panels) and pSPL (bottom panels) as a function of lateral displacement from the source for four different acquisition scenarios. Figure 11a shows the computed SEL and pSPL for a 4130 in$^3$ air gun array, representative of dual-source acquisition fired every 10 s. Observe the directivity pattern related to the spatial configuration of the array, which comprises three subarrays. Figure 11b shows the results for a 3280 in$^3$ air gun source, representative of a two-subarray source used for triple-source acquisition fired every 7.5 s. The 3280 in$^3$ array shows a reduction of approximately 2.5 dB in SEL and approximately 4.5 dB in pSPL at vertical incidence relative to the 4130 in$^3$ array. Despite the reduction in volume, the reduction in sound output is modest due to the reduced firing interval. Figure 11c shows the SEL and pSPL for continuous shooting for one string with 40, 90, and 150 in$^3$ air guns fired randomly in time with an average interval of 292 ms (Hegna et al., 2018). The SEL and pSPL results in a reduction of approximately 10 and 14 dB relative to the 4130 in$^3$ air gun array at the vertical incidence direction, respectively.

Finally, the modeled output from the FSMV prototype used in continuous shooting mode is shown in Figure 11d. Observe the omnidirectional behavior of both air gun and marine vibrator sources used in continuous shooting mode. Table 1 shows the summary of the output levels of the sources at 0.5 km exclusion zones. In terms of pSPL, which has been associated with physiological damage to marine mammals (NOAA, 2016), the FSMV has by far the lowest output. If the calculations are limited to the bandwidth used for seismic imaging (0–100 Hz), Table 1 shows that the SEL of the FSMV is comparable to the output level of the air gun sources, which indicates that a similar image quality could be expected.

## Conclusions

Marine vibrators have many promising geophysical benefits, but they are yet to demonstrate robustness and reliability. Using knowledge of the physical laws that describe acoustic energy generation in water, we developed two marine vibrator systems that operate at the low- and high-frequency ends of the seismic frequency bands. The marine vibrator design uses large surface area and small displacements to achieve robustness and reliability. The source exploits resonance tuning to improve efficiency, especially at low frequencies where the efficiency challenges are greatest for all marine seismic sources. We have demonstrated that the full-source system is stable and can employ active harmonic distortion if required. Using synthetic data examples, we have shown the implications for processing marine vibrator data. Finally, we have demonstrated the environmental friendliness of the source compared to air gun sources. TLE

## Acknowledgments

We are grateful to PGS for permission to publish this work. Special thanks to Luka Baranic, Anthony Day, and all of our PGS colleagues for support and many useful discussions. We thank the team at GeoSpectrum Technologies Inc., Canada.

## Data and materials availability

Data associated with this research are confidential and cannot be released.

Corresponding author: okwudili.orji@yahoo.com

## References

Abma, R., 2018, Shot coding design for popcorn shooting: 88th Annual International Meeting, SEG, Expanded Abstracts, 56–60, https://doi.org/10.1190/segam2018-2995736.1.

Asgedom, E. G., O. C. Orji, and W. Söllner, 2019, Marine vibrator sources: Motion correction, deghosting and designature: 81st Conference and Exhibition, EAGE, Extended Abstracts, https://doi.org/10.3997/2214-4609.201901411.

Blackstock, D. T., 2000, Fundamentals of physical acoustics: John Wiley & Sons Inc.

Brenders, A., J. Dellinger, C. Kanu, Q. Li, and S. Michell, 2018, The Wolfspar field trial: Results from a low-frequency seismic survey designed for FWI: 88th Annual International Meeting, SEG, Expanded Abstracts, 1083–1087, https://doi.org/10.1190/segam2018-2996201.1.

Chelminski, S., 1961, Acoustic wave impulse generator repeater: U.S. Patent 3249177A.

Dellinger, J., A. Ross, D. Meaux, A. Brenders, G. Gesoff, J. Etgen, J. Naranjo, G. Openshaw, and M. Harper, 2016, Wolfspar, an "FWI-friendly" ultralow-frequency marine seismic source: 86th Annual International Meeting, SEG, Expanded Abstracts, 4891–4895, https://doi.org/10.1190/segam2016-13762702.1.

Dragoset, W. H., 1988, Marine vibrators and the Doppler effect: Geophysics, **53**, no. 11, 1388–1398, https://doi.org/10.1190/1.1442418.

Feltham, A., M. Jenkerson, N. Henderson, M. Girard, V. Nechayuk, and A. Cozzens, 2018, Geophysical testing of a marine vibrator integrated projector node (MV-IPN) at Seneca Lake: 80th Conference and Exhibition, EAGE, Extended Abstracts, https://doi.org/10.3997/2214-4609.201800996.

Hampson, G., and H. Jakubowicz, 1995, The effects of source and receiver motion on seismic data: Geophysical Prospecting, **43**, no. 2, 221–244, https://doi.org/10.1111/j.1365-2478.1995.tb00133.x.

Hegna, S., T. Klüver, and J. Lima, 2018, Making the transition from discrete shot records to continuous wavefields — Methodology: 80th Conference and Exhibition, EAGE, Extended Abstracts, https://doi.org/10.3997/2214-4609.201800998.

Hegna, S., T. Klüver, O. Orji, and J. Lima, 2019, The continuous wavefields method: Using electro-mechanical sources: 89th Annual International Meeting, SEG, Expanded Abstracts, 4019–4023, https://doi.org/10.1190/segam2019-3209867.1.

Kinsler, L. E., A. R. Frey, A. B. Coppens, and J. V. Sanders, 2000, Fundamentals of acoustics, 4th edition: John Wiley & Sons Inc.

Klüver, T., S. Hegna, and J. Lima, 2018, Making the transition from discrete shot records to continuous wavefields — Real data application: 80th Conference and Exhibition, EAGE, Extended Abstracts, https://doi.org/10.3997/2214-4609.201800999.

Laws, R., D. Gerez, C. Ocampo, M. Supawala, and L. Na, 2017, A comparison of image quality and potential environmental impact for two types of air gun: 87th Annual International Meeting, SEG, Expanded Abstracts, 101–105, https://doi.org/10.1190/segam2017-17674813.1.

Laws, R. M., D. Halliday, J.-F. Hopperstad, D. Gerez, A. Supawala, A. Özbek, T. Murray, and E. Kragh, 2019, Marine vibrators: The new phase of seismic exploration: Geophysical Prospecting, **67**, no. 6, 1443–1471, https://doi.org/10.1111/1365-2478.12708.

Landrø, M., and L. Amundsen, 2018, Marine vibrators, part I: Geo ExPro, **15**, no. 3, 52–53.

Morse, P. M., and H. Feshbach, 1953, Methods of theoretical physics: McGraw-Hill Book Comp.

NOAA, 2016, Technical guidance for assessing the effects of anthropogenic sound on marine mammal hearing — Underwater acoustic thresholds for onset of permanent and temporary threshold shifts: NOAA Technical Memorandum NMFS-OPR-55.

Orji, O., M. D. C. Oscarsson-Nagel, W. Söllner, Ø. Trætten, B. Armstrong, D. Nams, and P. Yeatman, 2019, Marine vibrator source: Modular projector system: 89th Annual International Meeting, SEG, Expanded Abstracts, 52–56, https://doi.org/10.1190/segam2019-3215325.1.

Proffitt, J. M., 1991, A history of innovation in marine seismic data acquisition: The Leading Edge, **10**, no. 3, 24–30, https://doi.org/10.1190/1.1436807.

Rietsch, E., 1977, Computerized analysis of vibroseis signal similarity: Geophysical Prospecting, **25**, no. 3, 541–552, https://doi.org/10.1111/j.1365-2478.1977.tb01186.x.

Roy, D. A., R. Rekos, C. Brideau, T. Lawry, and C. Corrada, 2018, A marine vibrator to meet the Joint Industry Project specification: 88th Annual International Meeting, SEG, Expanded Abstracts, 97–101, https://doi.org/10.1190/segam2018-2997347.1.

Söllner, W., and O. C. Orji, 2018, Marine vibrator source acceleration and pressure: US 2018/0052245 A1.

Tenghamn, R., 2006, PGS shows off electrical marine vibrator to capture 'alternative' seismic source market: First Break, **24**, no. 1, 33–36.

# SEG WORKSHOP

**SEG Summer Research Workshop: Data Analytics and Machine Learning for Exploration and Production**
10–13 August 2020 | Denver, Colorado

## Call for Abstracts
**Submission deadline: 30 April**

**Suggested topics include:**

- Seismic interpretation
- Seismic processing
- Other geophysical methods & multiphysics data integration
- Reservoir characterization
- Wellbore
- Natural language processing applications
- Advances in algorithms

**Register by 10 June and save!**

**seg.org/events**

# SEG/DGS WORKSHOP

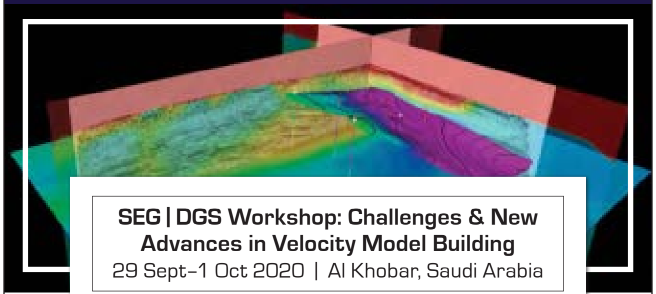

**SEG | DGS Workshop: Challenges & New Advances in Velocity Model Building**
29 Sept–1 Oct 2020 | Al Khobar, Saudi Arabia

## Call for Abstracts
**Submission deadline: 15 May 2020**

**Suggested topics include:**

- Role of acquisition
- Near surface
- Non-seismic methods
- Borehole seismic
- Wave equation tomography
- Waveform inversion
- Anisotropic velocities
- Big data & machine learning
- And more ...

Image source – Cui et al., https://doi.org/10.1190/tle34121474.1

**seg.org/events**

# SEG/SPE WORKSHOP

**Advanced Geoscience Applications in Drilling and Well Placement Workshop**
25–26 August 2020 | Kuala Lumpur, Malaysia

## Call for Abstracts
**Submission deadline: 30 April**

**Suggested topics include:**

- Well planning and modeling of reservoir characterization
- Advances in geoscience measurements for drilling and well placement
- Cost effective real-time geosteering and imaging
- Pore pressure and fracture gradient in complex geological setting
- Industry 4.0 (IR 4.0) applications of cloud, artificial intelligence and machine learning
- And more...

**seg.org/events**

# SEG WORKSHOP

**Complex Overburden and High End Imaging Workshop**
22–23 September 2020 | Kuala Lumpur, Malaysia

## Call for Abstracts
**Submission deadline: 30 April**

**Suggested topics include:**

Model Building and Imaging Under Complex Overburdens

- Near surface and weathering layers
- Carbonate platforms/pinnacles
- Gas cloud
- And more ...

High End Imaging

- Advances in full waveform inversion for strong velocity contrasts
- Artificial intelligence or machine learning
- New imaging algorithms
- And more ...

**seg.org/events**

# Automation of marine seismic data processing

Andrew Long[1] and Tony Martin[2]

https://doi.org/10.1190/tle39040264.1

## Abstract

Marine seismic data sets contain highly redundant information. Data analytics and machine learning-based solutions should provide opportunities to reduce turnaround and improve confidence levels in output data volumes. A proof-of-concept (POC) thrust regime example from Indonesia illustrates that parameter testing can almost be eliminated if existing project parameter data can be mined from a database. Where quality control (QC) is required for complex challenges such as noise removal, supervised classifiers are a platform that can enable rapid global quantitative decisions based on relevant data attributes, moving behind the subjective art of observational QC. Finally, many early processing steps depend on reasonable knowledge of the velocity model in addition to the explicit dependence of imaging steps. A POC Monte Carlo-based model building exercise in West Africa used an efficient tomographic platform to demonstrate that turnaround can be reduced from 90 days to only a few days, even when the starting model was significantly wrong. These examples illustrate that a lot is already within our reach, and the development of embedded feedback loops will improve the level of automation further, particularly if humans can learn to let the data speak for itself.

## Introduction

The proposed application of automated processing to towed-streamer marine seismic projects broadly follows three considerations: (1) parameterization with minimal testing, (2) accelerated quality control (QC), and (3) derivation of the velocity model. This sequence acknowledges that appropriately conditioned data are required to build any model. How much further can we progress to full automation? Sheridan and Verplank (1978) provide a relevant 10-stage hierarchy of automation levels in which level seven (the computer does the entire job and tells the human what it did) represents the highest level of automation, where manual decisions still outrank the computer. Complete delegation of decision making to algorithms will conceivably be as much of a psychological barrier as it will be a technological innovation. In our proof-of-concept (POC) examples, we advocate the use of pragmatic solutions that can exploit the redundancy of information recorded by modern marine seismic surveys. The machine learning-type QC described by Bekara and Day (2019) is placed in the context of rapidly validating the parameterization of processing modules with data analytics solutions. Strategic data compression, onboard and onshore teams working in concert with common big data platforms, and the use of deep learning, data analytics, and Monte Carlo methods for automated velocity model building are all demonstrated to be relevant when streamlining project complexity and reducing project turnaround.

## Bridging the vessel-office distance

Seismic vessel operations are complex enterprises that depend on the seamless integration of many systems and platforms to control a vast array of data collection. Modern vessels routinely tow 16–18 multisensor streamers with 8–10 km length, representing a receiver array with up to 17 km$^2$ of sensors, and record 2–10 TB of seismic, navigation, and ancillary data each day. The size of the recorded data volumes are a direct function of the number of channels recorded and the sample rate. While real-time condition-based monitoring of vessel performance data is already streamed to virtual instrument rooms in office locations (Courtenay, 2019), enabling data analytics and proactive management of critical systems, it remains impractical to transmit all of the uncompressed seismic data recorded each day to the office in near real time using geosynchronous satellite networks. Seismic data processing during the acquisition stage of any project must either be: (1) pursued onboard using available human and computing resources, (2) pursued onshore as the frequency of physical data drops allow, or (3) pursued onshore with strategic data subsets transmitted by satellite (possibly with data compression to reduce file sizes) and processed onshore in parallel with onboard activities.

Most streamer vessels have onboard human and computer resources that enable some form of data processing during acquisition. Fast-track preliminary interpretation products are correspondingly delivered in interim form during acquisition and in final form soon after the completion of acquisition using abbreviated processing flows (e.g., Walker et al., 2019). Processing flows use either testing parameterization or production parameterization with the final choice of parameters in each step. Traditionally, production processing with the full-integrity workflow sequence does not begin until the physical data are received in the office via scheduled data drops.

Assuming that near real-time processing at the rate of acquisition is desired in an office, 2 TB of uncompressed seismic data representing one wavefield component from one day of towed multisensor streamer acquisition will take aproximately one year to transmit using a standard 512 Kbps geosynchronous satellite connection. This reduces to approximately three days using a 64 Mbps connection that represents the upper bandwidth limit typically used for projects seeking near real-time transmission. It is therefore evident that such data must be heavily compressed to enable complete transmission in less than one day, though this remains uncommon. Alternatively, we can transmit strategic subsets of data to the office each day (e.g., shot gathers from one streamer only). Critical onboard QC, such as line acceptance decisions and parameterization of noise removal procedures, only requires subsets of field data (representative combinations of shot gathers, common channel ensembles, or near-field hydrophone

[1]PGS, West Perth, Australia. E-mail: andrew.long@pgs.com.
[2]PGS, Surrey, United Kingdom. E-mail: tony.martin@pgs.com.

data). Such data can be robustly transmitted using low rates of data compression and modest satellite bandwidth connection. Office support of vessel personnel enables rapid and robust decisions for the production processing steps possible within the acquisition timeframe of a project, but the majority of production processing is completed after the acquisition stage.

The frequency of physical data drops from the vessel to the office is linked to the rotation of vessel crew using either large vessel or helicopter transfers (typically between every two and five weeks). This critical path drives the time lag between the acquisition of each sail line and the onset of production processing. The time taken to acquire enough sail lines within swaths with sufficient crossline aperture for full testing of 3D algorithms, such as surface-related multiple elimination and migration, is determined by the length of each line and the overall shooting plan. Hence, full-volume QC may not be possible before much of the physical data have been received in the office.

Alternatively, if high rates of data compression (probably 50–100) are acceptable, all of the daily data could be efficiently streamed to the office, and production processing of the decompressed data could commence without waiting for physical data drops. Perhaps it is time for the industry to accept that data compression/decompression using modern algorithms is as acceptable as the effective signal compression introduced by sparsity-promoting inversion solutions, multichannel transforms, and seismic migration.

## Data analytics and processing automation

Testing, validation, and production administration are time consuming for any processing project. Testing is performed to optimize the parameters for each specific step in the processing sequence. Depending on the challenge the step is attempting to address and the complexity of the data, processing testing can require a lot of interactivity with the data, which can be both prolonged and computer-resource intensive.

As indicated, the amount of seismic data processed annually by a globally active contractor can be significant, especially when each step in the sequence has unique characteristics. If the contractor's historical activity can be used to construct a database of parameters applied to all data sets, it can be mined to extract the most appropriate parameters for the data processing. This is based on similarity criteria and considering geologic setting, processing challenges and objectives, acquisition geometry, environmental conditions, and specifics of the processing sequence. The collective expertise and experience of contractor personnel stored in a database is an undeniably powerful tool for reducing turnaround. The data could be mined to focus testing parameterization and reduce testing turnaround or to bypass testing altogether.

A 400 km$^2$ POC test was run with data from Indonesia, where key processing parameters for all steps in both the data domain preprocessing and migration were mined from a database. No testing was performed, and all workflows were actioned end on end. The resulting raw migration was then compared to the full-integrity processing project whose parameters were excluded from the database and which was run in advance of the testing. Figure 1 shows a comparison of the data from the (independent) full-integrity work compared to that where parameters have been determined in advance of the project and run without testing.

The migrated stacks look similar. However, quantitative comparison metrics were run, including correlation analysis, normalized root-mean-square difference (NRMSD), and signal-to-noise (S/N) content, to further analyze the two volumes. QCs were run after each key processing step, but at no point did they affect the original (mined) parameter choices, and for brevity, only the final comparisons are shown. Such metrics are common to 4D processing and are therefore a good indicator for comparing the full-integrity

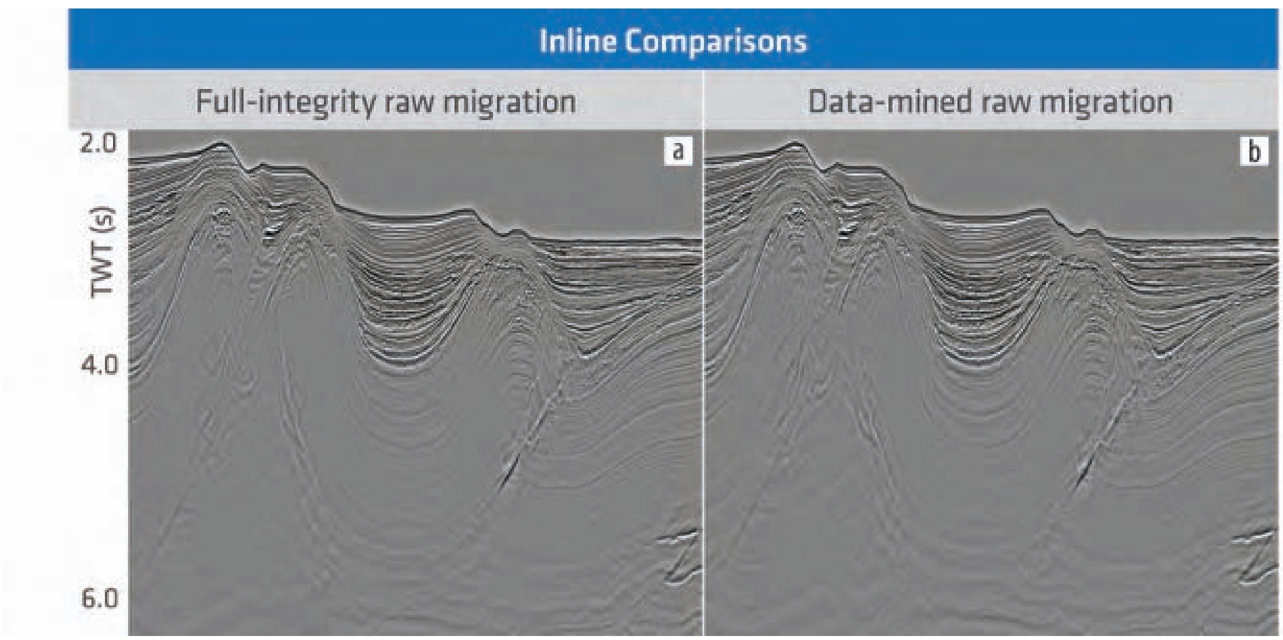


**Figure 1.** (a) A raw migration stack response comparison of a full-integrity processing project. (b) An automated approach using data mining of a parameter database.

volume and the automated equivalent. Correlation analysis between the two volumes (Figures 2a and 2b) and NRMSD (Figure 2c) highlight that deeper data are slightly noisier. Figure 2d suggests that the automated processing nevertheless preserved phase integrity. The S/N content in Figure 3b indicates that the full-integrity data have a slightly better response (notably 30–70 Hz), albeit marginal. Overall, the data quality from the database-mined processing automation is equivalent to the full-integrity process and was achieved in one-third of the time taken to create the full-integrity volume. As with all seismic processing projects, an equivalent level of success cannot always be expected. However, as such parameter databases become more sophisticated and better populated, the principles herein should be broadly applicable.

The only caveat in achieving comparable results in this processing automation POC work is the use of an a priori velocity model in the migration, which for comparison sake was taken from the full-integrity project. In a later section, we consider automation of the velocity model used for depth migrations, but first we address the obvious question of how the parameter selection can be efficiently validated.

## Automated QC: Supervised large volume noise removal

Most onboard line acceptance and QC activities during marine seismic acquisition are based on the assessment and removal of noise in many thousands of shot records. Once the field data are accepted, modern seismic data processing flows typically have 15 to 20 major components, each having unique characteristics managed by intermediate data outputs. Traditional QC has relied heavily on visual inspection of the prestack and poststack results of multiscenario parameter testing and attribute generation. However, the simultaneous assessment of many attributes is subjective, empirical, and challenging.

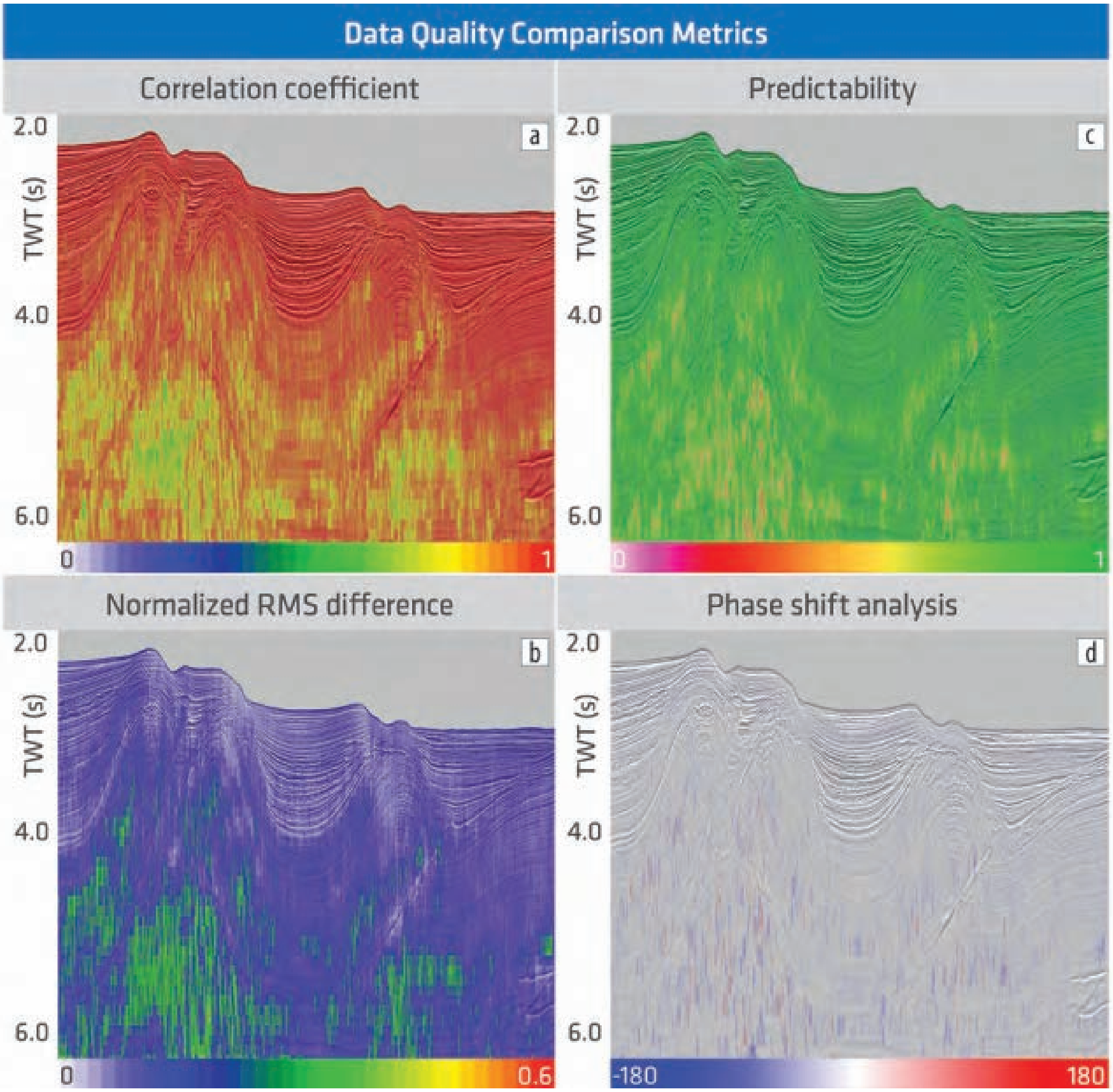


**Figure 2.** (a) Correlation coefficient. (b) Predictability. (c) NRMSD. (d) Phase.

Marine seismic data sets contain highly redundant information, so data analytics and deep learning-based solutions provide opportunities to reduce turnaround and improve confidence levels on output data volumes. As previously alluded to, early-stage processing QC occurs in concert between onboard and onshore resources, enabled by satellite transmission and data compression. As the volume of data in a typical survey has increased over time, QC practice has moved toward assessing global attribute maps that are computed from the data, such as root-mean-square amplitude or S/N maps. However, such simplistic tools require frequent cross-checks with the seismic data. The focus is on detecting outliers and anomalies, and humans cannot understand the visualization of more than two or three attributes at a time. Clearly, we want to compute as many informative attributes as possible to give a better sampling of the filtering performance. This can be facilitated by using statistical data mining techniques to analyze the different attributes. Correspondingly, Bekara and Day (2019) describe a relevant POC supervised learning framework for automatic denoise classification that expands on the unsupervised outlier detection methodology of Spanos and Bekara (2013). Their example applies to one step (denoise) of a processing flow, of which there will be several in practice. Six sail lines evenly dispersed throughout a semicompleted multisensor streamer survey were split into training and validation data sets of raw shot gathers. Shot gather-based multidimensional statistical attributes measuring the similarity between the output of various degrees of noise removal and the difference between input and output were computed within time-spatial windows. Similarity will increase with increasing signal leakage into the filtering.

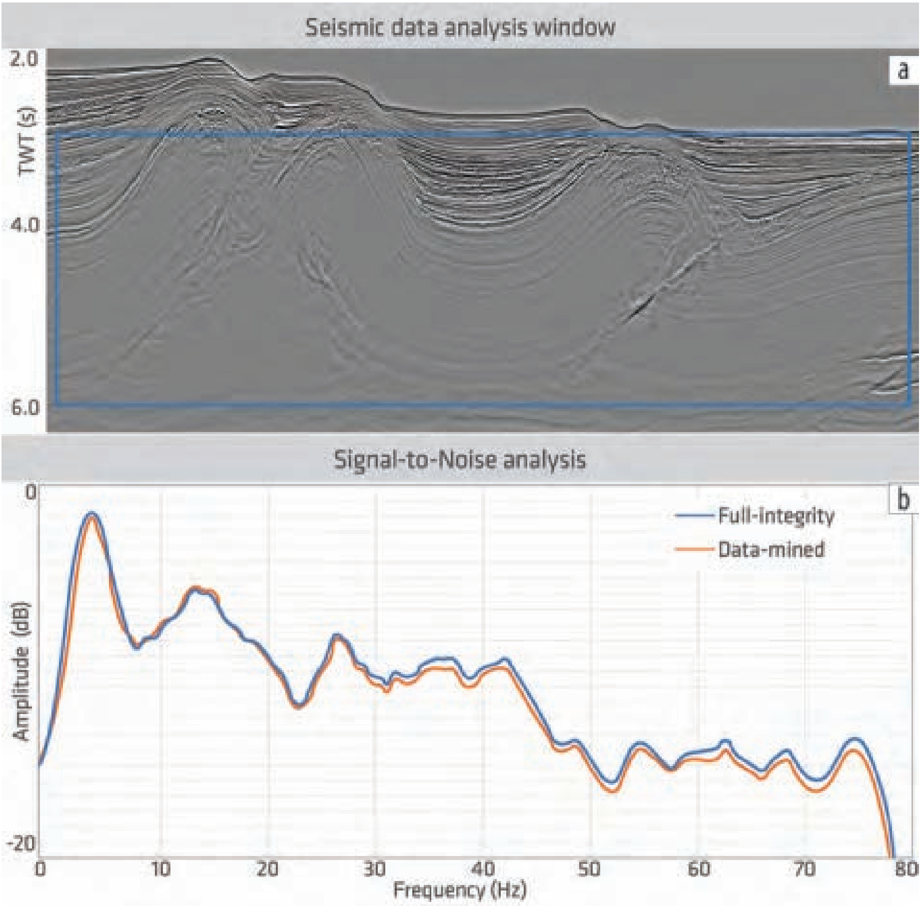


**Figure 3.** (a) Analysis window used to compute the S/N attribute. (b) S/N comparison of the full-integrity and data-mined results.

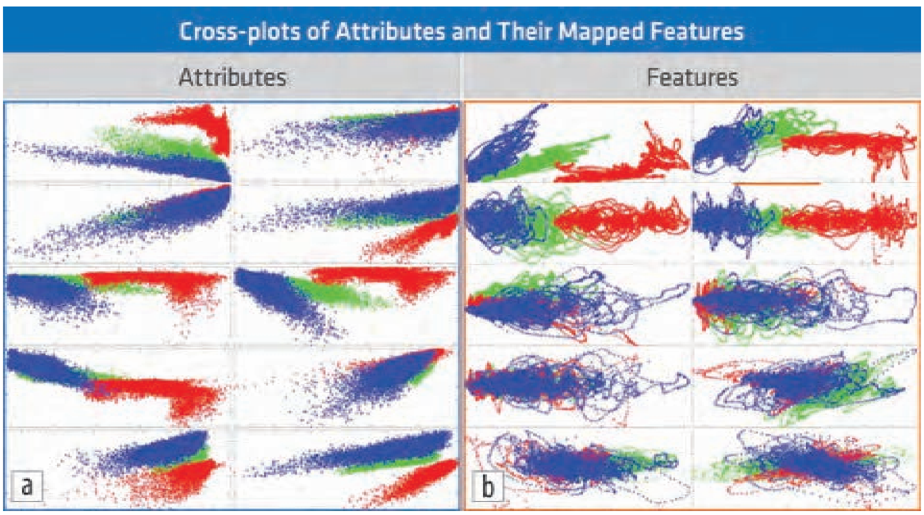


**Figure 4.** (a) Crossplot of five attributes and (b) the equivalent crossplots of five principal components computed after spatial augmentation of the attributes. Each dot within the crossplot distribution of the three colors of red (mild), green (optimal), and blue (harsh) represent one filtered shot gather. Note that visual separation between the different clusters has improved for the primary principal components, and the corresponding decision space yielded negligible false-positive results by comparison to the result based on attributes. From Bekara and Day (2019).

The crossplots of five different attributes computed from three test lines are shown in Figure 4. These are only shown to validate the attributes, which are overlaid for the optimal, harsh, and mild filtering cases using a three-color code (mild is blue, optimal is green, and harsh is red). There will always be hidden correlations between the individual attributes due to their common origin. Their dimension can also be extremely large, making the subsequent classification problem harder. The task of decorrelating the attributes to extract useful structure is called "feature extraction." It is a mapping process that transforms each vector of attributes into an optionally lower dimensional vector of features. Often, the features tend to have a better cluster-discrimination power compared to the attributes. Key linear feature extraction procedures are principal component analysis (PCA) and independent component analysis (ICA) (Hyvärinen et al., 2001). To take the spatial consistency of the filtering outcome into consideration, attributes from adjacent shots are merged with the attributes of the central shot, resulting in an augmentation of the total number of attributes for the central shot. Figure 4b shows the cluster of features obtained after applying a nonlinear mapping (spatial augmentation with 20 shots followed by PCA) on the cluster of attributes in Figure 4a. A supervised classification based on support vector machines (Cristianini and Shawe-Taylor, 2000) was constructed using the training data, yielding three decision spaces corresponding to optimal, mild, and harsh filtering. When using the attributes to train the machine learning classifier, those selected were informative, as the training error for all three scenarios was negligible (< 3%). The validation error for harsh and mild filtering was similarly small; however, about 20% of the optimal filtering points were initially misclassified as mild or harsh filtering. This error significantly decreased (from 20% to 1%) when the machine learning classifier was trained instead with the features. As noted in the previous section, the POC example may not necessarily be as successful elsewhere for this equivalent processing step. Other major processing components would need different attributes within the same learning framework. However, the strategy of making better-informed decisions with more data references should remain robust.

Figure 5 shows a tricolor decision map for every available shot in the POC study. Subsequent evaluation of the shot locations,

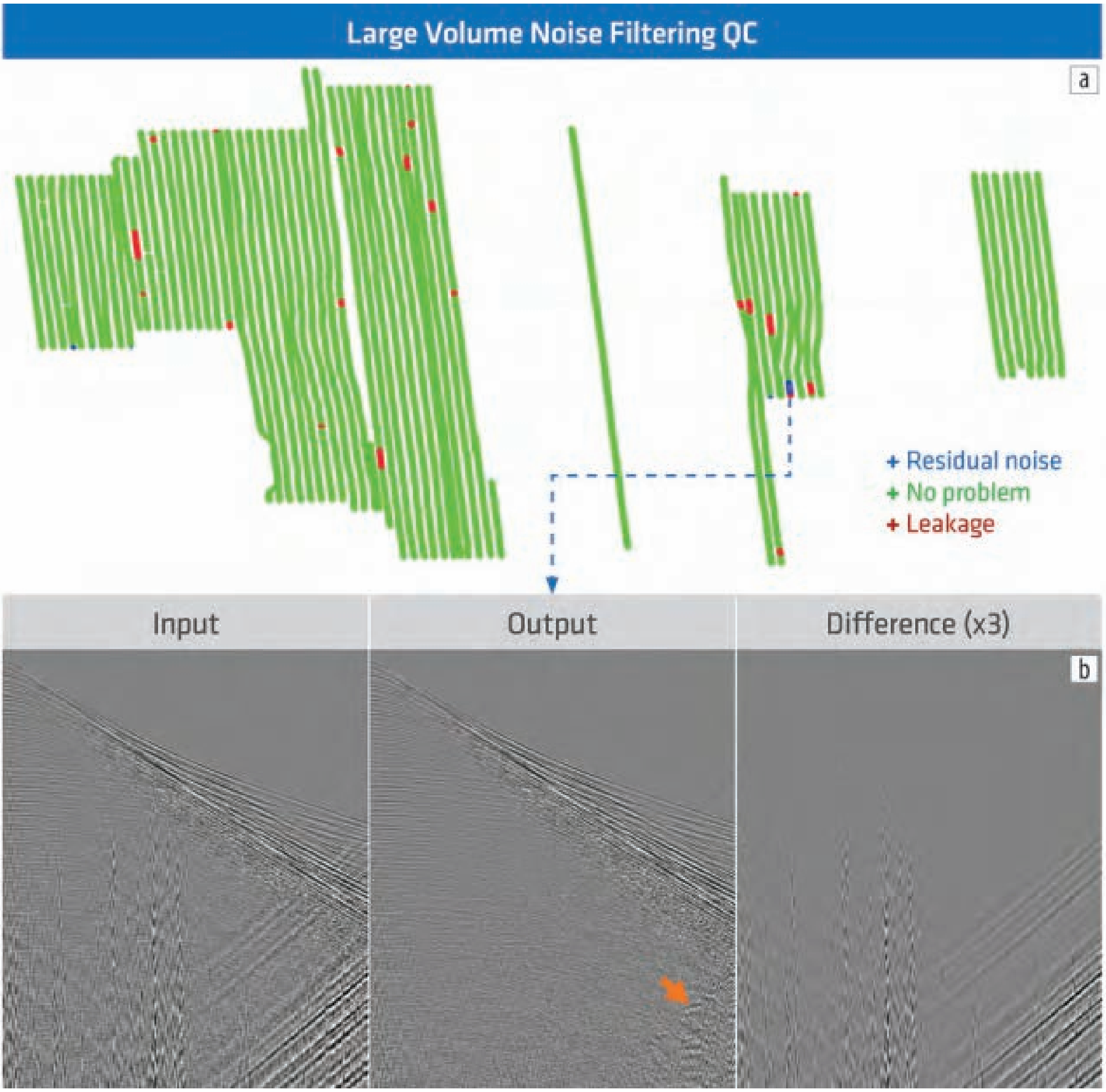


**Figure 5.** (a) Classification of all shot locations. (b) An example of a shot gather identified as requiring residual noise removal. The decision map contains one point for each shot gather location. The colors follow the same scheme used in Figure 4.

identified by blue points, would result in additional residual noise removal. Red points correspond to false positives produced when training the solution with attributes.

In the dynamic offshore environment, the described approach would help focus attention on any priority areas with potential problems, thereby optimizing the use of resources working within challenging timeframes. More generally, supervised classifiers should enable global quantitative decisions based on many relevant data attributes, moving behind the subjective art of observational QC. While the POC example shown is for validating and classifying denoise, the philosophy could be extended to other major processing steps. Looking forward, the development of feedback loops will enable processing flows with even higher levels of automation. For example, level eight in the hierarchy of Sheridan and Verplank (1978) is "computer does whole job and tells human what it did only if human explicitly asks."

## Automated velocity model building

Any fast-track products or progressive interpretation deliverables, such as angle-range gathers and stacks, explicitly depend on the early availability of an accurate velocity model for the entire data set. Simple velocity picking by onboard personnel or by office personnel using remote sessions to the onboard computers is robust during acquisition. A reasonable starting model can be produced rapidly with a short time lag after the receipt of data in the office. If data compression is acceptable to the client, there is no technical reason why highly compressed (and possibly subsampled in time) shot gathers could be transmitted to the office in near real time for input to full-waveform inversion (FWI), especially given that irreversible signal distortion from high compression rates is generally prevalent at higher frequencies of negligible relevance to FWI. Therefore, an FWI-based velocity model could in principle be ready when the physical data drop is received by the office, enabling zero wait to progress to demultiple, assuming that all shot domain denoise pursued on the vessel met the project technical ambitions. Furthermore, if elements of the demultiple workflow have also been completed on the vessel and/or in the office before the physical data are received, the time between data receipt and the commencement of imaging will be further reduced (e.g., Saint Andre et al., 2010).

More generally, model building for depth imaging is one of the largest bottlenecks in processing workflows as well as one of the most critical steps. Such models are used to provide an image of the subsurface, from which a range of probabilities and volumetric estimates may be made and drilling campaigns planned and then actioned. Although FWI represents the pinnacle of velocity model building (VMB) for many practitioners, its high computational cost makes it impractical for scenario testing of different model realizations or uncertainty. Deep model building is often challenging for standard streamer lengths, even if cycle-skipping-mitigated full-wavefield FWI is achievable (e.g., Ramos-Martínez et al., 2019). Considerable scope still exists for pragmatic non-FWI solutions to augment faster processing workflows.

Bell et al. (2016) describe the use of a Monte Carlo simulation that enables multiple realizations in order to derive estimates of the uncertainty of an individual velocity model. The method performs multiple random perturbations of a starting model followed by tomographic inversion. This platform uses an efficient

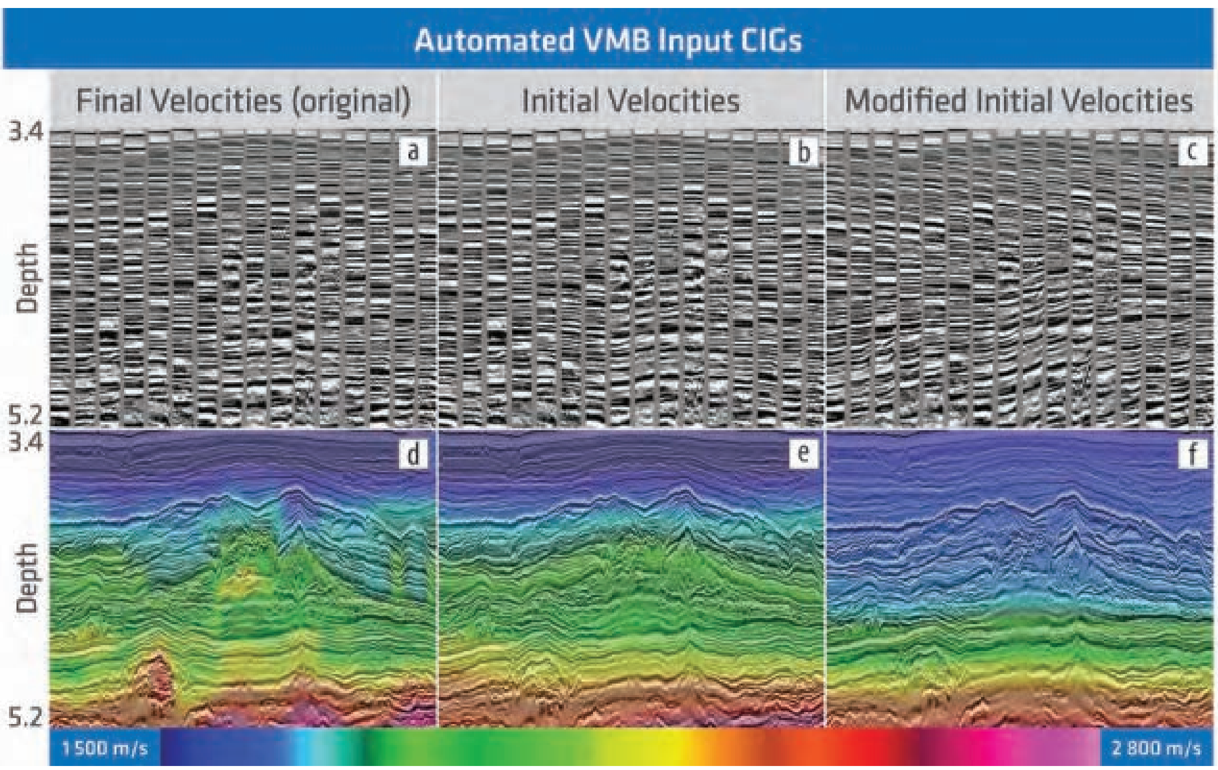


**Figure 6.** CIGs for the (a) final tomographic model, (b) initial model for (a), (c) modified and locally erroneous initial model, and (d)–(f) migrated stacks with corendered velocities corresponding to CIGs in the upper row.

beam migration to establish the initial ray kinematics of the invariant data, which comprise wavelets extracted from the data through a multidimensional dip scanning process (Sherwood et al., 2008), performed within the migration model space generating the observed data. The process of model perturbation is performed in a residual migration and applies the differential kinematic to the observed data, consistent with the applied perturbation. Rather than look at the uncertainty of a single model and the imaging products, the methodology can also be adapted to create a depth imaging velocity model from scratch using either a benign or incorrect starting point through the same Monte Carlo simulation of the model space.

The starting point for the full automation of VMB in Martin and Bell (2019) begins with the same steps of determining what the data support in the model space prior to creating a randomly generated model population. Once generated, the population is tomographically inverted, and statistical analysis is performed on the model updates prior to reintroducing a pass of random model generation. The process is repeated with the goal to produce a model that explains the data by producing flat common-image gathers (CIGs) that have a zero residual for tomographic inversion. This is quantified by determining moveout-related metrics after each pass of the simulation. Convergence of the solution determines how many iterations are used.

A 500 $km^2$ data set from West Africa was used in a POC test to reduce the time taken to produce a model by removing human intervention. Two initial models were tested: the starting model used for the actual tomographic model building project and one where the initial model was modified to incorporate a locally varying error up to 10% in the starting model. Once randomly perturbed, the secondary starting model could be locally up to 15% too fast or slow. The results were checked against the final tomographic model, which was built using the same data and generated in 90 days.

Figure 6 shows three sets of CIGs and three stacks with their associated velocities corendered on the seismic sections. Figures 6a and 6d are the result of the 90-day model building exercise. The central image shows the starting point for the automated Monte Carlo model building process. The starting CIGs in Figures 6b and 6c show a significant level of moveout, as the model was up to 15% wrong. The results in Figures 7b and 7c show the product of the automated model building. Gather flatness is equivalent to the conventional approach (Figure 7a), and the corendered velocity models closely resemble the model built in 90 days.

Progressive analysis of metrics on moveout show an equivalent level of convergence in the resulting models, irrespective of the starting point (Figure 8). The workflows were initiated by a geophysicist who had no prior knowledge of the data or models, and no well constraints were available to confirm the accuracy of any of the resulting models. The implications of this approach are considerable. While the original model building project took 90 days, both automated models were achieved in less than an order of magnitude of that time.

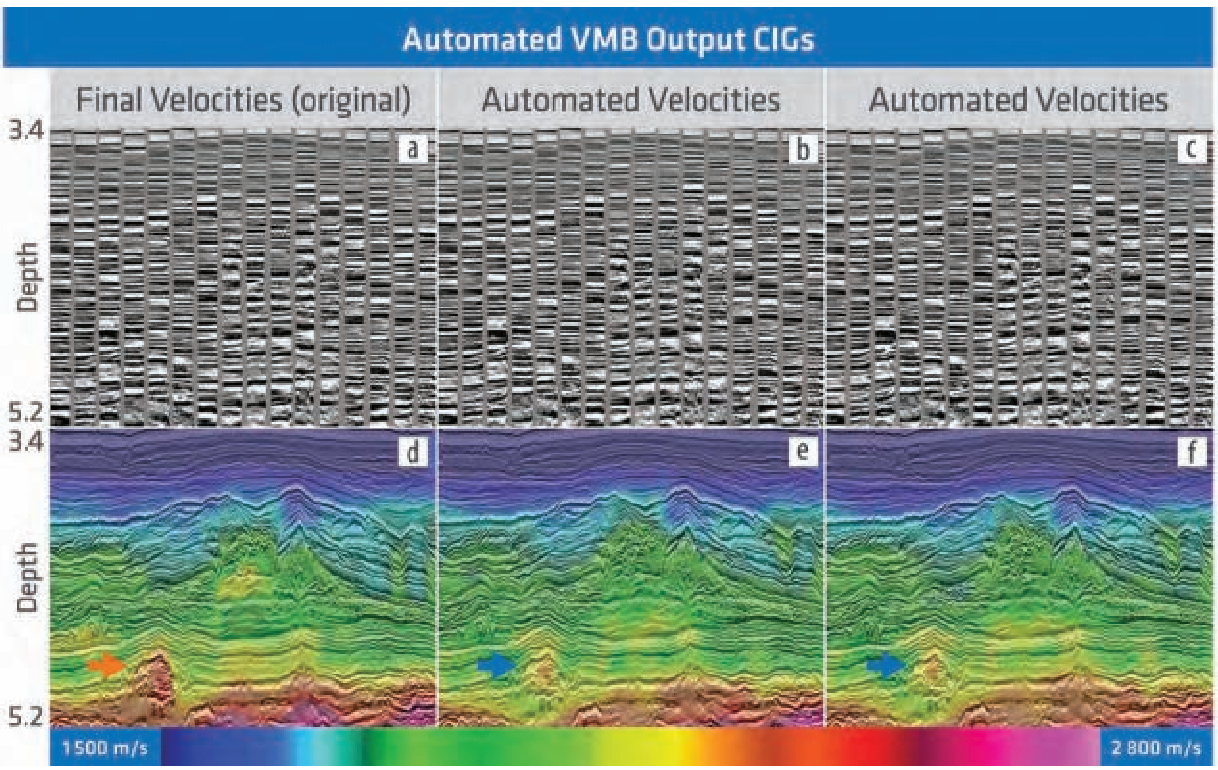


**Figure 7.** CIGs for the (a) final tomographic model, (b) final automated model starting with Figure 6b, (c) final automated model starting with Figure 6c, and (d)–(f) migrated stacks with corendered velocity models corresponding to CIGs in the upper row. The orange arrow in (d) shows the location of the masked and updated geobody (channel). Blue arrows in (e) and (f) show the channels captured with the automated approach. The automated models in (e) and (f) otherwise show a strong correlation with the model built during a conventional velocity model workflow.

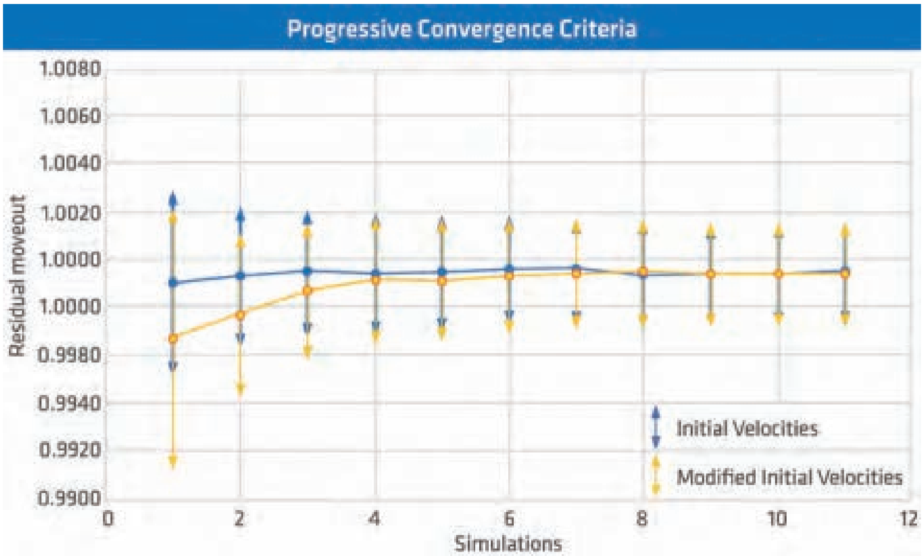


**Figure 8.** Moveout convergence criteria QC. The blue curve using a starting model was derived from semblance-based velocity picking. The orange curve using a starting model is shown in Figure 6b. Both blue and orange curves converge to the same level of moveout.

## Summary

The progress from the sequential series (with many steps and interactive QC events in legacy seismic processing flows) to full automation will occur in a piecemeal fashion as the industry learns to embrace what will essentially be a hands-off paradigm. Towed-streamer marine seismic surveys can acquire vast data volumes each day, presenting an early-stage project challenge to cost-effective near real-time streaming of the data to onshore supercomputer facilities using geosynchronous satellite networks. An acceptance of high rates of data compression and/or the sharing of strategic subsets of data with onshore resources is the pragmatic solution to initiate production processing early during the acquisition stage.

Our POC example demonstrated that a collectivized digital experience database can be mined to fully parameterize several consecutive processing steps without human intervention. An efficient QC system is correspondingly necessary to validate such an approach. A supervised learning example of efficient denoise QC is demonstrated as being a potentially efficient platform for using all of the data acquired to augment better acquisition QC decisions in less time. It presumably heralds the way to similarly augment more efficient QC for other steps in a typical processing flow.

Automated parameterization validated with efficient and robust QC platforms is also particularly relevant for automated VMB, as data conditioning is inevitably required before VMB, including FWI. Although FWI represents the pinnacle of model building VMB for many practitioners, considerable scope still exists for pragmatic non-FWI inversion solutions to augment faster processing workflows. Correspondingly, an efficient wavelet-based beam migration platform was shown in a large POC study to accurately recover depth velocity models using Monte Carlo-based tomographic inversion of moveout residuals, even when the starting model was highly inaccurate. Overall, a pragmatic combination of supervised deep learning, data analytics, and efficient imaging solutions can deliver substantial reductions in project turnaround while balancing human interaction and full automation. Further iterations of this workflow with embedded feedback loops would improve the level of automation. TLE

## Acknowledgments

We thank Suhail Butt and Khairom Baharom for help with the Indonesian data test, Marcus Bell for help with the automated velocity model building, and PGS for permission to publish this work.

## Data and materials availability

Data associated with this research are confidential and cannot be released.

Corresponding author: andrew.long@pgs.com

## References

Bekara, M., and A. Day, 2019, Automatic QC of denoise processing using a machine learning classification: First Break, **37**, no. 9, 51–58.

Bell, A. C., L. Russo, T. Martin, D. van der Burg, and B. P. Caselitz, 2016, A workflow to quantify velocity model uncertainty: 78th Conference and Exhibition, EAGE, Extended Abstracts, https://doi.org/10.3997/2214-4609.201601098.

Courtenay, P., 2019, Building a dream team: Oilfield Technology, **12**, no. 5, 13–15.

Cristianini, N., and J. Shawe-Taylor, 2000, An introduction to support vector machines and other kernel-based learning methods: Cambridge University Press, https://doi.org/10.1017/CBO9780511801389.

Hyvärinen, A., J. Karhunen, and E. Oja, 2001, Independent component analysis: John Wiley & Sons.

Martin, T., and M. Bell, 2019, An innovative approach to automation for velocity model building: First Break, **37**, no. 6, 57–66.

Ramos-Martínez, J., L. Qiu, A. A. Valenciano, X. Jiang, and N. Chemingui, 2019, Long-wavelength FWI updates in the presence of cycle skipping: The Leading Edge, **38**, no. 3, 193–196, https://doi.org/10.1190/tle38030193.1.

Saint Andre, C., N. Khaled, L. Bovet, J. Brittan, M. Bekara, T. Martin, and M. Phillips, 2010, Angola wide azimuth towed streamer (WATS): 3-D SRME whilst shooting: 80th Annual International Meeting, SEG, Expanded Abstracts, 3416–3420, https://doi.org/10.1190/1.3513558.

Sheridan, T., and W. Verplank, 1978, Human and computer control of undersea teleoperators: MIT Technical Report.

Sherwood, J. W. C., K. Sherwood, H. Tieman, and K. Schleicher, 2008, 3D beam prestack depth migration with examples from around the world: 78th Annual International Meeting, SEG, Expanded Abstracts, 438–442, https://doi.org/10.1190/1.3054840.

Spanos, A., and M. Bekara, 2013, Using statistical techniques to improve the QC process of swell noise filtering: 75th Conference and Exhibition, EAGE, Extended Abstracts, https://doi.org/10.3997/2214-4609.20130884.

Walker, M., D. Davies, C. Hill, C. Page, P. Smith, and A. Irving, 2019, Full-cycle iterative processing: When is "good", good enough? A 4D North Sea case study: 81st Conference and Exhibition, EAGE, Extended Abstracts, https://doi.org/10.3997/2214-4609.201901578.

# In-situ combustion front monitoring and tracking using InSAR

Mohammad Bazargan[1], Pieter Bas Leezenberg[2], and Anthony R. Kovscek[1]

https://doi.org/10.1190/tle39040272.1


## Abstract

Interferometric synthetic aperture radar (InSAR) is used to locate the combustion front during field application of the in-situ combustion (ISC) enhanced oil recovery process. As the combustion front propagates through the reservoir during ISC, lateral surface deformation occurs on the order of 1–100 mm/year, depending on the reservoir depth and overlying strata, with a unique time derivative signature. Monitoring using InSAR benefits from the existence of a thin (tens of centimeters) high-temperature (600°C) combustion front to accurately determine the front position. This can inform reservoir and production engineering design decisions. Analytical and numerical examples of a homogeneous, isotropic, and horizontal reservoir show that regardless of the depth of the reservoir, the combustion front is positioned at the local maximum of the rate of surface deformation. These results are consistent with analytical solutions for distribution of point stress in the earth. This result is applied to the field case of Suplacu de Barcau, Romania, that has a long history of ISC. For the Suplacu Field, surface deformation rate data were generated using InSAR for the time periods of 12 March 2003 to 28 July 2010 and 29 October 2014 to 19 June 2017. The time derivative of surface deformation (surface velocity) suggests the advancement of the combustion front, consistent with reservoir engineering analyses in the literature. Importantly, the predicted positions of the combustion front match the available historical data for Suplacu in 2006 and 2010. We have also predicted the position of the combustion front in 2017 using the most recent InSAR data.


## Introduction

In-situ combustion (ISC) is an enhanced oil recovery method in which air is injected into a crude oil reservoir to burn a small fraction (approximately 3%–5%) of the oil in place to produce heat that reduces oil viscosity and combustion gases that drive oil forward. The combustion front is the volume of reservoir where oxidation of crude oil components and the release of combustion heat occurs. Practical design of ISC includes finding the optimum air injection rate and managing the combustion front to obtain orderly propagation. For safety reasons, it is important to be certain that the combustion front does not enter open production wells. In the field, the combustion front is typically a few to tens of centimeters thick. Accurate estimation of the combustion front position on the field scale using numerical simulation is challenging because of the very fine spatial resolution required to resolve front dynamics (Gutiérrez et al., 2009).

The applicability of interferometric synthetic aperture radar (InSAR) data has been shown to be relevant to the reservoir engineering aspects of several oil fields (Leezenberg and Allan, 2017). Active satellite systems, such as radar, send a signal to the earth's surface and measure the reflected signal's phase and amplitude. The difference between two sequential phase measurements is due to ground elevation. Thus, InSAR measurements are used to measure surface movements between successive passes of orbiting satellites with an accuracy of ±1 mm (Leezenberg and Allan, 2017).

This work was based on SAR data from Envisat and Sentinel satellites acquired every 12–30 days with a resolution of 5 × 20 m. These sensors have two different look angles, and images were processed using the Antares persistent scatterer InSAR framework, generating up to 500,000 measurement points over the field. Images are unwrapped as described by van Leijen (2014). Differences in look angles were taken into account by projecting to vertical using the incidence angle of every pixel. This assumes that deformation is mainly vertical.

The availability and configurability of SAR imagery is undergoing a surge in recent years. In this work, we show that InSAR measurements are useful to locate the very thin combustion front during ISC in a commercial field project.

## Application of InSAR to ISC

When a combustion front propagates through a crude oil reservoir (Figure 1), the maximum temperature (approximately 600°C) and heating rate (approximately 10°C–30°C/minute) always occur at the combustion front (Penberthy and Ramey, 1966). The rate of temperature change is positive ahead of the combustion front and negative behind it. Because the reservoir temperature changes dramatically during ISC, the resulting thermal expansion/contraction of rock and fluids is significant. As shown in Figure 1, from time $t_1$ to $t_2$ ($=t_1 + \Delta t$), the zone ahead of the front experiences elevation uplift (positive $\Delta Z$), whereas the zone behind the front undergoes subsidence (negative $\Delta Z$). The elevation/subsidence rate is proportional to the temperature change versus time. Thus, the combustion front that has the maximum heating rate $\left(\frac{dT}{dt}\right)$ has the maximum deformation rate $\left(\frac{dZ}{dt}\right)$. Clearly, ISC front propagation creates a unique signature of deformation rate versus distance. The reservoir deformation rate is positive ahead of the front and negative behind the front. The maximum reservoir deformation rate corresponds to the location of the combustion front.

We now consider analytical and numerical treatments to relate the maximum reservoir deformation rate at the combustion front to the surface deformation rate. For a homogeneous and isotropic 2D medium, where the combustion front position is a point of

[1]Stanford University, Energy Resources Engineering Department, Stanford, California, USA. E-mail: mozarg@stanford.edu; kovscek@stanford.edu.
[2]SkyGeo Inc., San Mateo, California, USA. E-mail: pieterbas.leezenberg@skygeo.com.

thermal stress, we intuit that the surface deformation rate must be maximum at the same position. Boussinesq's analytical solution (Sterret, 1985; Das, 2013) for point/line load stress distribution inside the medium shows that bulb-shaped stress profiles are formed with the maximum stress at each depth located above/below the point load stress point position. Approximating the combustion front as a thermal stress point/line analytical solution suggests that the maximum surface deformation is located at the combustion front position.

Nevertheless, the real problem is more involved. Apart from heterogeneity and anisotropy, heat and mass transport and geomechanical phenomena take part. Numerical simulation of ISC together with geomechanical models is needed to analyze the problem more accurately. To support the intuitive analysis, we consider homogenous and isotropic numerical examples to investigate the surface deformation rate caused by ISC front propagation.

## Example 1: Simulation of thin high-temperature combustion front

Depending on the combustion design parameters, accurate numerical simulation of ISC may require grid block sizes of no more than a few millimeters (Bazargan and Kovscek, 2018). This grid block size is orders of magnitude smaller than the feasible grid block size used for numerical simulation at the field scale. The existence of a thin combustion front is a major challenge for ISC simulation at the field scale. Conversely, the existence of such thin high-temperature combustion fronts favors InSAR and helps us locate the front position accurately. Thus, it is important that in our numerical simulation example, we appreciate this thin high-temperature combustion front. In the first example, we have used 1D ($x$ direction) propagation of a combustion front in the media that is simulated using grid blocks with $\Delta x$ = 3.048 mm length. There is one layer in the $y$ direction with $\Delta y$ = 6.096 cm and 100 layers in the $z$ direction with $\Delta z$ = 6.096 cm. The distance between injector and producer is 304.8 cm. To avoid boundary effects, 30 grid blocks with $\Delta x$ = 30.48 cm before the injector and after the producer have been placed. The model contains 1060 × 1 × 100 grid blocks.

All of the grid blocks have 32% porosity. The first $z$ layer ($z$ = 1) of grid blocks between the injector and producer have oil saturation ($S_o$) of 0.1 and permeability of 10 Darcy. The rest of the grid blocks have no oil and zero permeability. Hence, these blocks do not contribute to the mass transfer calculation. A conventional three-step reaction model has been considered to represent the oxidation of crude oil. The reaction model and parameters, heat of reaction, and other rock and fluid properties are chosen (Bazargan and Kovscek, 2018). The medium is homogenous and isotropic. Linear elastic behavior has been considered in the geomechanical modeling. Rock properties are obtained from Panait-Patica et al. (2006). Geomechanical parameters are obtained from Domenico (1977) for unconsolidated sands.

Numerical simulation has been performed using the CMG software STARS. The consistency and convergence of the numerical model has been assured using spatial and temporal refinement

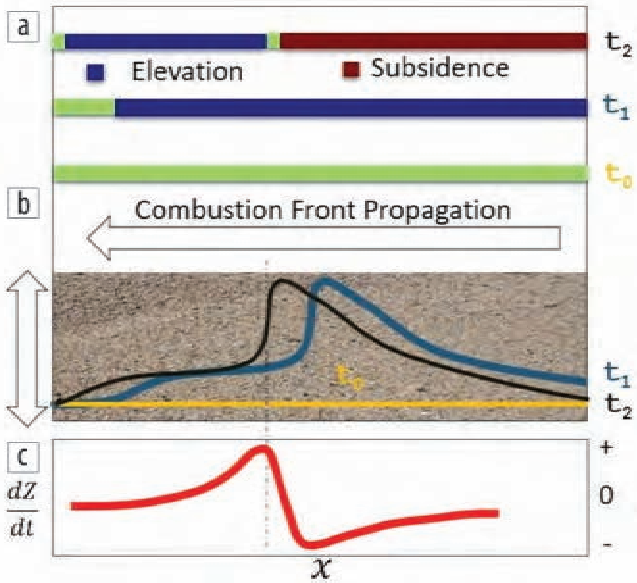


**Figure 1.** (a) Regions of reservoir thermal expansion and contraction. (b) Schematic combustion front temperature profiles at two times. (c) Resulting rate of change of elevation at $t_2$. Note that front propagation is from right to left.

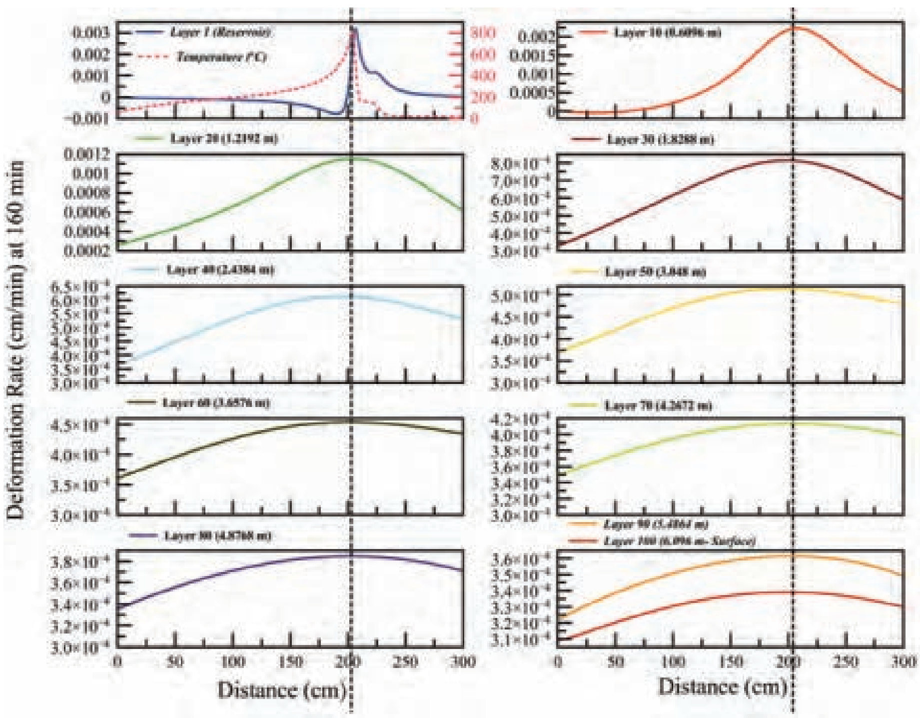


**Figure 2.** Example 1. Simulation of deformation rate at 160 min for 10 layers above the reservoir (layer 1) up to the surface (layer 100).

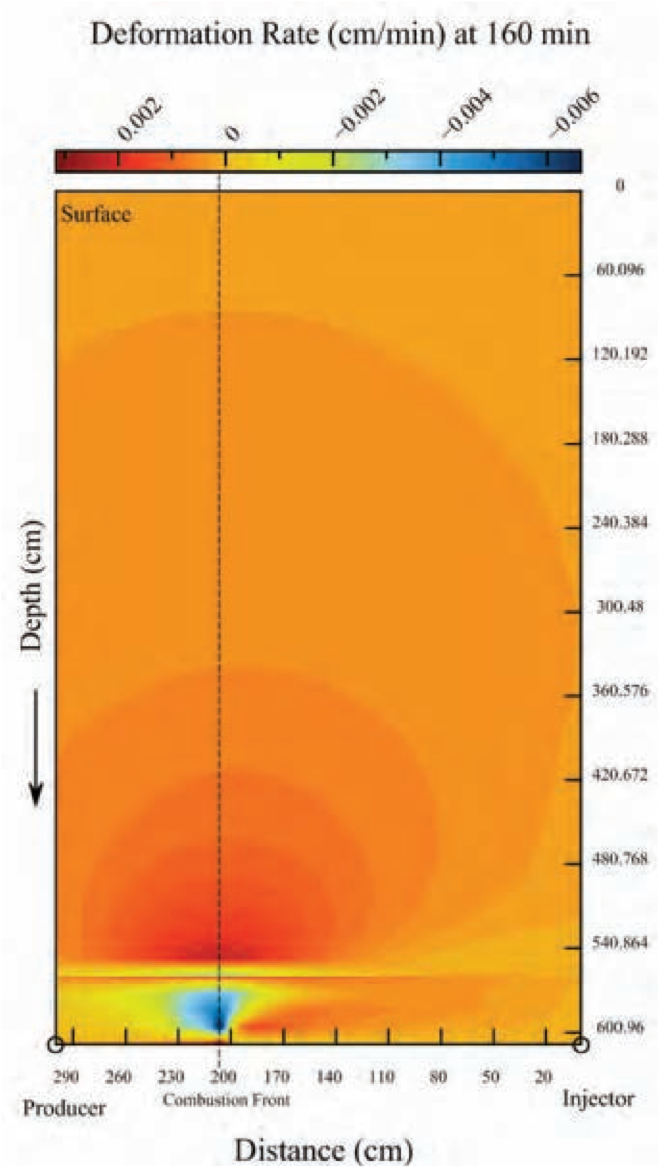


**Figure 3.** Example 1. Simulation of deformation rate versus depth when the combustion front propagates at 160 minutes after ignition.

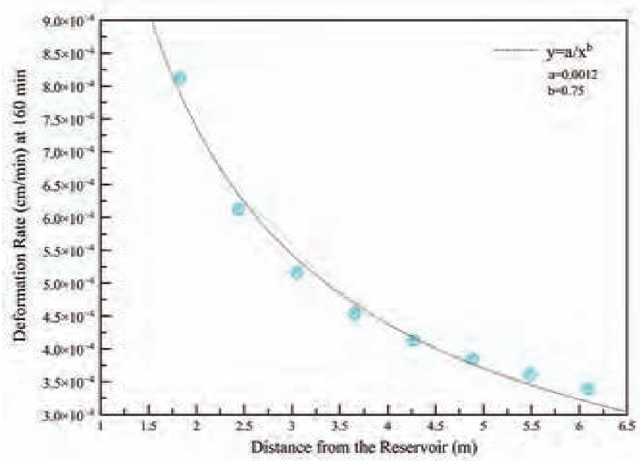


**Figure 4.** Example 1. Simulation of maximum deformation rate versus distance when the combustion front propagates.

as described by Bazargan and Kovscek (2018). The temperature profile history shows that the combustion front propagates from injector to producer. Figure 2 shows the deformation rate at 160 minutes 10 layers above the reservoir up to the surface. As shown in Figure 2, at 160 minutes, the combustion front (with peak temperature of 820°C) is located 204 cm from the injector. Because no heat loss is considered in the model, the peak temperature is larger than the observed value in combustion tube experiments (Bazargan et al., 2011). While analyzing the deformation rate of the reservoir (layer 1), we see the trend summarized in Figure 1. For all layers above the reservoir, we observe that the maximum deformation rate is located at the combustion front position. This result strongly supports the idea of using the maximum deformation rate for locating the combustion front. We see from Figure 3 that bulb-shaped stress profiles are produced inside the medium when the combustion front propagates in the reservoir. As shown in Figure 3, fine grid blocks are needed to simulate ISC phenomena and its relevant deformation profiles.

An important observation from Figures 2 and 3 is that the deformation rate decreases and the deformation rate profile spreads with vertical distance from the reservoir. The decrease is initially sharp (approximately 51% per meter for layer 10), then it is dampened (approximately 9% per meter for layer 90). In Figure 4, we plotted the maximum deformation rate versus distance from the reservoir. Interestingly, we see that the decrease in the maximum deformation rate fits the power law model ($y = ax^b$); exponent $b = -3/4$. According to Boussinesq's solution, the power law model with exponent $-3/4$ explains the distribution of vertical stress inside elastic media due to a line load. Thus, we expect a maximum surface deformation rate of 60 mm/year for a reservoir with an average depth of 100 m (Figure 8). Whereas, for a 3000 m deep reservoir, we expect a maximum deformation rate of 4.68 mm/year. Importantly, there appears to be enough temporal resolution to determine the position of the front once a year, even for the 3000 m deep reservoir.

Clearly, the length scale in this numerical example is not the reservoir scale. Ideally, we should simulate the reservoir scale using fine grids to accurately demonstrate the applicability of our method. Unfortunately, this is not feasible, and upscaling techniques must be implemented. Simulations using upscaled grid blocks have considerably smaller peak temperatures (due to volume averaging) and consequently smaller deformation rates. Simulation at the field scale underestimates the maximum deformation rate we could observe during actual ISC. Such results are, thus, conservative estimations of field trends. As described next, we use state-of-the-art upscaling techniques to obtain the deformation rate profiles.

## Example 2: Areal propagation of combustion front at reservoir scale

To show the trend of deformation rate caused by ISC at the reservoir scale, we apply an upscaling procedure originally proposed by Zhu et al. (2011) and Bazargan et al. (2011), which is implemented by Priestley et al. (2013) for Suplacu de Barcau Field simulation. Reservoir properties and kinetics parameters are obtained from Priestley et al. (2013) and Glatz (2011). Both $x$ and $y$ directions contain 40 grid blocks with $\Delta x = \Delta y = 2.4$ m. The media is simulated with 11 layers in the $z$ direction (from the reservoir to the surface) with $\Delta z = 6$ m. The reservoir layer contains oil with $S_o = 0.85$. The layers above have no oil and zero permeability.

Figure 5 shows the temperature profile in the reservoir layer 863 minutes after air injection. Peak temperature is 425°C, and the combustion front has traveled to the middle of the simulation grid at 863 minutes. Figure 6 shows the deformation rate for both reservoir and surface layers at 863 minutes. Comparing Figures 5 and 6, we see that the locations of maximum deformation rate for both reservoir and surface layers align with the combustion front position. Thus, we conclude that for a homogenous and isotropic medium with horizontal layers, the location of the maximum deformation rate of the surface is an accurate indicator of the combustion front position.

For a real reservoir case, the effect of heterogeneity and dipping layers may need to be considered and extra processing steps (similar to the seismic processing procedure) added. Furthermore, for a specific reservoir and area, the spatial and temporal resolution of InSAR data must be evaluated. Deep reservoirs and thickly vegetated areas decrease the temporal and spatial resolution, respectively.

## Field case: Suplacu de Barcau

The Suplacu de Barcau Field has a history of ISC dating to 1964 (Panait-Patica et al., 2006). Suplacu is a relatively shallow (35–200 m) and small dip (approximately 5°) reservoir with an average thickness of 10 m (Carcoana, 1990). The combustion front temperature is estimated to be approximately 600°C. These are favorable conditions to leave a strong surface deformation signal measurable by InSAR during ISC. Due to vegetation and nonhomogeneous distribution of structures (for radar scattering), the spatial resolution of InSAR measurement points is moderate (Figure 7). SAR data for time periods of 12 March 2003 to 28 July 2010 and 29 October 2014 to 19 June 2017 were used for analysis. The reservoir boundaries and advancement of the combustion front for 1964–2010 have been reported by Priestley et al. (2013). In Suplacu, an ISC pilot started in 1964 on a 1.25-acre inverted five-spot pattern. Upon incredibly favorable results (30 × increase in oil production), the area expanded to a 5-acre nine point. Between 1967 and 1971, six nine-point patterns were added to sustain 15 MMscf/day of air injection. In 1980, the air injection was increased to 65 MMscf/day through 50 air injection wells. Forming a line drive, a 5 km combustion front was created to follow the dip of the reservoir. In three years, the combustion front was extended to approximately 8 km through 100 air injection and 500 producer wells, with a total air injection rate of 100 MMscf/day. In 1984, the second combustion front was established approximately 900 m north of the existing project, but it was abandoned in 1997 due to limited success. Cyclic steam injection has been used to stimulate oil wells and ease oil production. The locations of air injection and cyclic steam wells in 2006 and 2010 are shown in Figure 9. Obviously, the combustion front should be located between the producer and injector. Compared to 1998, the

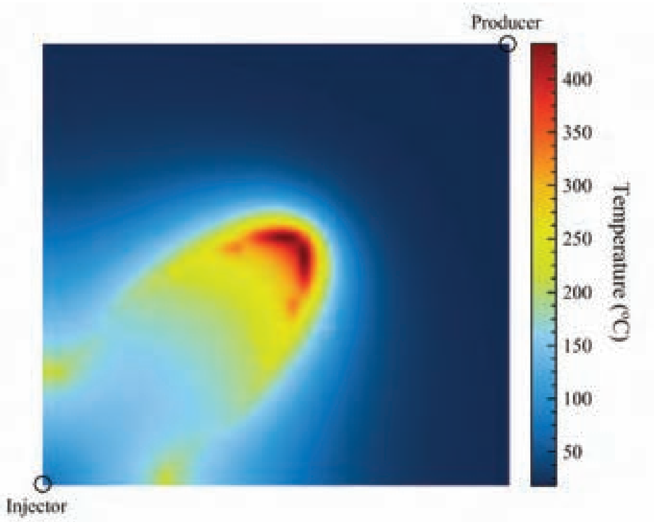


**Figure 5.** Example 2. Simulation model. Aerial view of temperature profile at 863 minutes. The aerial dimensions are 96 × 96 m.

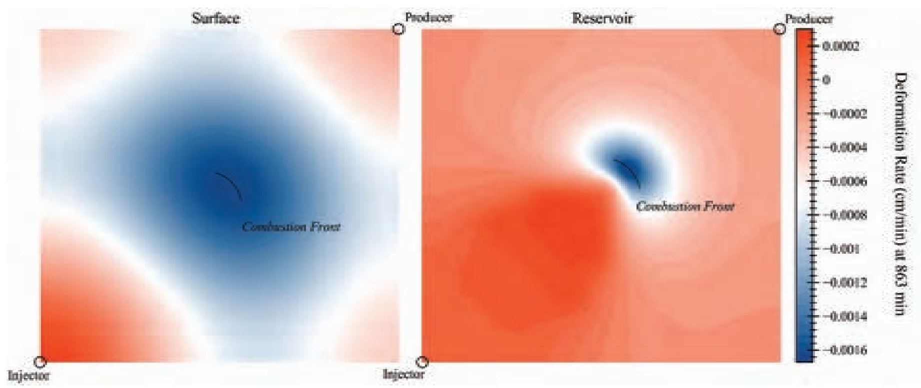


**Figure 6.** Example 2. Simulation of deformation rate for the (a) reservoir layer and (b) surface layer at 863 minutes.

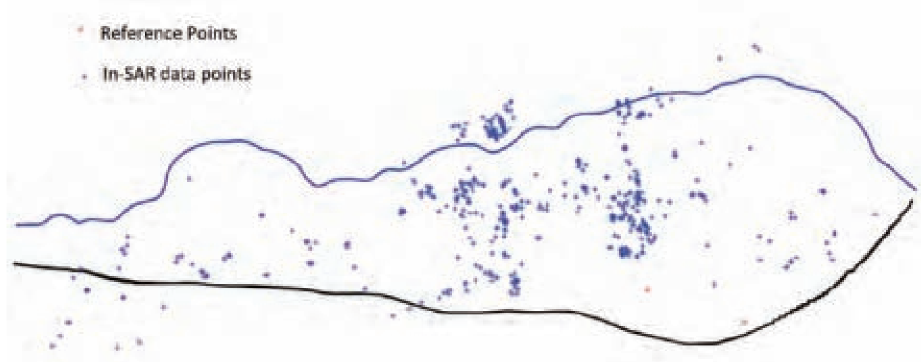


**Figure 7.** Reference points and InSAR data points from 12 March 2003 to 28 July 2010 in Suplacu de Barcau.

locations of air injection wells in 2006 have not considerably changed. In 2010, as shown in Figure 9, the oil production wells, close to the combustion front, have been replaced by air injection wells. Thus, we see a considerable change in the location of air injection wells in 2010 compared to 2006. The significant change in location of injection wells from 2006 to 2010 does not cause confusion about the location of the combustion front.

The reservoir boundaries and advancement of the combustion front for 1965–2010 have been reported by Priestly et al. (2013). This information is sufficient for us to proceed to analysis without reservoir simulation or upscaling. We apply our method to locate the combustion front in 2006, 2010, and 2017 using InSAR. Figure 7 shows the InSAR data points available from 12 March 2003 to 28 July 2010. We have transformed the satellite map into the reservoir map by using two reference points, exactly located by GPS on both maps. As mentioned earlier, spatial density of the data is moderate due to vegetated areas and urban structures. Fortunately, we have good data resolution in the areas where we suspect the front is located. Temporal resolution, on average is about 1 month for each of these points. Thus, we are able to obtain the surface deformation rate based on InSAR data. The next step is smoothing the raw deformation rate data and interpolating inside the boundaries of the Suplacu Field. We have used a robust quadratic regression (rloess) method for smoothing the data. Interpolation has been performed by implementing the natural-neighbor method. Both methods are implemented in MATLAB.

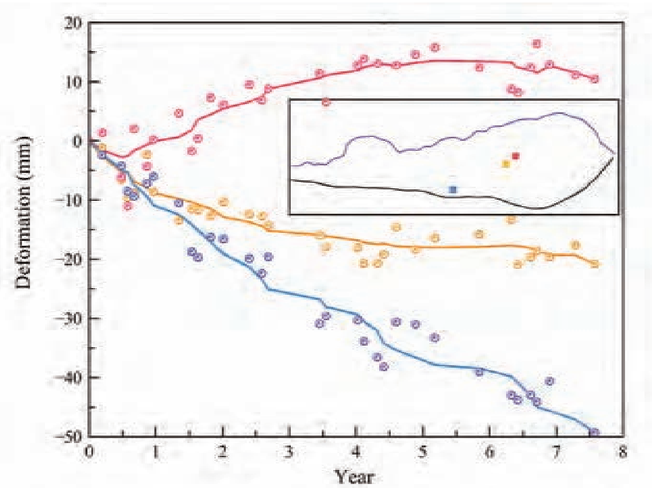


**Figure 8.** InSAR deformation of three points in a time series together with areal-averaging data during 7.5 years of ISC operation. Inset shows the location of the positions in the field in plan view. Front propagation is from the south to the north.

Figure 8 demonstrates time series (not in map view) from three points on the land surface above the reservoir to show that there is a change in deformation rate as the combustion front migrates. That is, InSAR shows how the surface velocity changes with time. It shows the deformation recorded for three surface points above the reservoir for 7.5 years. The inset within the figure shows the location of these three points on the ground surface. Recall that the front progresses from south to north. Both raw data and averaged data are shown in Figure 8. Note that the total deformation is over 10 mm at all points.

We see from Figure 8 that for two of the points (blue and orange), the combustion front has passed these positions because the deformation is constant and negative. The blue point is farther away from the combustion front than the orange point. The blue point shows more rapid negative deformation than the orange point. For the third point (red), we see a positive deformation rate until approximately 5.5 years, consistent with an approaching front. Then, we observe a peak and decline in deformation (negative deformation rate). This shows that the combustion front has reached this position at approximately 5.5 years. We conclude that the InSAR data in this field case are meaningful.

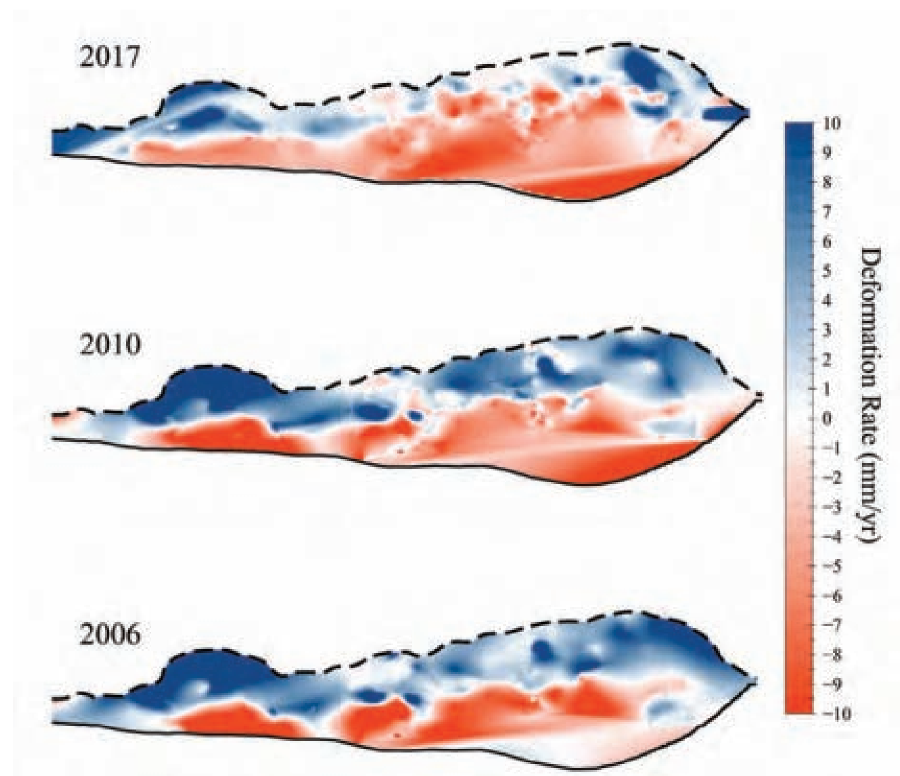


**Figure 9.** Deformation rate of Suplacu de Barcau Field obtained by InSAR data for 2006, 2010, and 2017.

Figure 9 shows the deformation rate of the Suplacu Field for 2006, 2010, and 2017. As shown in Figure 9, except from the regions in which the spatial data resolution is poor (see Figure 7), the deformation rate of Suplacu during ISC follows the pattern described in Figure 6. Because the reservoir has small dip, we expect the combustion front to be located at the local maximum of deformation rate. Comparing 2006, 2010, and 2017 maps, it is clear that the combustion front has moved northward in the plan view.

Figure 10 compares the predicted combustion front location based on local maximum of the surface deformation rate obtained from InSAR with actual data reported by Priestley et al. (2013) for 2006 and 2010. We see that the predicted combustion data are precisely located between the injection and production wells. It is interesting that the effect of a single air injection well on the southeast portion of the reservoir is predicted by using our method.

Based on the positive match between our prediction and reported data for location of the combustion front in 2006 and 2010, we predict the combustion front for 2017. Figure 11 shows our predicted combustion front for 2006, 2010, and 2017.

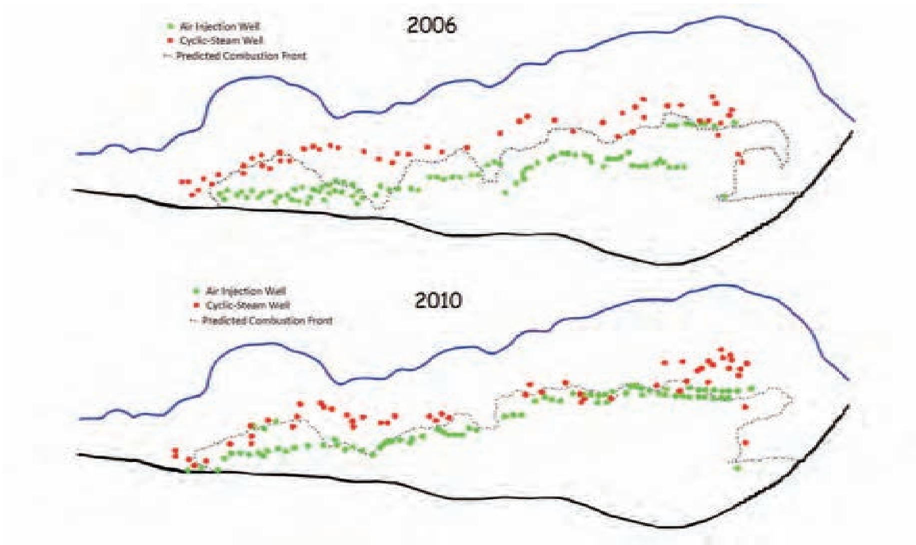


**Figure 10.** Air injection wells, oil production wells, and predicted combustion front (gray dashed line) for 2006 and 2010. The blue and black lines are the north and south reservoir boundaries, respectively.

## Future work

We have used a relatively shallow reservoir with near zero dip angle. Although the spatial resolution of the InSAR data was moderate, the temporal resolution was satisfactory for analysis. In future work, we would like to apply our method to a deeper reservoir that has smaller temporal resolution but greater spatial resolution. Also, similar to seismic processing procedures, we can add processing steps to include highly heterogeneous reservoirs with steeply dipping layers.

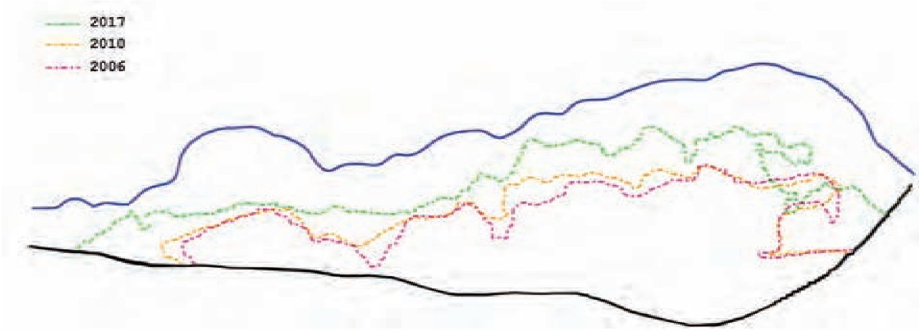


**Figure 11.** Predicted combustion front position for Suplacu de Barcau Field in 2006, 2010, and 2017. The blue and black lines are the north and south reservoir boundaries, respectively.

## Conclusion

We have shown that when the combustion front propagates inside a reservoir, it causes deformation at the surface above the field that is detectable by InSAR. Depending on the reservoir depth, geomechanical properties of the overburden, and surface conditions, the temporal and spatial InSAR signal is variable. We have demonstrated through two numerical simulation cases (one subreservoir-scale model using fine grids and one field-scale simulation using an upscaling technique) that the maximum deformation rate at the surface corresponds to the position of the combustion front in the reservoir if the layers are horizontal. We have applied our methodology in Suplacu de Barcau, which has a long history of ISC. We have concluded that the surface deformation rate follows the pattern suggested through numerical simulation. Moreover, the location of the combustion front determined by our method matches the historical data in 2006 and 2010. We have used InSAR, applied our method, and determined the location of the combustion front in 2017. TLE


## Acknowledgments

We acknowledge, with gratitude, the financial support of Ecopetrol and additional funding by the SUPRIA Industrial Affiliates.


## Data and materials availability

Data associated with this research are available and can be obtained by contacting the corresponding author.


Corresponding author: mozarg@stanford.edu


## References


Bazargan, M., and A. R. Kovscek, 2018, Pulsating linear in situ combustion: Why do we often observe oscillatory behavior?: Computational Geosciences, **22**, no. 5, 1115–1134, https://doi.org/10.1007/s10596-018-9741-9.

Bazargan, M., B. Chen, M. Cinar, G. Glatz, A. Lapene, Z. Zhu, L. M. Castanier, M. Gerritsen, and A. R. Kovscek, 2011, A combined experimental and simulation workflow to improve predictability of in situ combustion: Presented at Western North American Region Meeting, SPE, https://doi.org/10.2118/144599-MS.

Carcoana, A., 1990, Results and difficulties of the world's largest in-situ combustion process: Suplacu de Barcau Field, Romania: Presented at Enhanced Oil Recovery Symposium, SPE, https://doi.org/10.2118/20248-MS.

Das, B. M., 2013, Advanced soil mechanics, fourth edition: CRC Press, https://doi.org/10.1201/b15955.

Domenico, S. N., 1977, Elastic properties of unconsolidated porous sand reservoirs: Geophysics **42**, no. 7, 1339–1368, https://doi.org/10.1190/1.1440797.

Glatz, G., 2011, In-situ combustion kinetics of a central European crude for thermal EOR: Presented at Annual Technical Conference and Exhibition, SPE, https://doi.org/10.2118/152363-STU.

Gutiérrez, D., F. Skoreyko, R. G. Moore, S. A. Mehta, and M. G. Ursenbach, 2009, The challenge of predicting field performance of air injection projects based on laboratory and numerical modelling: Journal of Canadian Petroleum Technology, **48**, no. 4, https://doi.org/10.2118/09-04-23-DA.

Leezenberg, P. B., and M. E. Allan, 2017, InSAR: Pro-active technology for monitoring environmental safety and for reservoir management: Presented at Western Regional Meeting, SPE, https://doi.org/10.2118/185648-MS.

Panait-Patica, A., D. Serban, N. Ilie, L. Pavel, and N. Barsan, 2006, Suplacu de Barcau Field — A case history of a successful in-situ combustion exploitation: Presented at SPE Europec/EAGE Annual Conference and Exhibition, https://doi.org/10.2118/100346-MS.

Penberthy, W. L., and H. J. Ramey, 1966, Design and operation of laboratory combustion tubes: SPE Journal, **6**, no. 2, https://doi.org/ 10.2118/1290-PA.

Priestley, A., J. A. Ruiz, P. F. Naccache, G. Glatz, and V. Crecana, 2013, Modeling in-situ combustion in a heavy oil field in Romania: Presented at Heavy Oil Conference, SPE, https://doi.org/10.2118/165490-MS.

Sterrett, R. J., 1985, Advanced soil mechanics: EOS, **66**, no. 42, 713–717, https://doi.org/10.1029/EO066i042p00714-02.

van Leijen, F. J., 2014, Persistent scatterer interferometry based on geodetic estimation theory: TU Delft.

Zhu, Z., M. Bazargan, A. Lapene, M. Gerritsen, L. M. Castanier, and A. R. Kovscek, 2011, Upscaling for field-scale in-situ combustion simulation: Presented at Western North America Regional Meeting, SPE, https://doi.org/10.2118/144554-MS.

# Years of Arabian Peninsula gravity exploration by Chevron and its legacy companies, including discovery of the Ghawar and Burgan super-giants

Robert Pawlowski[1]

https://doi.org/10.1190/tle39040279.1


## Abstract

Exploration of the eastern Arabian Platform in the 1930s and 1940s by Chevron and its legacy company Gulf Oil resulted in discovery of Kuwait's super-giant Burgan Field by Gulf Oil in 1938 and Saudi Arabia's super-giant Ghawar Field by California Arabian Standard Oil Company in 1948. Ghawar Field and Burgan Field are widely regarded as the first- and second-largest oil fields in the world, respectively. Gravity methods featured prominently in Gulf's and Chevron's subsurface explorations. Gravity mapping identified the Burgan structure and was important in delineating the Ghawar structural complex. Gravimetric technology continues to provide value for deep exploration in Chevron's Partitioned Zone concession in Saudi Arabia and Kuwait.


## Ghawar and Burgan super-giants: Early exploration successes

> *"After a round of orange juice and coffee, we took him out to see the gravity meter. He clambered into the truck and had a look through the reading microscope . . . . As he stepped down from the truck, he asked the Crown Prince if he wanted to look, but Saud laughed and said, 'I'm no engineer.' After much handshaking, they departed."*
>
> — Vignette of King Abdul Aziz Al Saud and Crown Prince Saud's 1939 visit to a California Arabian Standard Oil Company gravity field crew as described in Barger (2000) (reproduced with the kind permission of Selwa Press).

Exploration of the eastern Arabian Platform in the 1930s and 1940s by Chevron and its legacy company Gulf Oil resulted in discovery of Kuwait's super-giant Burgan Field by Gulf Oil in 1938 and Saudi Arabia's super-giant Ghawar Field by California Arabian Standard Oil Company (CASOC) in 1948 (Figure 1). Both companies are Chevron legacy companies. Gulf Oil merged with Chevron in 1985, whereas CASOC was a subsidiary of Standard Oil Company of California and later became Arabian American Oil Company (Aramco) in 1944.

Ghawar Field and Burgan Field are widely regarded as the first- and second-largest oil fields in the world, respectively. Although the volume of Ghawar Field's proven recoverable reserves is maintained as a state secret, numerous published outside estimates range between 74 billion and 140 billion barrels (Sorkhabi, 2010). Ghawar's cumulative oil production through 2007 was stated by International Energy Agency as being more than 66 BBO (IEA, 2008). Similar murkiness surrounds Burgan Field's proven recoverable reserves, though numerous published estimates range from 32 billion to 75 billion barrels (Sorkhabi, 2012), with most estimates falling within the middle to high side of the range.

Gravity methods featured prominently in Gulf's and CASOC's subsurface explorations. Paul Foote, former executive vice president of Gulf Research and Development Company, wrote of Gulf Oil's 1938 Burgan discovery (Foote, 1948):

> *"…a geophysical party left the laboratory (fig. 17) and arrived at Kuwait at the head of the … Gulf (fig. 18) where, in a few months, possibly the largest oil field in the world was discovered. Figure 19 shows the geophysical camp in the desert. During a single winter season, the entire country of Kuwait was covered by a complete*


**Figure 1.** The super-giant Burgan and Ghawar oil fields were discovered by legacy Chevron companies in 1938 and 1948, respectively. Gravity mapping identified the Burgan structure and was important in delineating the Ghawar structural complex.

[1]Chevron Energy Technology Company, Houston, Texas, USA. E-mail: rpawlowski@chevron.com.

*checkerboard of magnetic and gravity measurements. The structure finally selected was confirmed by the reflection seismograph and is now known as the Burghan anticline."*

The famous Gulf gravimeter, designed by Gulf Research and Development Company and fielded for regular geophysical operations in 1936, was a capable and precise instrument. Repeated gravity observations made at certain stations (20 to 30 observations per station) during the Kuwait field work resulted in Gulf concluding the probable, normally distributed error for a single observation in the Kuwait survey to be on the order of 0.04 mGal (Wyckoff, 1941) — a level of measurement precision adequate for much exploration work today. It can be seen in Figure 2 that the 43 kg Gulf gravimeter was more massive and less portable than modern meters like the Scintrex CG-5 (8 kg) and LaCoste & Romberg Model G meter (10 kg).

In Saudi Arabia, Max Steineke, CASOC's legendary chief geologist, advocated the identification and detailing of subsurface structures through a highly integrated methodology, one that included the gravity method because of its ability to delineate positive anomaly trends related to subsurface structures. The Proterozoic basement-cored En Nala antiform trend associated with the Ghawar Field was initially detected by surface mapping (e.g., "creekology"-style analysis of drainage and dissolution features), supplemented later by gravity mapping — this prior to World War II. Regarding exploration activity after the war, Aramco staff (1959) wrote:

*"…structure drilling supplemented by gravity-magnetic mapping was used to define wildcat locations in the Ain Dar and Haradh area …*

*"… The part of the En Nala axis surmounted by Ghawar shows a strong positive gravity anomaly (Fig. 3a.). In general, the coincidence between gravity mapping and structure is remarkably close.*

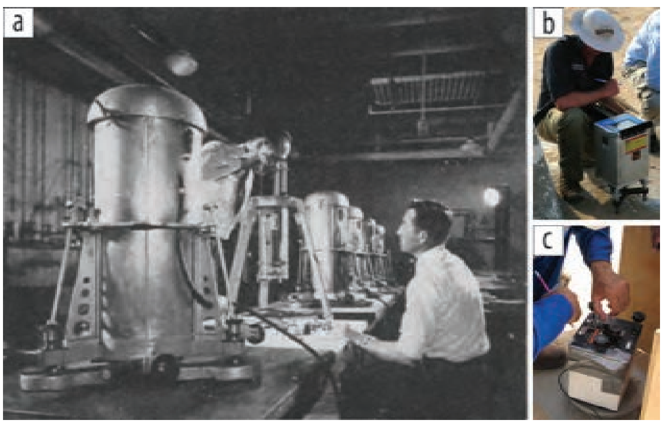


**Figure 2.** (a) The famous Gulf gravimeter. After a Gulf Oil R&D effort starting in late 1932, and a successful field trial in 1935, improved models were deployed in 1936 for Gulf's regular geophysical field operations (Wyckoff, 1941). The image is reproduced with permission of the American Philosophical Society from Figure 6 of Foote (1948). It is interesting to compare the Gulf gravimeter with smaller, lighter, and more portable modern gravimeters such as (b) the Scintrex CG-5 meter (Saudi Arabian Chevron Wafra Joint Operations photograph) and (c) the LaCoste & Romberg Model G meter (photo by author).

*In some areas, south Ain Dar, gravity control is better than shallow structure drill data."*

The efficacy of gravity anomaly contour mapping as a proxy for subsurface structure is a characteristic of the eastern Arabian Platform region's major producing structures and trends (Figure 3).

The success enjoyed by Gulf Oil and Chevron in detailing the Burgan and Ghawar basement-involved subsurface structures with gravity mapping is related to an extremely favorable distribution of rock bulk-average densities that occurs in the subsurface. With exception of the Permian Khuff carbonates, the Paleozoic section is primarily a siliciclastic section. Available analog data/evidence (e.g., published wireline density and porosity logs) from farther south in Saudi Arabia suggests that this clastic-dominated interval corresponds on average to a lower-density zone sandwiched between higher-density carbonate/evaporite units above and a higher-density basement complex below (Figure 4), making it an excellent target for gravity exploration methods (and probably magnetotelluric techniques as well). This aspect accounts for why the northerly trending, Proterozoic basement-cored mega-regional structural "arch" trends of the eastern Arabian Platform tend to be excellently expressed in gravity anomaly data (e.g., Qatar Arch trend, Ghawar/En Nala trend, Khurais/Wafra/Burgan trend).

## Chevron's deep exploration of the Partitioned Zone of Saudi Arabia and Kuwait

Moving to the present, gravimetric (and magnetic) methods continue to provide value for deep exploration in Chevron's

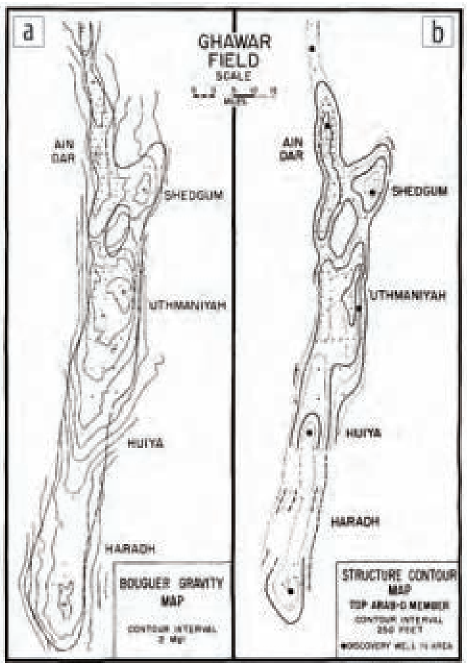


**Figure 3.** Ghawar Field, Saudi Arabia. The correspondence between (a) gravity contours and (b) the Jurassic Arab-D Member structure contours is remarkable. The image is reproduced from Figures 3a and 3b of Arabian American Oil Company Staff (1959). AAPG © 1959, reprinted by permission of the AAPG whose permission is required for further use.

Partitioned Zone concession in Saudi Arabia and Kuwait (Figure 5). Chevron and its legacy companies (Getty Oil Company, Saudi Arabian Texaco) have utilized gravity exploration techniques in the Partitioned Zone since the first gravity survey was executed there in 1949.

Although large volumes of oil have been produced since 1954 from the Partitioned Zone's Tertiary and Mesozoic reservoirs, its Paleozoic remains undrilled. Exploration and exploitation of deep opportunities is impeded by significant technological and geophysical imaging challenges. The carbonate-and-evaporite-prone Tertiary and Mesozoic sedimentary sequences for instance give rise to severe seismic-multiple interference and reduced signal-to-noise for seismic-event energy from the underlying Paleozoic section. Seismic data are therefore only partially adequate for resolving the Paleozoic geology, which is why gravity and magnetic anomaly data are useful for Paleozoic exploration.

Within the Partitioned Zone, gravimetric anomaly data are effective for mapping basement structural trends inherited from the Precambrian Amar Collision/Orogeny, as well as basement depressions where the Paleozoic reservoir-and-source-rock interval, if present, is likely to be thickest and best preserved. The Paleozoic-age fault framework originated from rejuvenation of the older basement structures, with the north–northwest-trending horst-graben architecture controlling the distribution of the main Paleozoic siliciclastic sediment trends. Periodically reactivated basement structures have contributed to the formation of structural and stratigraphic petroleum traps and acted as reefal nucleation centers.

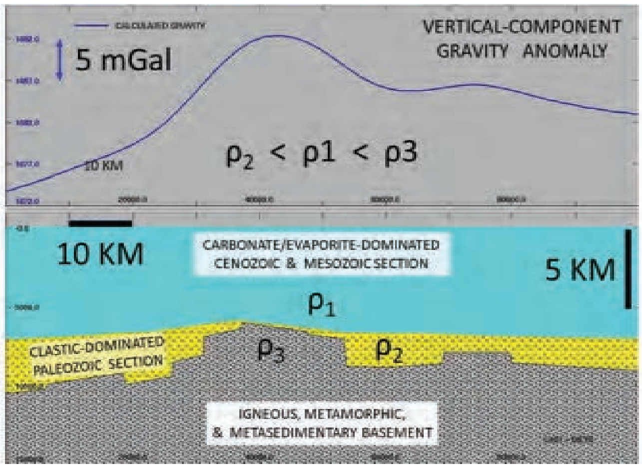


**Figure 4.** Arabian Platform deep-exploration concept illustrated with a conceptual cross section and modeled gravity anomaly. (Note: cross section is schematic and does not correspond to an actual location.) Sedimentary structures above basement level tend to be broad and low relief in nature, with the basement complex exhibiting greater structural relief. Consequently, the siliciclastic-dominated Paleozoic section represents a lower-density interval ($\rho 2$) adjacent to the higher-density basement complex ($\rho 3$), making it an excellent target for gravity exploration methods.

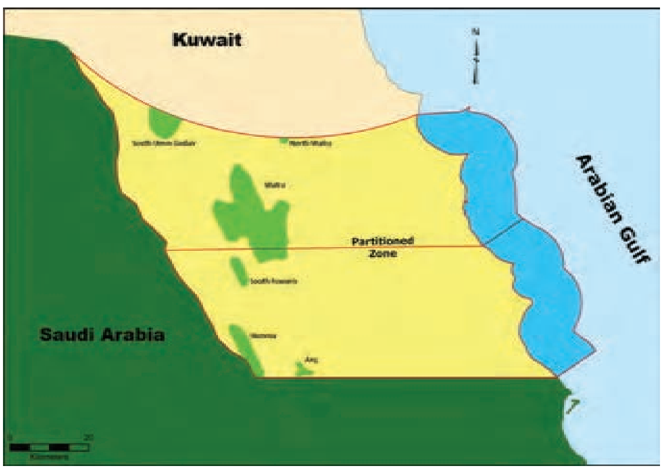


**Figure 5.** Saudi Arabian Chevron's Partitioned Zone concession. The six main field areas are Wafra, South Umm Gudair, South Fuwaris, Humma, Arq, and North Wafra. As with Burgan and Ghawar fields, Wafra Field is structurally controlled by a reactivated Proterozoic basement fault system, the associated horst-graben complex of which is well manifested in gravity anomaly data.

## A time line for Chevron's gravity exploration of the Arabian Peninsula

Chevron and its legacy companies (Gulf, Texaco, Getty Oil, Pacific Western) have a rich history of utilizing gravity and magnetic exploration methods in the Arabian Platform region, a history spanning more than eight decades.

### 1936 and 1937
### State of Kuwait: Exploration land geophysical surveying

Gulf Oil Company commences reconnaissance land geophysical surveys in Kuwait. Two Gulf gravimeters and three magnetometers (Schmidt vertical balances) are deployed (in addition to a seismic crew). Gravimetry proves useful for mapping subsurface structure, including the super-giant Burgan Field. In Kuwait, 4442 gravity stations and 2257 magnetic stations are observed (Boots and McKee, 1946).

### 1938
### Kingdom of Saudi Arabia: Exploration land gravity surveying

A CASOC gravity meter team arrives in Saudi Arabia to commence land gravity surveying in support of CASOC's structure-drilling program. Geologist Paul T. Walton was hired by Standard Oil of California to lead CASOC's first gravity-survey team, where the gravity work (as mentioned) contributed to the discovery of several major fields (Vaughan, 1999). Walton established himself as a great oil finder.

In 1948, Walton was hired by Jean Paul Getty to evaluate the prospectivity of the Partitioned Zone (or Neutral Zone, as it was then called). Getty was aware of Walton's successful and valuable exploration experience in Saudi Arabia and was hoping to secure an oil position for himself in the Middle East. During the Neutral Zone reconnaissance and evaluation, Walton was the first geologist to identify the possibility (and glimpse the potential) of a large prospective subsurface structure (today's super-giant Wafra Oil Field) from aerial observation of a low-relief topographic rise (Figure 5). In 1949, he went on to successfully negotiate the Neutral Zone concession for Getty's Pacific Western Oil Company (later to be organized as a component within Getty Oil), making Getty a major Middle East oil player.

Texaco's acquisition of Getty Oil in 1984 resulted in Saudi Arabian Texaco taking over Getty Oil's Partitioned Zone operations. Chevron's merger with Texaco in 2001 led to Chevron obtaining the Partitioned Zone concession (operated today by Saudi Arabian Chevron).

### 1949
### Partitioned Zone of Saudi Arabia and Kuwait: Exploration land gravity surveying

Aminoil's (American Independent Oil Company) and Pacific Western Oil Company's (later Getty Oil Company) Joint Operations acquires land gravity data (approximately 2100 stations) over most of the Partitioned Zone, prior to drilling the first wells in the zone. Gravity Meter Exploration Company conducts the gravity surveying.

### 2010
### Partitioned Zone of Saudi Arabia and Kuwait: Microgravity survey pilot study for near-surface geohazard detection

Wafra Joint Operations (Saudi Arabian Chevron's and Kuwait Gulf Oil Company's joint operating entity) executes a microgravity geohazard survey (conducted by WesternGeco Kuwait) in the southwest Partitioned Zone to assess the gravity method's efficacy for near-surface dissolution feature detection (karst and sinkholes).

### 2010
### Partitioned Zone of Saudi Arabia and Kuwait: Land gravity infill-survey to support deep-well planning

Wafra Joint Operations executes a 2D land gravity program in the southwest Partitioned Zone to assist well-location evaluation and planning for the zone's first Paleozoic well.

WesternGeco geophysical crew 3303 fields two surveyor teams and two gravity-meter teams to execute the nine-line, 611-station survey. Maintaining stable gravimeter temperatures in the convection-oven-like environment was a challenge, with constant winds and midday temperatures peaking as high as 55° C (130° F).

Land gravity data were acquired at a 500 m spacing along nine traverses to fill voids in existing gravity coverage and regions of poor-quality seismic imaging. Most gravity traverses were chosen to coincide with legacy 2D seismic lines.

### 2012
### Partitioned Zone of Saudi Arabia and Kuwait: Land gravity swath-survey for airborne gravity gradiometer evaluation

Wafra Joint Operations acquires a 500-station land gravity "swath survey" for use in verifying and evaluating the performance of an airborne full tensor gravity gradiometer (FTG) survey system (flown in late 2012 and early 2013).

Acquisition of a rectangular, 5 × 26 km swath of 500 land gravity stations by Daishsat Pty. Ltd. (Daishsat Geodetic Surveyors) was used to verify/evaluate performance of an airborne gravity gradiometer survey system deployed to the Partitioned Zone in 2012–2013. A Scintrex model CG-5 automated gravimeter used during the survey is shown in Figure 11.

**Figure 6.** Geophysical survey vehicles at Gulf Research Laboratories in 1936, prior to their shipment to Kuwait. The image is reproduced with permission of the American Philosophical Society from Figure 17 of Foote (1948).

**Figure 7.** Gulf Oil geophysical camp in Kuwait, 1936. The image is reproduced with permission of the American Philosophical Society from Figure 19 of Foote (1948).


**Figure 8.** (a) First-half 2010 microgravity surveying to assess the method's utility for near-surface geohazard characterization. (b) Partitioned Zone sinkhole. Chevron photographs.

### 2012 and 2013
### Partitioned Zone of Saudi Arabia and Kuwait: Airborne FTG and magnetic survey

Wafra Joint Operations executes an FTG, magnetic total intensity, and LiDAR survey (9923 line-km program) of the onshore and offshore Partitioned Zone to aid deep exploration. A 750 × 4000 m flight-line program was acquired by ARKeX Ltd. TLE


**Figure 9.** July 2010. (a) Real-time kinematic GPS surveying of gravity station locations. (b) Gravity meter reading, using the survey vehicle and a wooden shield to mitigate unwanted meter vibrations from wind and windblown sand. Chevron photographs.

**Figure 10.** July 2010. Gravity measurement being made on a tripod plate at a local survey base station with a Lacoste & Romberg Model G gravimeter. Wooden shield provides shade and mitigates unwanted meter vibrations from wind and windblown sand. Photo by the author.

**Figure 11.** October 2012. Partitioned Zone land gravity swath survey. Gravity measurement being made with a Scintrex model CG-5. gravimeter. Saudi Arabian Chevron Wafra Joint Operations photograph.


**Figure 12.** February 2013. Kuwait International Airport. Geophysical survey aircraft used during the Partitioned Zone 2012–2013 FTG survey. Saudi Arabian Chevron Wafra Joint Operations photographs. The nose boom magnetometer can be seen.

## Acknowledgments

I thank the managements of Chevron Energy Technology Company and Saudi Arabian Chevron for permission to publish this geophysical history. I am also grateful for the support of the Saudi Arabian Ministry of Energy, Industry and Mineral Resources. Selwa Press graciously allowed use of the opening vignette taken from the letters of Thomas C. Barger. The American Philosophical Society generously allowed republication of the excerpt from Paul D. Foote's 1948 paper as well as three photographs from the same paper (my Figures 2, 6, and 7). I acknowledge the American Association of Petroleum Geologists for its special fair use permission policy allowing republication of the illustration shown in my Figure 3. Finally, I thank the manuscript reviewers for their contributions in improving the article.

## Data and materials availability

Data associated with this research are confidential and cannot be released.

Corresponding author: rpawlowski@chevron.com

## References

Arabian American Oil Company Staff, 1959, Ghawar Oil Field, Saudi Arabia: Bulletin of the American Association of Petroleum Geologists, **43**, no. 2, 434–454.

Barger, T. C., 2000, Out in the blue: Letters from Arabia 1937–1940: Selwa Press.

Boots, P. H., and A. H. McKee, 1946, Geophysical operations in Kuwait: Geophysics, **11**, no. 2, 164-177, https://doi.org/10.1190/1.1437234.

Foote, P. D., 1948, The discovery of an oil field: Proceedings of the American Philosophical Society, **92**, no. 1, 15–25.

IEA, 2008, World Energy Outlook 2008: IEA, Paris, https://www.iea.org/reports/world-energy-outlook-2008, accessed 20 February 2020.

Sorkhabi, R., 2010, The king of giant fields: GEO ExPro, **7**, no. 4, 24–29.

Sorkhabi, R., 2012, The great Burgan Field, Kuwait: GEO ExPro, **9**, no. 1, 42–46.

Vaughan, R. H., 1999, Paul T. Walton (1914–1998), memorial: AAPG Bulletin, **83**, no. 5, 815–816.

Wyckoff, R. D., 1941, The Gulf gravimeter: Geophysics, **6**, no. 1, 13–33, https://doi.org/10.1190/1.1443704.

# GEOPHYSICS Bright Spots

COORDINATED BY JYOTI BEHURA

Welcome to a new collection of GEOPHYSICS Bright Spots. Below is a list of research that the editors found interesting in the latest issue of GEOPHYSICS. Although there are only two recommendations, there are more articles in the issue that present wonderful ideas and analysis. For example, one article that I found to be a great read is "Imaging of a fluid injection process using geophysical data — A didactic example" by Commer et al. in which the authors present an approach to image hydrologic properties that determine subsurface changes resulting from fluid injection. If that topic, or either of the topics presented in the following, pique your interest, please read the full GEOPHYSICS article.

## Modifying the seismic air gun to reduce its environmental impact

In marine seismic acquisition, data are commonly acquired using large air-gun arrays as the source and long hydrophone streamers as receivers. This acquisition system is robust, reliable, and generates data within the frequency band of interest for subsurface imaging (3–200 Hz). However, air-gun source arrays emit more sound at higher frequencies than needed for subsurface imaging, and these frequencies are not recorded because of the limited sampling of hydrophones (typically 2 ms). These high frequencies could disrupt the communication between marine mammals. Therefore, there is increased interest in reducing high frequencies generated by air-gun arrays. Various purpose-built source types have been invented or are under development. In "The impact of bubble curtains on seismic air-gun signatures and its high-frequency emission," Wehner and Landrø investigate the potential use of bubble curtains placed close to conventional air guns to mitigate these high frequencies. They conduct tank experiments using different configurations of a bubble curtain attached to an air gun (Figure 1). The experimental results indicate a reduced peak amplitude with an active bubble curtain, which leads to the mitigation of high frequencies. At the same time, low frequencies are practically unaffected by the bubble curtain. Upon comparing the experimental results to synthetic data, the authors attribute the reduction in peak amplitude to the buffer effect of the bubble curtain on the released air. Hence, a small bubble curtain concentrated around the gun ports could be an efficient and practical way to reduce high-frequency acoustic emissions. From a practical point of view, the authors are of the opinion that such bubble curtains can be installed easily on existing systems. These tank experiments may trigger further investigations resulting in field trials.

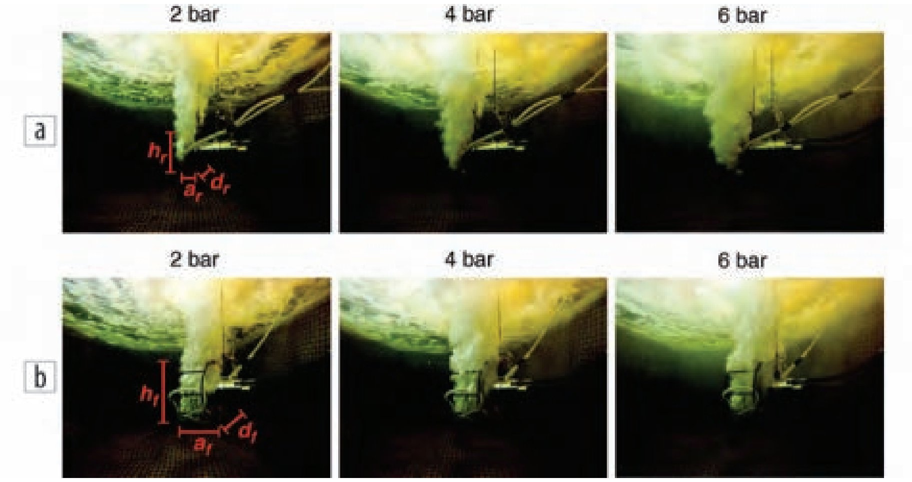


**Figure 1.** (Figures 4 and 5 from Wehner and Landrø.) Single air gun with (a) the bubble curtain directly injected at the gun ports and (b) injected at a metal frame attached to the gun. The amount of injected air increases from left to right, as indicated by the pressure values.

## Accounting for a time-varying sea surface in seismic modeling

Seismic data processing flows often ignore the spatial and temporal variations in the sea surface during marine seismic acquisition by assuming an idealized flat sea surface. However, weather patterns during data acquisition can generate rough sea conditions,

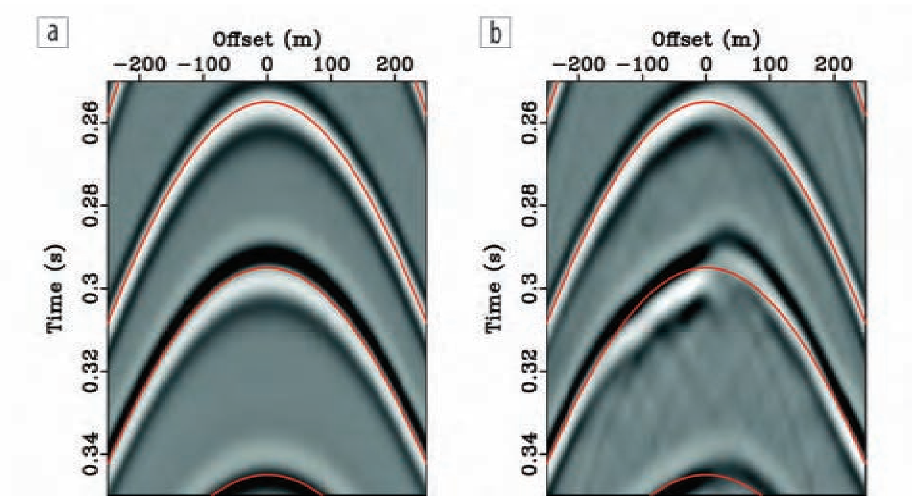


**Figure 2.** (Figure 8 from Konuk and Shragge.) Portions of shot gathers for (a) flat and (b) time-varying sea-surface profiles with 5 m significant wave height. The red lines indicate the theoretical traveltime surfaces corresponding to the event arrivals computed with a flat free surface. Note that rough sea conditions introduce traveltime perturbations to ghost and multiple reflections.

which can influence seismic full-wavefield behavior significantly by introducing spatial and temporal distortions to any seismic event interacting with the sea surface. Figure 2 shows these distortions on two different seismic data, simulated assuming flat and time-varying rough sea surfaces, with the traveltimes for the flat sea surface overlaid on both panels. Compared to the flat sea response, all events reflected from the time-varying sea surface exhibit various traveltime and amplitude perturbations due to the irregular sea-surface geometry. Improperly handling these distortion effects can degrade data quality severely and penalize seismic data resolution. There are numerous approaches for addressing this issue. However, these methods either face significant challenges in providing numerically accurate and stable solutions or are limited in their ability to model the full-wavefield phenomena. To investigate the effects of rough sea on seismic wave propagation, in "Modeling full-wavefield time-varying sea-surface effects on seismic data: A mimetic finite-difference approach," Konuk and Shragge develop and solve a new acoustic wave equation using a numerical scheme that employs a dynamic (i.e., moving) generalized coordinate system defined to be conformal to the assumed known time-varying sea surface. This sea-surface coordinate system allows the authors to model the full dynamic effects associated with this complex boundary. The developed method can accurately simulate seismic wavefield propagation on a moving mesh. Thus, it is a reliable tool for applications involving modeling, processing, imaging, and inversion of seismic data acquired in rough seas. TLE

# Reviews

Coordinated by Amit Padhi

**The Fossil Fuel Revolution: Shale Gas and Tight Oil**, by Daniel Soeder and Scyller Borglum, ISBN 978-0-128-15397-0, 2019, Elsevier, 354 p., US$127.50 (print), US$127.50 (eBook).

A fairly strong case could be made that one of the most significant events of the past 15 years was the development of major new sources of oil and natural gas in the United States. In addition to providing a large boost to a declining industry, it had a strong impact on global politics and the environment. For example, the United States is now much less dependent on oil imports, and new supplies of natural gas have enabled a large reduction in burning coal to generate electricity. This valuable book reviews the history of these developments in detail, with a focus on understanding how the industry got to its current state and what the immediate future may bring.

The key technologies that opened the new resources are hydraulic fracturing and advances in directional drilling. Together, they are now labe\led simply as fracking. The operational procedures were developed largely by the efforts of George Mitchell and his company to tap the gas resources of the Barnett Shale in Texas. Over many years, they found that by drilling horizontally along the shale beds and by modifying fracturing techniques, they could stimulate production from the entire volume of source rock. Mitchell's success in the late 1990s led numerous companies to adapt their methods to other shale basins, with eight more major plays coming into production between 2004 and 2009. Of note is the Bakken Formation in the northern plains, which was the first to include oil production starting in 2006.

More than half of the book discusses the geology of unconventional oil and gas resources compared to the conventional oil and gas fields that dominated the industry throughout the 20th century. This leads to summaries of numerous specific examples, including geologic setting, discovery and development history, and future potential. There are three groups of case histories: early successes in the United States, current and future plays there, and an outline of shale plays in the rest of the world.

The remaining sections of the book review the many complex issues related to the oil and gas industry in general and shale resources in particular. These include dealing with environmental risks and climate change, maintaining the security of energy supply to modern economies, setting equitable taxes and incentives for fossil fuels and renewable energy sources, and managing global concerns related to vast differences in energy resources between regions.

The authors do a commendable job of presenting multiple aspects of these debates, considering that the word "fracking" is now contentious and certain to generate heated argument between people who disagree as to whether or not it is a good thing.

While overall this is an excellent work, it could have been improved in a few ways. There are no details on new horizontal drilling technologies; the case histories are almost exclusively about the geologic work. Sections seem to have been written to stand independently, as numerous details are repeated several times. The illustrations are monochrome and appear to be mostly reprints from larger color originals, often making the details and captions nearly unreadable. The use of acronyms is sometimes excessive and not all are defined in the glossary or text.

Caveats aside, I would recommend this book to anyone interested in the current state of the oil and gas industry and its place in a world of rapid global warming.

— William R. Green
North Vancouver, British Columbia

**Mathematical Methods in the Earth and Environmental Sciences**, by Adrian Burd, ISBN 978-1-107-11748-8, 2019, Cambridge University Press, 596 p., US$64.99 (print), US$52 (eBook).

As the title indicates, this book is on mathematical methods used by earth and environmental scientists. As such, you will not find coverage of advanced topics important to theoretical geophysicists. You will, however, find coverage of topics of specific interest and use in earth and environmental sciences, such as calculating rough estimates of quantities, isometric and allometric scaling arguments, and dimensional analysis. These are topics not normally covered in standard texts on mathematical methods of physics. These particular topics are covered in some detail in the first chapter, along with useful examples from earth and environmental sciences.

The book is intended for earth and environmental science students and practitioners who have forgotten much of the basic mathematics they learned in their undergraduate years or for those who never learned it in the first place. Hence, the second and remaining chapters cover basic single-variable and multivariable calculus, linear algebra, probability, ordinary and partial differential equations, vector calculus, special functions, Fourier series, Fourier and Laplace transforms, and tensor analysis. This is convenient for those who need to review these topics, because they are all included in one book. Of course, this also means that there is not as much material covered as in standard mathematical texts. However, all of the basic and essential topics appear to be covered in sufficient detail. Topics of particular relevance to earth and environmental scientists that may not be found in standard mathematical texts are also covered including Monte Carlo methods, nondimensionalization, and scaling.

Each chapter contains, where possible, examples from earth and environmental sciences along with the basic mathematical development of the various topics. Chapters end with a section on further reading in which the author gives brief and useful descriptions of other books on the topics covered in the chapter. Exercises are interspersed throughout the text and included at the ends of chapters to help the reader better understand the topics.

Throughout the text, the author uses an easy-to-read conversational style to explain and prove rules and results. The website for the book contains additional resources, such as computer programs for numerical computations and exercise solutions for instructors.

If you need to review the basic mathematics used in earth and environmental sciences and do not want to dig out five or six mathematical texts to do so, this is the book for you.

— Edward S. Krebes
University of Calgary

**Geophysics: A Very Short Introduction**, by William Lowrie, ISBN 978-0-198-79295-6, 2018, Oxford University Press, 160 p., US$11.95 (print).

This book is one of more than 550 texts in the "Very Short Introduction" series published by Oxford University Press, which offers a stimulating and accessible means of studying a new subject. As the title implies, the book is short, but it is also quite comprehensive. It is written by an acknowledged expert in geophysics.

An overview of the subject is covered in Chapter 1, where the author explains the internal and external processes that affect the planet, as well as the principles and methods of geophysics that are used to investigate them. Chapter 2 discusses the solar system, the constituent planets, and their orbits. Kepler's laws of planetary motion are then presented, with a good historical review included. The chapter concludes with a discussion of the Chandler wobble, the effects of the moon and Jupiter on the earth's rotation, and the Milankovitch cycles of climatic variation.

In Chapter 3, seismology and the earth's internal structure are presented. From analyses of the earth's deepest interior to measurements made from earth-orbiting satellites, the author shows how geophysical exploration is vitally important in the search for mineral resources. The author also emphasizes our need to understand the history of our planet and the processes that govern its continuing evolution. This chapter will be familiar to most geophysicists, since it covers topics such as elastic deformation; seismic body waves (P- and S-waves); seismic surface waves and free oscillations; reflection, refraction, and diffraction of body waves and their paths through the earth; the internal structure of the earth; seismic tomography; the structure of the continental crust; and seismic noise. Again, the author includes many useful historical facts.

Earthquake seismology is developed in some detail in Chapter 4. Magnitude and intensity of earthquakes are discussed followed by secondary effects. Epicenter location and global seismicity are presented followed by a discussion of fault-plane solutions and focal mechanisms. Earthquakes at plate margins are then considered, together with earthquake monitoring and prediction methods. The author explains how analysis of seismic waves produced in earthquakes can reveal the internal structure of the earth.

Chapter 5 discusses the implications of gravity on the earth's shape, its variation with depth, the reference ellipsoid and geoid, satellite geodesy, tides, gravity surveying, Bouguer and free-air gravity anomalies, and the development of the three theoretical models underlying isostasy.

The earth's heat is considered in Chapter 6. Heat sources are discussed, together with the flow of heat through the earth's surface, the temperature inside the earth, thermal convection and mantle flow, and mantle convections and plumes. Geophysicists have established that the greatest source of energy powering geologic processes is the earth's internal heat. Deep inside the earth, the temperature is high enough to produce a fluid outer core of molten iron.

Chapter 7 explores this further and considers the earth's magnetic field. It begins with a description of the geomagnetic dynamo and geomagnetism. Essentially, the author explains that it is the motion in this molten iron layer that produces the earth's magnetic field, which shields the planet against harmful radiation from the sun and outer space, making the planet habitable. The magnetic field also magnetizes rocks during their formation, leaving a permanent record of the ancient field and its direction that geophysicists have learned to use to interpret past motions of the continents and tectonic plates. The sun's effect on the earth's magnetic field is then discussed, followed closely by a description of the magnetic fields of other planets. The magnetic properties of rocks are then considered. The chapter concludes with a discussion of paleomagnetism, the apparent polar wander and continental drift, geomagnetic polarity reversals, oceanic magnetic anomalies, and plate tectonics.

The final chapter is a refreshing treatise that summarizes some of the technical and political developments and implications of geophysics in our modern world.

The book's content is well organized, and the text is generously illustrated with many quality diagrams, figures, tables, and images. The book is also supplemented at the end with a list of useful introductory books on earth sciences, specific topics in geophysics, and geophysical textbooks for more in-depth reading.

In summary, this book provides an excellent and comprehensive introductory overview of the science of geophysics.

— William A. Sandham
Glasgow, United Kingdom

## Laurence (Larry) Richard Lines
## 7 March 1949–25 November 2019

Larry Lines' voicemail greeting, "Hello, hello, hello," was a cheerful arpeggio that conveyed his welcoming spirit and generous enthusiasm. His characteristic handshake reinforced his love of people and his wonderful ability to engage. Larry's gentle but formidable dedication to his family, friends, and colleagues was deeply enriching. His contributions to the science of geophysics and service to our profession are legion and profoundly inspirational. Larry served as editor of Geophysics in 1997–1999, coeditor of the *Canadian Journal of Exploration Geophysics*, and published widely on key topics in geophysics, including tomography, inversion, migration, and interpretation. He was president of the Society of Exploration Geophysicists (SEG) in 2008–2009. In recognition of his extraordinary services, he received many awards and honors, including SEG Honorary Membership in 2000 and the Canadian Society of Exploration Geophysicists (CSEG) Medal in 2017. Larry passed away on 25 November 2019 after a short but valiant battle with cancer. He made many memories for us while helping to build numerous futures.

### The early years

*Larry was born on 7 March 1949 in Athabasca, Alberta, Canada, to Laurence and Agnes (Richards) Lines. After 18 years growing up on the family farm, Larry went on to earn degrees from the University of Alberta (UofA) (BS 1971, MS 1973) and the University of British Columbia (UBC) (PhD 1976).*

Larry Lines: "A cheerful glow in the midst of the geophysics community … "

**William (Bill) Cumming:** Larry Lines became my first geophysics colleague when we shared a bench desk at UBC in 1974–1976. His thesis was more entertaining than mine, and he was generous in acknowledging any contribution, however incidental. In response to the many tributes that he received over the decades for his contributions to research, education, and the geophysical profession, Larry would attribute his success to his roots on an Athabasca farm and the support of his family and colleagues. His style of leadership was subtle, marked by gentle manners, active kindness, and good humor in service of a resolute dedication to principle.

### Living on Tulsa time

*After graduate school, Larry began his career in exploration geophysics. He married Shirley Pritchard in Calgary in 1978, and they moved to Tulsa, Oklahoma, USA, where Larry and Shirley raised two children, Wendy and Andrew.*

**Sven Treitel:** Larry actually visited Amoco's Tulsa center several years before he joined us. The late Tad Ulrych at UBC was his PhD advisor; he sent Larry to Tulsa to obtain data for his thesis. We were all so impressed with Larry's knowledge of exploration seismology that we persuaded our Calgary office to offer him a job, with the option of a later transfer to Tulsa. At Amoco, Larry rapidly made a name for himself as one of our most innovative and prolific research scientists, quickly managing to become widely known in industry and academe through his many publications, some of which I was privileged to coauthor with him. This collaboration lasted for some two decades. During this time, Larry and I established the closest of friendships, one that had endured and grown until his untimely passing. Larry had a sparkling personality. He was such a gentle soul who always saw the good in people. He leaves a gaping void in all who were privileged to know and work with him.

**Sam Gray:** I met Larry when I interviewed for a job at Amoco's research lab. I was immediately struck by how gracious he seemed, and I knew I wanted to work there. I got the job, fortunately in the same group as Larry, and my first impression was reinforced every day. I also learned quickly how knowledgeable and brilliant he was, and I got to witness firsthand some of the earliest applications of inverse theory in geophysics. Only gradually did I learn about Larry's sense of humor — gentle, in keeping with his personality, but always to the point. Luckily, Larry and I kept up during his second career in academia. The mutual dedication between Larry and his students was clear, and it inspired all.

## Back in Canada

*In 1993, Larry's work shifted from industry to academia, and he moved from Amoco's Research Center to Memorial University of Newfoundland in St. John's as a Chair in Applied Seismology. Returning to Canada also meant a cooler climate, perfect for enjoying daily walks with a beloved Alaskan Malamute. Each of Larry's Malamutes — Aurora, then Denali, then Pearl — were his constant companions, and the pair walking together were a comforting fixture in each of Larry's home communities. Larry had a chance to return to his native Alberta and University of Calgary (UofC) from Newfoundland. He left the decision up to Shirley. She said that they were going!*

**Don Lawton and Bernhard Mayer:** With his return to Alberta in 1997, Larry's career continued to flourish as a professor in the Department of Geology and Geophysics at UofC. He successfully led numerous research grants and consortia, educated hundreds of students, and brought deep integrity and enjoyment to his academic and professional communities. He had an exceptional blend of skills and values: his love and knowledge of science, his insatiable curiosity and enjoyment of learning, his unmatched way of connecting with people from all walks of life, and his uncanny ability to share a song in his soothing bass voice (in choir or in the classroom). Throughout his career, he published more than 50 peer-reviewed journal papers and hundreds of refereed conference contributions that are frequently cited in the academic community and widely utilized by industry practitioners. From 1997 to 2002, Larry held the CSEG Chair in Exploration Geophysics at UofC. Furthermore, he served as director of the Consortium for Heavy Oil Research by University Scientists, was associate director of the Consortium for Research in Elastic Wave Exploration Seismology (CREWES) and the Fold-Fault Research Project, and cogenerated several million dollars in research funds. From 2002 to 2007, Larry was head of the Department of Geology and Geophysics. During his tenure at UofC, he instructed six different undergraduate courses in two departments and taught four graduate courses. He supervised or cosupervised a highly impressive number of 73 graduate students. His numerous conference presentations and publications ensured that new academic knowledge was rapidly taken up in practical applications in industry. Larry was a tremendous academic citizen, a great human being and friend, and a truly kind man. We cannot remember a single occasion when, upon being asked to take on a duty or task, Larry would not have said with a happy face "Yes of course, I'd be glad to!" A graduate memorial scholarship is being established in Larry's honor at UofC. More information can be found at https://netcommunity.ucalgary.ca/larrylinesmemorialaward.

**Gary Margrave:** I met Larry when he joined the faculty at UofC, and right away, I recognized a kindred spirit. Immensely knowledgeable and incredibly congenial, Larry was the perfect colleague and friend. I've never known anyone else with such a profound combination of wisdom, humility, and friendliness. We had many common interests in geophysics, and I often benefited from his insight, which was always offered in a way that both complimented and, if need be, gently corrected. Larry was always a role model for gracious professional conduct. We are nearly the same age, and while I retired several years before Larry, I was very much looking forward to a continued "senior" collaboration following his retirement this past September. Now sadly, without Larry, I can hear him saying "The future ain't what it used to be."

**Brian Russell:** I met Larry in 1976 in Calgary at the start of our careers with Amoco and Chevron. Over the course of our long friendship we spent a lot of time on the same committees, first the *TLE* Editorial Board and then the SEG Executive Committee, and in Larry I observed the most hardworking (and soft-hearted) individual I have ever known. In 2002, I had the good fortune to go back to UofC as Larry's "mature" graduate student. The next four years were the most stimulating of my life, as Larry expertly guided

**Above:** Wearing a cap bearing the insignia of his beloved New York Yankees, Larry pitches in the UofC departmental softball game. **Left:** Larry with one of his Malamutes as a pup.


UofC and CREWES faculty — Rob Stewart, Don Lawton, Larry Lines, and Gary Margrave.

me to my PhD. Since we lived very close to each other in Calgary, my favorite memories are our weekend walks with his beloved Malamutes at the park between our houses. I will miss Larry very much.

**Mauricio Sacchi:** I met Larry in 1997 when I moved to Alberta, but I knew about his work because he was one of my scientific heroes when I was an undergraduate working on wavelet estimation and deconvolution. Larry's contributions to geophysics are impressive; he has worked on deconvolution, tomographic inversion, reverse time migration, amplitude variation with offset inversion, heavy-oil production, reservoir geophysics, etc. Larry's modesty and friendly nature have had a significant imprint on many of us and, undoubtedly, he will be missed.

**Kris Innanen:** I met Larry in 1998, when he visited UBC near the start of my degree. My impression then was of a thoughtful man who transmitted scientific ideas so gently that it could be days before you realized you had learned something. This hasn't really changed much in the intervening years, especially the last 10 in which I worked closely with him at UofC. In trying to say a brief word about what was essential about Larry, I thought of his questioning of students during their (rather stressful) oral exams — asking deep questions, and then struggling to be tough in getting the answers against his natural tendency to help the student through. He would lose that struggle pretty often. We would rib him for it, and he would tell us he'd be tougher next time. He never was. But, that was the man — committed to his science but with a prevailing instinct for human kindness. I will miss that, and him, greatly.

**Satinder Chopra:** Larry was a man of many individual traits. I first met him when I started volunteering for the *CSEG Recorder* in September 2000 and later got to know him more when I interviewed him. My next significant collaboration with him was when we compiled the contributed papers for a heavy oils workshop into a book published by SEG in 2010. This led us again to serve together as coeditors for the *Canadian Journal of Exploration Geophysics*. I always found Larry a humble human being, approachable, friendly, always kind and smiling, generous with his time and effort, and above all an engaging person. We will treasure Larry's wonderful memories forever.


Larry Lines and Rachel Newrick during the CSEG 2017 Symposium.

**Daniel Trad:** Larry was shining sunlight on a cloudy day. He was always friendly and open to help with his generosity. His contributions to geophysics were abundant, but his amazing gentleness was even bigger. He would have such a warm presence that we all felt about him like family. He contributed to CREWES over the years in many ways, but probably the part we will remember the most was his friendship and warm mentorship.

**Doug Schmitt:** Larry would always joke to me about our reversing latitudes from our Albertan origins (his in the north and mine in the deep south) to the southerly UofC and the northerly UofA. Despite this geographical complication, we came to work together on issues related to heavy-oil exploration and characterization. A particular high point of this was our joint organization of what may have been the best-attended SEG Development and Production Forum on topics related to the geophysics of heavy oils, bitumen-related topics, along with a field trip to the oil sands at Fort McMurray in 2007. This led to the popular SEG volume *Heavy Oils: Reservoir Characterization and Production Monitoring*.

**Phil Bording:** Larry's motto was always upbeat and positive — "Let's write a paper" and on occasion "let's write a book," and so many of his collaborators and I did. We used the Treitel motto of using known models to generate data, and if the results were good, then try real seismic data. Not long ago, Larry started rewriting our book on waves and called me last summer with a great deal of pride. He had finished 17 chapters, and now it was my turn to do editing and writing. I will finish the new book slowly but surely over the next year or so. Many a day and evening were spent with Dr. Lines and his family. He had an amazing memory and could tell you who drove in the winning run to win the World Series or the winning goal in a Stanley Cup hockey game for any year of your choice. I will miss him.

**Rob Stewart:** Larry was an excellent scientist, but also a character. He was adept at not just seismic analysis, but song and skits. At one department event, he had several of us dress as The Spice Girls and perform the song, "Wannabee." In another musical event, Larry organized the "CREWES Brothers" in a takeoff on the Blues Brothers singing, "Rollin', rollin', rolling" with words he adapted for geoscience. While he had numerous pastimes (his encyclopedic knowledge and love of baseball were legendary), Larry's technical writing and thinking were always impeccable. We've used his and Dr. Rachel Newrick's classic book, *Fundamentals of Geophysical Interpretation*, extensively in courses. His paper on least-squares inversion has more than 800 citations alone. It was always wonderful to work with Larry on geophysical topics but also in writing about the university-industry interaction, how to effectively communicate geophysics, and in composing tributes to other geophysicists. Larry could turn our thinking upside down with "cooperative inversion" as well as correct our "frowns into smiles."

Larry dances with his wife, Shirley, during the Presidential Jam at the 2010 SEG Annual Meeting in Denver, Colorado.

**Rachel Newrick**: A cheerful glow in the midst of the geophysics community went out when Larry passed away. At conferences, we will miss the moment when Larry catches our eye and waves in recognition. His animated interest in our latest work will no longer be part of the experience at technical meetings. Dog photos will no longer appear randomly in seismic presentations, yet Larry lives on within all of us.

The day after Larry's passing, 18 students in London, England, were interpreting a seismic line from our textbook, and I had yet another reason to reflect on how immense his influence was and how in some way he helped all of us grow.

*Larry is survived by his loving wife, Shirley; children, Wendy (Craig) Benoit and Andrew (Sarah) Lines both of Calgary; and grandchildren, Ruby and Alice of Calgary. Larry is also survived by his four brothers, Gordon (Dolores), Robert (Mon), Ron (Lorraine), and Darren (Wanida); as well as numerous other relatives and friends.*

*With these recollections and tributes, we commemorate our good friend Larry Lines. We honor his fine life, well lived. He enriched us and our science, and we will long remember and treasure him.*

— By Don Lawton, Rob Stewart, Sven Treitel with many of Larry's friends

## The Leading Edge

# Errata

The October 2019 *TLE* article by Connolly, "Elastic reflectivity vectors and the geometry of intercept-gradient crossplots," contained two errors in Table 2 on page 763. In Table 2, the $c_3$ coefficient for the "gradient" AVO parameter was incorrectly published as –2k. It should be −4k. Additionally, in the bottom row of the $c_3$ coefficient column, the term $\cos\chi + 4k\sin\chi$ should be $\cos\chi - 4k\sin\chi$. The corrected table is presented here.

**Table 2.** Coefficients of equation 5 for AVO parameters and angle-dependent reflectivities.

| AVO terms | | $c_1$ | $c_2$ | $c_3$ |
|---|---|---|---|---|
| Intercept | A | 1 | 0 | 1 |
| Gradient | B | 0 | −8k | −4k |
| Curvature | C | 1 | 0 | 0 |
| | $R(\theta)$ | $1 + \tan^2\theta$ | $-8k\sin^2\theta$ | $1 - 4k\sin^2\theta$ |
| | $R(\chi)$ | $\cos(\chi) + \sin(\chi)$ | $-8k\sin(\chi)$ | $\cos\chi - 4k\sin\chi$ |

The March 2020 *TLE* article by Alexandrov et al., "Normal faulting activated by hydraulic fracturing: A case study from the Barnett Shale, Fort Worth Basin," contained an error in the third author's affiliation and e-mail address. Umair bin Waheed's correct affiliation is King Fahd University of Petroleum and Minerals, and the correct e-mail address for the author is umair.waheed@kfupm.edu.sa.

# Announcements

## Nominees for SEG Board of Directors

The following Active Members have been selected by the SEG Committee on Nominations and have agreed to be candidates for the 2020–2021 SEG Board of Directors:

**President-elect**
Guillaume Cambois and Anna Shaughnessy
**Second vice president**
Bruce Shang and Huasheng Zheng
**Treasurer**
Pete Cramer and Xuri Huang
**Director at large**
Mohammed Badri and Sherif M. Hanafy
**Director at large**
Johannes Douma and Brandy Hawkins

In addition to the Board of Directors election, all Districts are holding elections for one new representative. The nominees are:

**District 1**
Patrice Nsoga Mahob and Tania Mukherjee
**District 2**
Frank Brown and Tracy Stark
**District 3**
Karen Christopherson and Sarah Gach
**District 4**
Debotyam Maity and Douglas Schmitt
**District 5**
Carmen Dumitrescu and Rachel Newrick
**District 6**
Javier Nuñez Ariza and Ana Curcio
**District 7**
Anton Bogrash and Yuriy Ivanov
**District 8**
Horst Rueter
**District 9**
Uche Irene Aigbokhai and Isaac Muneji Marobhe
**District 10**
Sankhadip Bhattacharya and Shokhrukh Shomurodov
**District 11**
Yonghyun Chung and Yang Liu
**District 12**
Ahmad Riza Ghazali and Teck Kean Lim

Nominations in writing, signed by at least 40 Voting Members and accompanied by the written consent of the candidate and a brief biography, ready for publication, may be submitted prior to 15 May. The biographies of the Board candidates and their position statements will be published in *TLE*. Survey & Ballot Systems Inc. will handle SEG elections again this year and will send ballots by 15 June. Eligible voters who have a valid e-mail address on file with SEG will receive personalized pass-code information in an e-mail. Voting will end on 31 July with results announced in early August. The new Board will begin its term at the end of the 2020 Annual Meeting and complete its term at the end of the 2021 Annual Meeting. Elected District Representatives will serve a two-year term beginning 1 August 2020.

Active, Emeritus, Honorary, Life, and Associate members are eligible to vote on all matters submitted to the membership; however, members failing to pay dues by 1 June will not be eligible to vote in the 2020 election. TLE

# Membership

Applications for Active membership have been received from the candidates listed below. This publication does not constitute election but places the names before the membership at large in accordance with SEG's Bylaws, Article III, Section 5. If any member has information bearing on the qualifications of these candidates, it should be sent to the SEG president within 30 days.

### Requirements for membership

Active: Eight years of professional experience practicing or teaching geophysics or a related scientific field. Membership applications and details of other types of membership, including Associate, Student, and Corporate, may be obtained at https://seg.org/membership.

### For Active membership

Abdeldayem, Abdelaziz (Arab Republic of Egypt)
Abdulla Alarabi, Shaima Ibrahim (UAE)
Adeleye, Aji (UK)
Ajiboye, Saheed (USA)
Akinbode, Olisa (Nigeria)
Alawadhi, Muneera (Kuwait)
Al Habsi, Ahmed (Oman)
Alhammadi, Miaad (UAE)
Al-Ismaili, Ali (Oman)
Allo, Paulus Tangke (Indonesia)
Al-Mahmeed, Mona (Kuwait)
Almubarak, Yousef (Saudi Arabia)
Al Qatari, Haidar (Saudi Arabia)
Alreesh, Wesam (Kuwait)
Alshafei, Ali (Saudi Arabia)
Alshammari, Abdullah (Saudi Arabia)
Al-Shehri, Eman (Kuwait)
Al Wadhahi, Taimur (Oman)
Anderson, Edward (UK)
Bacon, Bradley (USA)
Barnett, David (USA)
Becel, Anne (USA)
Bellian, Jerome (USA)
Black, Robert (Oman)
Boucard, Daniel (France)
Bradbury, Neil (Canada)
Camacho, Hilario (USA)
Cao, Chenghao (China)
Carley, Shane (USA)
Carotti, Diego (Oman)
Chen, Suyang (UK)
Chen, Yingpeng (UAE)
Chowdhury, Bidyut (India)
Craddock, Andrew (Australia)
Davie, William (UK)
De Freminville, Thibault (France)
Ding, Liangbo (China)
Ebed, Atef (UK)
Ehanire, Alexander (Nigeria)
El Asrag, Ramy (Oman)
Fan, Yijing (Singapore)
Farhan, Bassam (Kuwait)
Farouq Ali, S. M. (USA)
Froneberger, Mark (USA)
Fu, Boye (China)
Fu, Chao (China)
Gesbert, Stephane (Netherlands)
Ghazali, Faizan Akasyah (Malaysia)
Gill, Claire (UAE)
Gupta, Menal (USA)
Habsi, Nasser (UAE)
Hamilton, Angus (Kuwait)
Hand, Nicolas (Australia)
Haumonte, Luc (France)
He, Jiahuan (China)
He, Tao (China)
Hugonnet, Pierre (France)
Ibeneme, Ikechukwu (Nigeria)
Ion, Dumitru (Saudi Arabia)
Jacobs, Rhonda (USA)
Jagger, Martin (UAE)
Jasbinsek, John (USA)
Jin, Jing (Singapore)
Joshi, Rahul (India)
Kumar, Jyoti (Malaysia)
Kumar, Sanjeev (Kuwait)
Kurin, Evgeny (Russian Federation)
Laurent, Olivier (France)
Lima, Isabela (Germany)
Li, Sijia (China)
Liu, Pandeng (China)
Liu, Weihua (China)
Liu, Yujin (China)
Louro, Vinicius (Brazil)
Lovheim, Leon (Norway)
Lu, Li (Canada)
Luo, Miao (China)
Machado, Marcos (Brazil)
Madden, Sammuel (USA)
Maia, Daniel (Brazil)
Majhi, Nirban (India)
Majid, Maziah (Malaysia)
Malone, Andrew (Kuwait)
Matende, Kitso (Botswana)
Ma, Xinhai (China)
Membrouk, Mohamed (Kuwait)
Mender, Jufriady (Kuwait)

Mihaljevic, Ivica (UAE)
Mudavakkat, Anandan (Kuwait)
Mugumya, Firminus (Uganda)
Naumann, Sören (Norway)
Neves, Fernando (France)
Norris, Justin (Australia)
Nwaka, Gozie (Nigeria)
Obaid, Khalid (UAE)
Onaneye, Omololu Alfred (South Africa)
Oropeza, Simon (USA)
Pica, Antonio (France)
Prout, Martin (UK)
Purbokusumo, Riyanto (Kuwait)
Qi, Qunli (UAE)
Rasouli, Vamegh (USA)
Retailleau, Matthieu (France)
Rice, Shawn (USA)
Rodriguez, Arnold (USA)
Sarkar, Sebabrata (USA)
Schjolberg, Kolbjorn (Netherlands)
Selvakumar, Arjun (USA)
Sen, Ashok (Kuwait)
Sharma, Subhash Kumar (India)
Shen, Hui (China)
Shi, Suzhen (China)
Silveira, Renato (Brazil)
Singh, Shwet (Kuwait)
Singh, Sunil (Kuwait)
Steiner, Stefan (UAE)
Sun, Shan (China)
Takacs, Erno (Hungary)
Talbi, Sami (UAE)
Tang, Jian (China)
Tarde, Cyril (France)
Tertrais, Bertrand (UAE)
Vera Rodriguez, Ismael (Norway)
Vivin, Lilas (France)
Wang, Daxing (China)
Wang, Enjiang (China)
Wang, Yi (USA)
Webb, Andrew (UK)
Wu, Dakui (China)
Yamanaka, Motoyoshi (UAE)
Yao, Menglin (China)
Youssef, Tahar (Oman)
Zhao, Mingqiu (UAE)
Zhou, Keming (China)
Zou, Changchun (China)

### For transfer to Active membership

Allroggen, Niklas (Germany)
Alsaad, Ali (Saudi Arabia)
Anandito, Muhammad (Indonesia)
Anantharamu, Venkatesh (USA)
Andrade, Hector (Mexico)
Bucknill, Michael (Australia)
Chin Tee, Ang (Malaysia)
Contreras, Fabio (Mozambique)
Cunningham, Craig (USA)
Falkovskiy, Alexander (Canada)
Gaines, David (USA)
Gao, Yingjie (China)
Grant, Ashley (Australia)
Hawkins, Brandy (USA)
Hobro, James (UK)
Hoy, Torben (Norway)
Kozawa, Takeshi (Japan)
Latter, Julie (Canada)
Leslie, Stephen (USA)
Msezane, Bhekithemba (South Africa)
O'Connell, Daniel (USA)
Pearce, Paul (USA)
Ras, Paul (Netherlands)
Tatanova, Maria (Brunei Darussalam)
Vargas-Jimenez, Carlos (Colombia)
Westerman, Julius (USA)

# Calendar

*Conference and workshop dates remain in flux due to the effects of coronavirus disease 2019 (COVID-19). The following dates were accurate as of 23 March 2020. For the latest updates, please check https://seg.org/events/events-calendar.*

## APRIL 2020

### POSTPONED (NEW DATE TBD)
URTeC One Day Workshop: Boosting Production, Cutting Costs, Testing New Technologies and Analytics
https://urtec.org/workshops/denver2020
**Denver, Colorado, USA**

### POSTPONED UNTIL 12–16 APRIL 2021
16th Multidisciplinary Conference on Sinkholes and the Engineering and Environmental Impacts of Karst
http://www.sinkholeconference.com
**San Juan, Puerto Rico**

## MAY 2020

### POSTPONED UNTIL 3RD QUARTER 2020
Offshore Technology Conference
http://2020.otcnet.org
**Houston, Texas, USA**

### POSTPONED UNTIL 10–11 NOVEMBER 2020
2nd Joint SBGf-SEG Workshop on Machine Learning
https://seg.org/events/second-workshop-on-machine-learning
**Rio de Janeiro, Brazil**

### POSTPONED (NEW DATE TBD)
Asia-Pacific Geophysics Student Conference
http://apgsc.ustc.edu.cn
**Hefei, Anhui, China**

### 20 MAY
2nd SEG Virtual Student Conference
https://www.eventbrite.co.uk/e/2nd-european-virtual-student-conference-registration-89226830853
**Virtual**

## JUNE 2020

### 2–4 JUN
SEG/AGU Advances in Distributed Sensing for Geophysics Workshop
https://seg.org/events/distributed-sensing-for-geophysics
**Houston, Texas, USA**

### 14–19 JUN
18th International Conference on Ground Penetrating Radar
http://gpr2020.csmspace.com
**Golden, Colorado, USA**

## JULY 2020

### POSTPONED UNTIL 2021 (DATE TBD)
9th International Geosciences Student Conference
http://igsc2020.rwth-aachen.de
**Aachen, Germany**

### 20–22 JUL
Unconventional Resources Technology Conference
https://urtec.org/2020
**Austin, Texas, USA**

### 20–24 JUL
Summer Research Workshop: Maintaining True Seismic Amplitudes from Sensor to Image
https://seg.org/events/maintaining-true-seismic-amplitudes-from-sensor-to-image-workshop
**Park City, Utah, USA**

## AUGUST 2020

### 10–13 AUG
Summer Research Workshop: Data Analytics and Machine Learning for Exploration and Production
https://seg.org/events/data-analytics-and-machine-learning-for-e-and-p
**Denver, Colorado, USA**

### 12–13 AUG
Summer NAPE
http://napeexpo.com/summer
**Houston, Texas, USA**

### 17–19 AUG
Offshore Technology Conference Asia
http://2020.otcasia.org
**Kuala Lumpur, Malaysia**

### 25–26 AUG
SEG/SPE Advanced Geoscience Workshop: Applications in Drilling and Well Placement
https://seg.org/events/applications-in-drilling-and-well-placement
**Kuala Lumpur, Malaysia**

## SEPTEMBER 2020

### 13–14 SEP
2nd SEG/DGS Workshop: Advances in Quantitative Seismic Reservoir Characterization
https://seg.org/events/reservoir-characterization-2020
**Bahrain**

### 14–17 SEP
The 14th Middle East Geosciences Conference and Exhibition
https://geo-expo.com
**Bahrain**

### 22–23 SEP
Complex Overburden and High End Imaging Workshop
https://seg.org/events/complex-overburden-and-high-end-imaging-workshop
**Kuala Lumpur, Malaysia**

### 29 SEP–1 OCT
SEG/DGS Workshop: Challenges and New Advances in Velocity Model Building
https://seg.org/events/velocity-model-building
**Al Khobar, Saudi Arabia**

## OCTOBER 2020

### 11–16 OCT
SEG International Exhibition and 90th Annual Meeting
https://seg.org/am
**Houston, Texas, USA**

### 25–27 OCT
Seismic Processing Advances for Reservoir Characterization Workshop
**Muscat, Oman**

# Episode 74: Dave Monk reassesses survey design in light of modern processing techniques

The following is an excerpt from SEG's podcast, Seismic Soundoff. In this episode, host Andrew Geary previews Dave Monk's upcoming Distinguished Instructor Short Course and book titled, "Survey design and seismic acquisition for land, marine, and in-between in light of new technology and techniques." In this engaging conversation, Dave and Andrew discuss how full-waveform inversion impacts survey design, the research breakthroughs needed for the next evolution of seismic surveys, and one group that may not realize that this course is for them. Listen to the full episode at https://seg.org/podcast/post/8946.

**Andrew Geary: What questions helped guide your reassessment of survey design?**

**Dave Monk:** How should I design a survey, given that I may want to use compressive sensing? Why do my data not look like the data that I'm used to interpreting? What's changed, and how should I be interpreting data today?

I think one of the most important changes is full-waveform inversion. People ask, how should I design a survey if I know I'm going to use full-waveform inversion? And what sort of bandwidth do I need to ensure that I get in the data to make full-waveform inversion useful to me at the end of the day?

**Geary: What differences could arise while utilizing this classic survey design with something like full-waveform inversion?**

**Monk:** Surveys that we designed five to 10 years ago were limited in the amount of equipment that we could deploy. They were often limited in offsets between the source and the receiver. When we're doing full-waveform inversion, we need to get some very long offsets. So, surveys that were shot five years ago are not necessarily appropriate if we're going to use full-waveform inversion.

The other issue with full-waveform inversion is that we need to get some very low frequencies into the ground and recover them. New sources are being developed that allow us to put much lower frequencies into the ground. If we didn't have that information in the older surveys, we couldn't start the full-waveform inversion process.

**Geary: What research breakthroughs are needed to improve seismic surveys in the future?**

**Monk:** That's a really interesting question. We know how to solve the problems associated with imaging in the earth; we just haven't had the computer power in the past to be able to implement the solutions. We know how to do full-waveform inversion, but until recently, we certainly were not able to do it.

Things are changing. We can solve some problems that we've known how to solve. But there are a couple of problems that haunt geophysicists, including areas of the world that exhibit really strong interbed multiples. We don't know yet how to solve that problem. If somebody came up with a solution to that, I'm sure the industry would be beating a path to their door, because there are certain areas of the world where that problem exacerbates the issue to see the subsurface. I'm thinking of places like the Gulf of Suez or offshore Canada. So, I think breakthroughs in the area of solving the problem of interbed multiples are going to change what we do in the future.

**Geary: While reading the description of your course, who may not realize that it is for them?**

**Monk:** The seismic workflow starts with the person who designs the survey, and then people go and acquire it, and the end product is something that goes to the interpreters. I think those are the people that may look at this and say, "This is a seismic survey design. It's at the other end of the workflow. I'm not sure that this is for me." But they're wrong, because they need to understand how the data are derived that end up on their desk so they can do the interpretation.

**Geary: What excites you about the future of this topic?**

**Monk:** Technology development, no matter what industry it is, takes a long time. I have a presentation about technology and show that it takes 20 to 25 years for any technology to mature from initial concept to commercialization. We happen to be in a time where there are a lot of technologies that are reaching that 25 years. So, I think it's the right time to do it, and that's what excites me about the topic. TLE